HYBRID BIOMIMETIC PLATFORMS BASED ON AMPHIPHILIC BLOCK COPOLYMERS

Inauguraldissertation

Zur Erlangung der Würde eines Doktors der Philosophie

vorgelegt der

Philosophisch-Naturwissenschaftlichen Fakultät der Universität Basel

von

Stefano Di Leone

Basel, 2021

Genehmigt von der Philosophisch-Naturwissenschaftlichen Fakultät auf Antrag von

Prof. Dr. Wolfgang Meier

(Universität Basel)

und

Prof. Dr. Uwe Pieles

(Fachhochschule Nordwestschweiz FHNW)

Prof. Dr. Cornelia Palivan

(Universität Basel)

Prof. Dr. Erik Reimhult

(Institut für Biologisch inspirierte Materialien)

Prof. Dr. Marcel Mayor

(Dekan)

Basel, den 22.06.2021

Dedicated to my grandfather Nino

A person that I always have in my heart

Aknowledgments

First of all, I thank the committee members Prof. Wolfgang Meier, Prof. Uwe Pieles, Prof. Cornelia Palivan and Prof. Erik Reimhult for evaluating my thesis. A big thank to Prof. Wolfgang Meier and Prof. Cornelia Palivan for supervising my work in these four years, allowing me to develop my scientific and my soft skills. I thank very much Prof. Erik Reimhult for being my co-referee and Prof. Edward Constable for chairing my defense.

A special thank goes to the Swiss Nanoscience Institute, the Swiss National Science Foundation, the NCCR Molecular System Engineering and the University of Basel for financial support.

I want to thank my former and previous colleagues for the team-work during our collaboration and fruitful conversation, or simply for the splendid time passed together in the office and outside. Especially I thank Ricco, Saziye, Myrto, Ioana, Dimitri, Andrea, Alessandro, Shabnam, Moritz, Maryame and Maria, together with my office neighbours of the second floor Dalila, Giacomo and Guglielmo. I wish you the best for your future and I know I will miss you all.

Now I want to write some lines about the most important friends, which somehow contributed in these years to my personal growth. Myrto thanks for your continuous support, you always have nice and motivating words for me both in private and career life. I appreciate a lot your open-mindness and especially your patience you had for taking care of me as a supervisor; and when I say “take care” I mean like an older sister, because this is the impression you gave me. Andrea, thanks for the funny conversation and time spent together in the lab and outside. Sazi thank you for your enlightening teaching about membranes and how to work in a professional way. Riccardo, you are my best German friend; since the beginning I could feel we would have built a special friendship. Thanks to Michal, with whom I share a lot of tastes and hobbies, also the sense of humour. Raoul, my Swiss friend, clever, kind and pleasant, I always enjoy to pass my time with you. Julian, the first Swiss friend I had, with a soul similar to an Italian. With you, I could easily overcome the boundaries between our cultures, starting from the language. Raphi and Sami, my crazy guys, funny and smart, actually two potential Italian speakers (amazing pronunciation). I always enjoy to teach you new Italian words and way of saying from my dialect. Thanks to Panos, my stubborn Greek friend.

For all the Italians or Italian speakers, I will carry from now on the conversation in my native language, so everyone can clearly understand how important for me you are.

In primis un grazie ai miei genitori, mamma e papà, per essermi stati sempre vicini, anche se a distanza. Per avermi dato il vostro supporto e i vostri preziosi consigli. Se sono quello che sono, in gran parte lo devo a voi. A mia madre, per avermi consolato nei momenti difficili e avermi dato la forza di andare avanti, per avermi contattato ogni giorno con la premura che solo una madre puo' avere per il proprio figlio. A mio padre, esempio di padre di famiglia e di uomo con grande forza di volontà e pazienza. Grazie a mio fratello, per essermi stato vicino, a modo suo. Grazie a mio zio Guido, che nonostante il suo celato e forte senso di nazionalità ha accettato la mia partenza ed è sempre pronto a riabbracciare il nipote al suo ritorno, riempiendolo di affetto e bei momenti insieme. Grazie ai miei parenti, che mi hanno scritto e pensato, chi piu' e chi meno, da quando sono fuori dall'Italia: zia Licia, zia Franca, zio Beppe, zia Paola, zia Ale e zia Francesca. Grazie a mio nonno Nino, punto cardine della mia crescita, nella cui filosofia di vita e modo di pensare mi rispecchio molto. Mi sarebbe piaciuto parlargli della Germania e della Svizzera, popoli per cui lui aveva tanta stima, e di come si vive all'estero, a lui che si lamentava continuamente degli italiani.

Un grazie alla mia Cristina, per l'amore che mi dimostri ogni giorno e per l'entusiasmo con cui portiamo avanti la nostra relazione nonostante le difficoltà della distanza. Per i sacrifici e le rinunce che fai pur di venire da me a Basel. Per la tua dolcezza. Perchè sei speciale, anche coi tuoi piccoli difetti.

Un grazie speciale va ad Eugenio, il mio migliore amico. No, molto di piu, un fratello per me. Colui con cui vivo quasi in simbiosi, condividendo esagerata euforia per identiche passioni e hobby, a partire dai gusti musicali. Colui che non sto piu nella pelle di rivedere di persona dopo pochi mesi di lontananza, come se non ci vedessimo da anni. Colui con cui litigo per piccole cose, come si fa tra fratelli, per poi fare subito pace. Grazie per esserci, senza di te non sarebbe lo stesso.

Grazie ai miei migliori amici: Aurelio, Peppe, Gad, Giannelli. Persone di cui ho una stima senza eguali, condivido gli interessi e non pochi modi di pensare, e i quali sono rimasti in contatto con me dal primo giorno in cui ho messo piede fuori dall'Italia. Grazie per avermi insegnato tante cose, per tutti i momenti passati insieme, di persona o online. Perchè per la

nostra amicizia non esistono barriere. Mi mancate, e a volte sono nostalgico dei tempi spensierati dell'università.

Grazie a Titti, per il supporto in questi anni, per il suo affetto incondizionato anche quando le nostre strade si sono separate e per la maturità con cui abbiamo affrontato i cambiamenti. Grazie ai miei amici d'infanzia Simone, Giorgio, Tuan e Massimo. Grazie ai vecchi amici con cui sono periodicamente in contatto e che fanno di tutto per vedermi quando torno in patria: Cristian, Germana, Teo, Rosanna, Valeria, Stefano Rossello, Gianni (l'uomo erectus), Genovesi, Ignazio, Bart, Dario, Cristina, Anelli e Lorenzo.

Grazie a i miei nuovi amici italiani conosciuti a Basel: Pezzman, Maddalena, Matteo, Raffaele, Gianluca,Vincenzo e Rosy. Grazie ad Angelo, dopotutto se ora mi trovo a Basilea lo devo anche a te. Mi hai insegnato tanto, sei la persona piu' saggia che conosca. Infine, ma non ultima per importanza, Miranda, la mia sorella mancata. Propositiva, entusiasta, piena di energia e sempre pronta aiutare, con te non ci si annoia mai. Di te mi posso sempre fidare, sei importante per me.

…well, at this point is better that I stop writing, I thanked people enough for today, considering that I could start crying if I keep on thinking about all the special people that surround me. I hope I did not forget anyone. With my PhD I close another chapter of my life, but the most important thing for me is that I could share all of this with you.

With pure love,

Stefano

Table of Contents

List of Figures

List of Tables

Abbreviations

7-ADCA = 7-aminodesacetoxycephalosporanic acid

ADAse = artificial deallylase

α-He = α-hemolysin

AFM = atomic force microscopy

AR = amplex red

BAM = brewster angle microscopy

BSA = bovine serum albumine

CLSM = confocal laser scanning microscopy

cyt c = cytochrome c

DCC = N,N'-dicyclohexylcarbodiimide

DPPC = 1,2-dihexadecanoyl-sn-glycero-3-phosphocholine

DPPE = 1,2-dipalmitoyl-sn-glycero-3-phosphoethanolamine

DMAP = 4-dimethylaminopyridine

DMF = dimethylformamide

DMPC = 1,2-dimyristoyl-sn-glycero-3-phosphocholine

DOPC = 1,2-dioleoyl-sn-glycero-3-phosphocholine

DOPS = 1,2-dioleoyl-sn-glycero-3-phospho-L-serine

DOTAP = 1,2-dioleoyl-3-trimethylammonium-propane

ECM = extracellular matrix

EDS = 1-ethyl-3-(3-dimethylaminopropyl)carbodiimide

FTIR = Fourier-transform infrared spectroscopy

H_2O_2 = hydrogen peroxide

HPLC = high pressure liquid cromatography

Hys = histidine

LB = Langmuir-Blodgett

LC = liquid condensed

LE = liquid-expanded

Liss Rhod PE = 1,2-dipalmitoyl-*sn*-glycero-3-phosphoethanolamine-*N*-(lissamine rhodamine B sulfonyl)

LS = Langmuir-Schaeffer

MeOH = methanol

MloK1 = *Mesorhizobium loti*

MOXA = 2-methyl-2-oxazoline

sNHS = sulfo-N-hydroxysulfosuccinimide

OmpA = outer membrane protein A

OmpF = outer membrane protein F

PB = phosphate buffer

PB-b-PEO = poly(butadiene)-block-poly(ethylene oxide)

PBD = polybutadiene

PBD-*b*-PEO = poly(butadiene-*b*-ethylene oxide)

PBS = phosphate buffer saline

PDMS-b-PMOXA = poly(dimethylsiloxane)-block-poly(2-methyl-2-oxazoline)

PEG-g-PEO = poly(ethylene glycol)-grafted-poly(ethylene oxide)

PGMA-*b*-PPO-*b*-PGMA = poly(glycerol monomethacrylate)-*b*-poly(propylene oxide)-*b*-poly(glycerol monomethacrylate)

PGME = phenylglycine methyl ester

PHA = polyhydroxylalkanoates

PHEMA-b-PBMA-b-PHEMA = poly(2-hydroxyethyl methacrylate)-block-poly(n-butyl methacrylate)-block-poly(2-hydroxyethyl methacrylate)

PIB = polyisobutylene

PMOXA-b-PDMS-b-PMOXA = poly(2-methyl-2-oxazoline)-block-poly(dimethylsiloxane)-block-poly(2-methyl-2-oxazoline)

POPC = 1-palmitoyl-2-oleoyl-sn-glycero-3-phosphocholine

POPE = 1-palmitoyl-2-oleoyl-sn-glycero-3-phosphoethanolamine

PVC = polyvinylchloride

QCM-D = quartz crystal microbalance with dissipation

SALB = solvent-assisted lipid bilayer

SAPM = solvent-assisted polymer membrane

SAV = streptavidin

SSBM = solid-supported bilayer membrane

SPR = surface plasmon resonance

SUV = small unilamellar vesicle

TDAB = tetradodecylammonium bromide

T_g = glass transition temperature

T_m = melting temperature

WT = wild type

YR = mutant

1. Scope of the thesis

Cell membranes are of great importance in numerous biological processes, and have been widely studied in the field of biochemistry and biophysics. That is the reason why it is crucial to understand the membrane properties in terms of morphology and architecture, together with the functions of each membrane component. For this purpose, artificial membranes have been developed and amphiphilic block copolymers represent ideal candidates for preparing these membranes. Polymeric membranes provide robustness and stability, and can mimic biological membranes, because they self-assemble in bilayers in aqueous environment. Thus, they have been employed for industrial and biomedical applications, such as catalysis, drug screening, biosensing, etc.

In this thesis, we design and create solid-supported membranes by combining different diblock and triblock amphiphilic block copolymers, specifically PDMS-b-PMOXA, by using different membrane preparation methods. Membrane properties were characterized by surface analytical techniques: isotherms of the monolayer at air-water interface were recorded; morphology, homogeneity and thickness of the different membranes were analyzed by AFM and force spectroscopy was employed for the mechanical properties of the polymer membranes; QCM-D was employed for quantifying the amount of biomolecules combined with membranes and the viscoelastic properties of the platform before and after the biomolecule recombination; the functionality of the combined biomolecules was monitored with the fluorimetry.

In the first part of the thesis, we investigate the field of hybrid membranes: the combination of copolymers and phospholipids led to a new generation of biomimetic materials that combines the mechanical resistance and chemical tunability of the polymers with the fluidity and biocompatibility of the lipids. Interestingly, when the physical state of polymer and lipids is not miscible, they separate in the membrane and form phase domains, which are similar to lipid raft found in biological membranes and are responsible for key functions in the cell (e.g. signalling, receptor trafficking). For the hybrid membrane preparation we deposited polymer-lipid monolayers onto silica supports by the controllable Langmuir-Blodgett transfer technique. Then we investigated the effect of different combination strategies on the accessibility of the model protein cyt c: either spontaneous insertion or covalent attachment through EDC/sNHS chemistry. Finally, we evaluated the peroxidase-like activity of cyt c after combining it with the membrane. We found that the phase domain separation was crucial for facilitating and controlling the protein recombination into a specific membrane domain (polymeric or lipidic).

The attachment strategy revealed to be better in terms of protein accessibility and also enhanced the cyt c activity.

In the second part of the thesis we explored the solvent-assisted method. This method was previously employed for preparing lipid membranes and we applied it on amphiphilic block copolymers here for the first time. We optimized the experimental conditions (e.g. polymer characteristics, solvent flow rate) and we combined the obtained membranes with different biomolecules. The combination was performed through the specific biotin-avidin interaction and was used to bind enzymes and DNA strands onto the membrane, preserving their functionality also in this case.

In the third part of the thesis, we added a fundamental research which was focused on combining the two main concepts of this thesis: we employed the SA method to prepare hybrid membranes composed of block copolymers and phospholipids in a fast and easy way.

2. Introduction

2.1. Biological membranes

Cell membranes are biological complex structures essential for all living organisms. Apart from compartmentalizing and protecting cells and cell organelles from their environment, they are involved in a multitude of biochemical processes: passive and active transport of ions through the membrane in order to maintain electrochemical gradients across the membrane; molecular recognition of specific molecules; enzymatic catalysis; cell signalling for control and coordinate activities of cell; and cell adhesion, which regulates cell migration and tissue development.

Cell membranes consist of proteins and oligosaccharides and phospholipids, and their content in the membrane influences critically their functions. Cell membranes are represented with the fluid mosaic model which consists of a self- assembled phospholipid bilayer, with the hydrophilic head groups oriented towards intracellular and extracellular spaces, while the hydrophobic chains face each other in order to isolate them from the environment. The formation of the bilayer is driven by hydrophobic interactions between the fatty acid chains. The structure of a cell membrane can be described by the "fluid mosaic model" proposed by Singer and Nicolson in 1972 (Figure 2.1-1). [1]

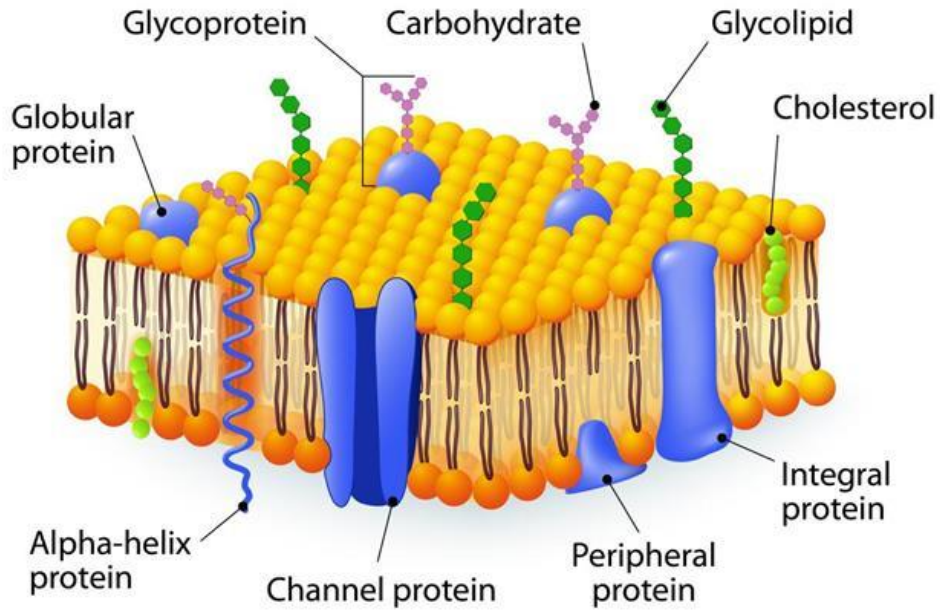

Figure 2.1-1. Fluid mosaic model of cell membrane.

In order to understand the functions of membrane proteins and individual membrane-related processes, biological membranes are widely studied. Artificial membranes have been employed as a simplified version of biological membranes for facilitating the investigation of membrane-related processes. Such artificial membranes can also find industrial applications, in the field of medicine or bio-engineering.

2.2. Biomimetic membranes

2.2.1. Phospholipids versus amphiphilic block copolymers

For obtaining a biocompatible and non-toxic membranes, phospholipids were mainly used for bio-mimicry, since they are natural components of biological membranes.[2] However, phospholipids present drawbacks, such as low mechanical stability, which facilitates chemical functionalization.[2,3] Amphiphilic block copolymers are able to overcome these constraints. Due to the higher molecular weights, block copolymers allow the formation of membranes with higher thickness and thus more resistance, even though less fluidity and less permeability (Figure 2.2-1). Lipid bilayers are relatively unstable compared to polymer membranes, which present improved physicochemical properties, namely high mechanical stability,[4–12] low permeability,[13] tunability,[14–16] biomimetic properties.[17]

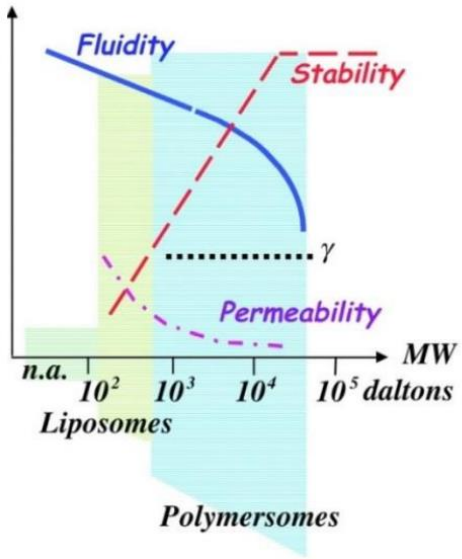

Figure 2.2-1. Schematic representation of membrane properties versus molecular weight of the amphiphile.[18]

Moreover, another advantage of amphiphilic blockcopolymers is their possibility to be designed and tuned with a different chain length and a variety of different functional ending group, in order to take control over the membrane assemblies, and the stimuli-responsiveness

of the system.[19,20] Amphiphilic diblock (AB) or triblock (ABA or ABC) copolymers have been already reported for their biomimetic properties[21]. Artificial membranes are formed by diblock and triblock copolymers,[18,20] which possess a phospholipid-like structure. Among these, PMOXA-b-PDMS copolymer is a good candidate to mimic biological membranes, due to its biocompatible properties. Also, PMOXA-b-PDMS-b-PMOXA triblock copolymers possess the required structure to form membranes.[22–24] Due to its biocompatibility, non-toxicity, and high flexibility, the hydrophobic PDMS block is suitable for development of biomaterials.[25,26] Furthermore, the presence of the tertiary amine in the backbone chain, makes it almost no detectable by enzymes and thus increasing its stability in biological environments.[27] Formation of membranes is possible by self-assembly process in aqueous media.

At a specific concentration, defined as critical micellar concentration (CMC) which is characteristic for every amphiphile, self-assebly process takes place. Micelles, vesicles, or worm-like structures, are formed in these process in order to reach thermodynamic equilibrium and minimize the free energy of the system.[6,28] The self-assembly process is driven by the so-called hydrophobic effect, which force the amphiphiles to withdraw their hydrophobic part in order to reduce contact with the aqueous solution. Several factors influence the self-assembly: the geometry and chemical composition; the polydispersity index of the amphiphile, the preparation method adopted, and external factors, e.g. pH, solvent or temperature.[29] The resulting structures can be predicted from the molecular packing parameter (P), related to the hydrophilic / hydrophobic ratio of the amphiphile.[23,30,31] P is a dimensionless value and it is defined as:

P = vp / al p (1)

Where v and l are the volume and the length of the hydrophobic tail, and a is the area occupied by the hydrophilic head group.[32,33] P characterize the morphology of the self-assemblies: spherical micelle ($0 < P \leq 1/3$), cylindrical micelle ($1/3 < P \leq 1/2$), or bilayer structure, such as vesicle ($1/2 < P \leq 1$).[33,34]

2.2.2. Polymer self-assembly

Amphiphiles can undergo two main categories of self-assembly: planar membranes and spherical compartments. These different structures presents their advantages and drawbacks, and can find different applications. Planar membranes have a 2D architecture and include: i) Langmuir monolayers at the air-water interface,[14] ii) freestanding membranes,[35] and iii) solid-supported membranes (Figure 2.2-2).[18]

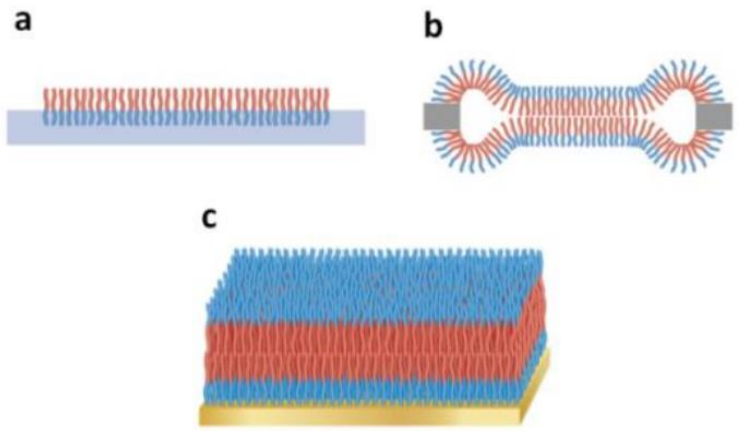

Figure 2.2-2. Models of planar membranes: (a) Langmuir monolayer, (b) freestanding membrane, and (c) solid-supported membrane.[36]

Freestanding membranes have been widely used for understanding the membrane interaction with proteins in terms of insertion mechanism and functionality after the combination. By monitoring the change in the conductance of the system, for example, it was possible to observe the membrane protein insertion.[37,38] However, the low stability of free-standing membranes due to the limited lateral tension makes them of scarce interest for technological applications.[39,40] Langmuir monolayers and solid-supported membranes will be described in detail in the following sections.

2.2.3. Micelles and vesicles

Vesicles and micelles represent 3D spherical compartments (Figure 2.2-3), which can encapsulate and transport compounds like proteins, drugs or enzymes.[41,42] The encapsulated molecules are this way protected by external stimuli and this make vesicles particularly appealing for bio-medical applications.[43]

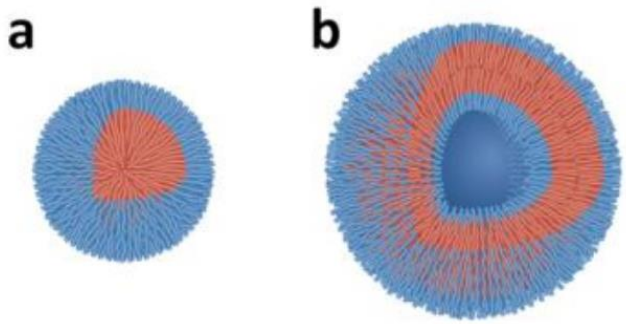

Figure 2.2-3. Models of spherical compartments: (a) micelle and (b) vesicle.[6]

By controlling the hydrophilic/hydrophobic ratio or the molecular weight of the hydrophobic block of the polymer used, it is possible to tune the dimensions of the vesicles formed.[29] For example, when a PDMS-b-PMOXA diblock copolymer with low molecular weight of the PDMS block was employed, it self-assembled into micelle and nanoparticles instead of vesicle.[29] Most of polymer membranes are symmetric and are obtained by self-assembling AB or ABA amphiphilic block copolymers. However, asymmetric ABC triblock copolymers are interesting candidates to achieve a directional protein combination with membranes or to create membranes with different properties at each surface.

Micelles have a 3D architecture, with a hydrophobic core and a hydrophilic shell. Micelles do not possess a membrane's structure, nevertheless they are employed in application such as drug delivery.[44] In this case, the encapsulation works with drugs which are water insoluble and which can be entrapped in the hydrophobic core of the micelle, and then delivered and released in a specified area of the body through induced stimuli like change of pH and temperature, or by conjugation with some antibody. The great advantage of micelle relies in their small size (< 100 nm) which allows them to circulate in the organism for a long time without being recognized, keeping the cargo protected by proteins or phagocytic cells.

2.3. Langmuir monolayers

2.3.1. Langmuir technique

The Langmuir technique allows the investigation of amphihilic molecules at the air-water interface, this way enabling the investigation of their behaviour and interactions at the interface. Langmuir monolayers consists in a single membrane leaflet and were widely studied as a membrane model.[45] The self-assembly of molecules at the air-water interface to form a monolayer has been discovered by Irving Langmuir,[46] and it employs an apparatus called Langmuir trough. This instrument consists of: i) a hydrophobic Teflon trough, filled with an aqueous subphase (water or buffer); ii) two movable hydrophilic barriers; iii) a surface pressure sensor, called Wilhelmy plate. The procedure consists in spreading a solution of amphiphile, prepared in an organic and volatile solvent, such as chloroform, on the aqueous surface. Then the movable barriers close, inducing the packing of the amphiphiles to form a monolayer. The monolayer compression is recorded and represented as a surface pressure-area isotherm (Figure 2.3-1). Initially, the surface pressure value of 0 mN m^{-1} is representative of no interactions between amphiphile molecules occur and that the molecules are in the gaseous state. During

the compression, the molecules start to interact with each other and to form consequently, a monolayer in the LE, LC and solid states.[47] A further compression results in the collapse of the monolayer.[48] The Langmuir isotherm gives information about, stability, self-assemble and physical state of the monolayer.[49]

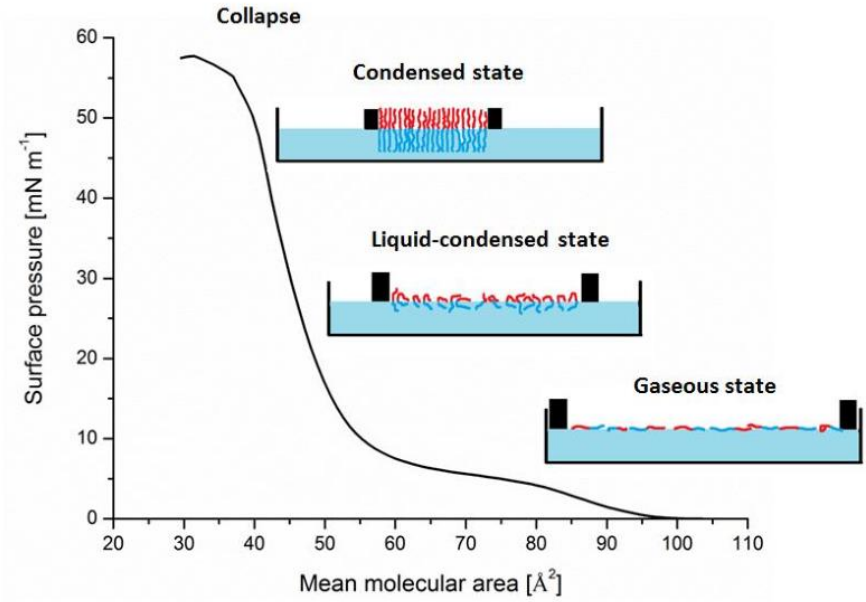

Figure 2.3-1. Langmuir isotherm of DPPC and the monolayer conformation during the compression (blue and red colours represent respectively the hydrophilic and the hydrophobic part of the molecule).[45]

2.3.2. Properties of the monolayers at the air-water interface

The shape of the isotherm depends from the monolayer characteristics and it can be influenced by different factors, like temperature, pH, size and structure of the molecules that are forming the monolayer. For example, fatty acids become ionized by inducing a change in pH, resulting in repulsive interactions between the molecules and a lower stability of the monolayer.[50] Length of the chain and degree of saturation are other parameters that influence monolayer formation.[51] The presence of the double bond in the hydrocarbon chain of the amphiphile hinder the flexibility of the chain and the adhesion between molecules.[52,53] Most important, the isotherms provide information about phase transitions of the monolayer at the air-water interface,[49] which are expressed by the change of the isotherm's slope.[54] Also for molecules with high molecular weight, such as amphiphilic block copolymers, it is possible to observe a change in the slope during the compression, until a plateau is reached. This plateau forms because of the rearrangement of the molecules during the monolayer compression, until the

formation of a densely packed film.[55] The hydrophobic and hydrophilic blocks' lengths, can also influence the shape of this plateau, as it was shown in previous works.[56] The two-component lipid-polymer monolayers typically exhibit intermediate characteristics between the polymers and lipids monolayers in terms of breaking point and phase transition value.

2.4. Solid-supported planar membranes

Amphiphilic molecules can form planar membranes on solid supports, so-called supported bilayer membranes. The solid support provides an improved stability of the membrane.[57] One great advantage of planar membranes on solid supports is in their possibility to be characterized by a variety of analytical methods, which is not possible for three dimensional membrane assemblies, allowing the quantification of membrane associated processes based on membrane-protein and protein-protein interactions. On the other hand, biomolecules combined with supported membranes may lose part of their functionality or denaturate after the combination, due to the interaction with the solid support.[58] In order to overcome this limitation and avoid contact between the combined biomolecule and solid support, supported membranes were optimized by introducing improvements based on electrostatic interaction (physisorption) such as polymer cushions or polyelectrolyte films, [36,57–59] and covalent bond between the amphiphile end-group and the surface (chemisorption), such as anchor as spacers groups,[58] which involves molecules like peptides, oligomers, or polymers.[57,60–63]

To date, different strategies have been applied to prepare planar membranes on solid supports, which will be explained in details in the following paragraphs. Common preparation techniques for such membranes are Langmuir film transfers,[64] vesicle spreading,[64,65] and vesicle fusion.[66,67] An emerging approach, called SALB method, consists of the deposition of a lipid dissolved in an organic solvent on a solid support, followed by an exchange of the solvent with an aqueous buffer.[68] This method can be applied also to polymer mixtures with proper adaption. The SALB method overcomes the limitation of vesicle fusion to form bilayers onto a limited number of substrates. Among the covalent attachment, two main strategies for preparation of the solid-supported films are the grafting from and the grafting to approaches (Figure 2.4-1). The "grafting from" strategy involves surface-initiated polymerization. This method provides good control over the brush thickness and homogeneity.[69] The "grafting to" strategy consists of the deposition of the prefabricated polymer onto the surface either by physisorption or by chemisorption.[70] The advantage consists in the simplicity of the method.[71] On the other hand, this strategy suffers some limitations, like the difficulty to obtain a densely packed film due to the steric repulsions between the polymer chains.[72]

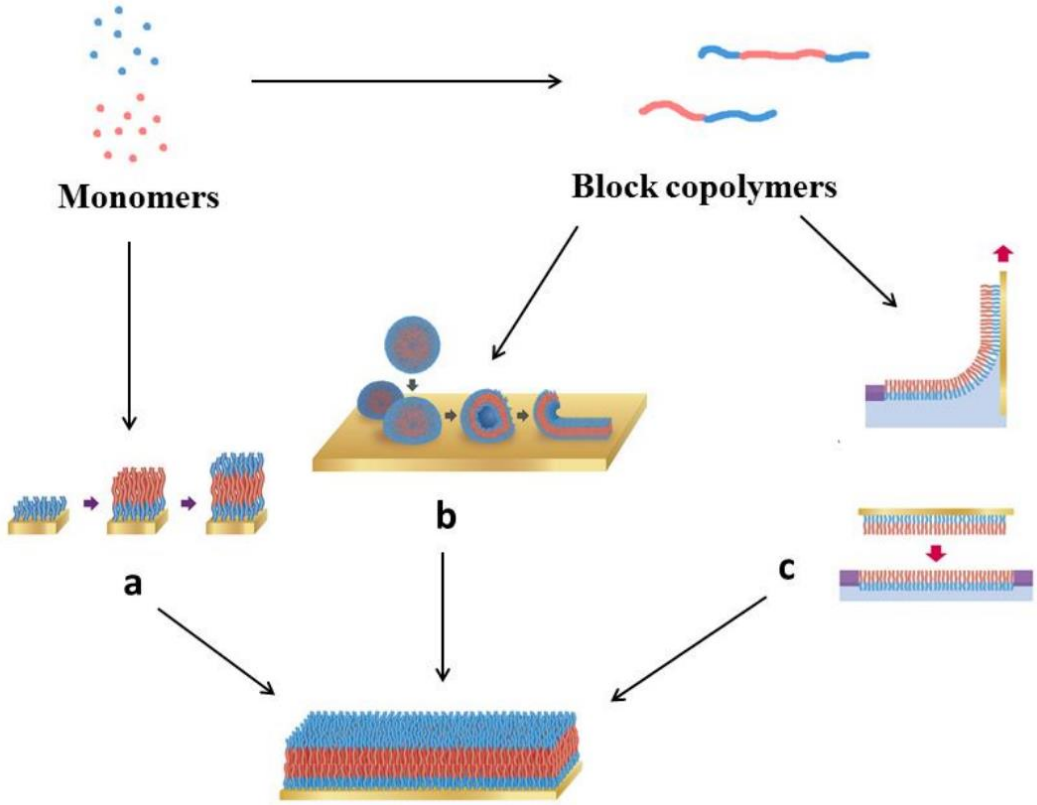

Figure 2.4-1. Strategies for preparation of solid-supported membranes: (a) surface-initiated polymerization (grafting from approach), (b) vesicles spreading (grafting to approach), and (c) LB and LS transfers (grafting to approach).[72]

2.4.1. Membranes prepared by surface-initiated polymerization

This approach involves of grafting amphiphilic molecules directly from the solid support. For this purpose, triblock copolymers are good candidates, since they possess a structure with a middle hydrophobic block and peripheral hydrophilic blocks. Such polymeric membranes can be prepared, by surface-initiated atom transfer radical polymerization.[70,73] For example, a previous work reported the synthesis of a biomimetic membrane, composed of PHEMA-b-PBMA-b-PHEMA triblock copolymer.[74] Even though this technique provides a good control over the brush density and thickness of the polymer and enables obtaining membranes with a biological-like architecture, the polymer chains are attached covalently to the surface. This affects the membrane lateral mobility and consequently reduces the possibility of protein insertion.[75] In order to overcome this limitation, non-covalent techniques (vesicle fusion, Langmuir transfer) have been applied for biomimetic membrane preparation.

2.4.2. Membranes prepared by vesicle fusion

Vesicle fusion is a straightforward method to obtain solid-supported membranes and it is commonly applied on lipids.[76–79] However, few studies concerning polymer vesicles spreading on solid supports are reported in literature.[15,80] In addition, real-time formation of the membrane can be monitored by SPR,[80] or by QCM-D.[81] Different parameters are influencing the membrane formation by vesicle fusion method, namely vesicle size, temperature, osmotic pressure, charge of the molecule and choice of solid support.[79] For example, it was observed that vesicles from different charged phospholipids interact differently with the slightly anionic silica support and the deposition pathway is also affected (Figure 2.4-3).[78] Depending on substrate properties, different assemblies can be obtained, and when the electrostatic interactions between the amphiphile and the support are strong, solid-supported planar membrane is successfully produced.

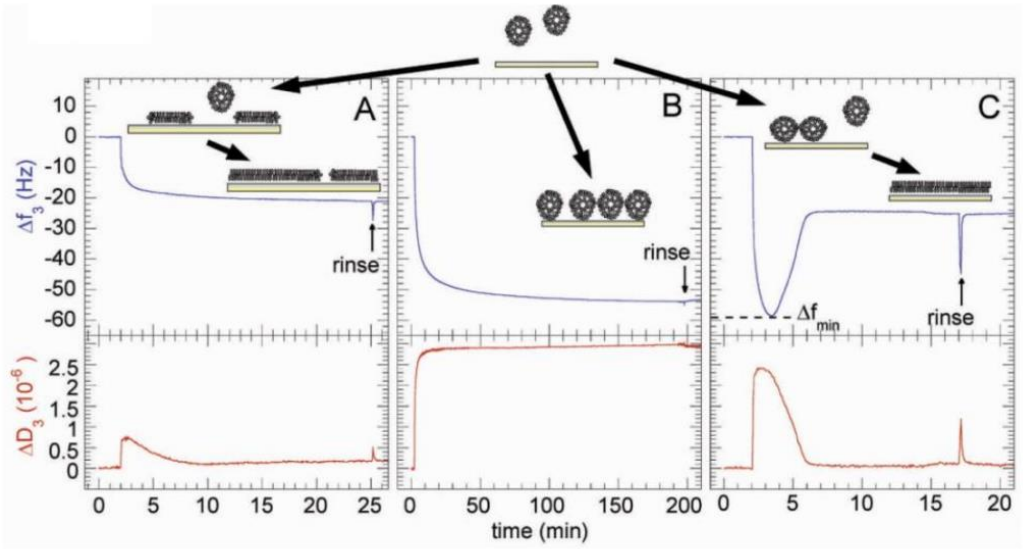

Figure 2.4-2. QCM-D data presenting deposition of SUVs onto silica substrate. The SUVs were formed by: (a) positively charged phospholipid, DOTAP, (b) 50% zwitterionic DOPC and 50% negatively charged DOPS, and (c) 80% DOPC and 20% DOPS.[82]

In the case of polymers, some factors have to be overcome in order to achieve the fusion of vesicles: the higher mechanical stability compared to lipids, the unfavourable thermodynamic conditions, and the loss of conformational freedom from the membrane packing. In another study, vesicles formed by lipoic acid-functionalized PB-b-PEO diblock copolymer were successfully fused onto a gold substrate.[80] It was observed that the bottom layer was covalently attached to the substrate, whereas the second layer was attached by hydrophobic interactions. Such a system is more similar to the biological membrane and improves the membrane fluidity,

compared to the one obtained with the surface-initiated polymerization (see previous paragraph). A quick rinsing with salt solution, a drying step, and a consecutive rehydration, increases the homogeneity of the bilayer, however some additional polymer aggregates attached to the bilayer surface could be still observed. The SPR and force spectroscopy measurements are techniques commonly used to evaluate the thickness of the obtained bilayer membranes.[83]

2.4.3. Membranes prepared by Langmuir transfer

Transfers of monolayers from the air-water interface onto solid support form membranes homogeneous and free of major defects. The advantage of this method is a control over the surface pressure to apply for the monolayer transfer, which directly affects the density of the monolayer. Moreover, the method can be applied to a variety of different substrates. The LB technique enables the deposition of more than one layer onto a solid support. Depending on the deposition strategy, different multilayer structure can be obtained: X-, Y-, and Z- type (Figure 2.4-6). Consecutive emersion and immersion of the substrate (Y-type deposition), results in the formation of a head-to-head and tail-to-tail multilayer.[49] Different strategies consist of multiple immersions (X-type) or emersions (Z-type) of the substrate. An important drawback of this method is related to a weak interaction between two monolayers, which can result in an incomplete monolayer transfer. In order to overcome this limitation, LS deposition technique can be applied.

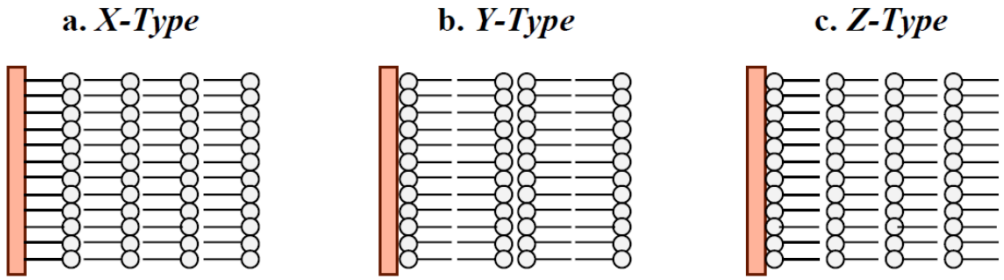

Figure 2.4-3. Strategies for multilayer transfer onto a hydrophilic substrate by LB technique.[49]

A bilayer membrane formation involves two processes: LB and LS transfers (Figure 2.4-7). During the LB transfer the substrate is dipped out from the water allowing attachment of the monolayer from the air-water interface onto the substrate with the hydrophilic part of the molecule.[84] The LS transfer allows the building of the second layer of the membrane through

hydrophobic interactions, by dipping a horizontally placed substrate, with a previously deposited first layer, into the sub-phase. Combination of LB and LS techniques allow the construction of asymmetric bilayers with mimicry properties, 88 separated from the solid support only by an ultrathin (1-2 nm) water film.[36]

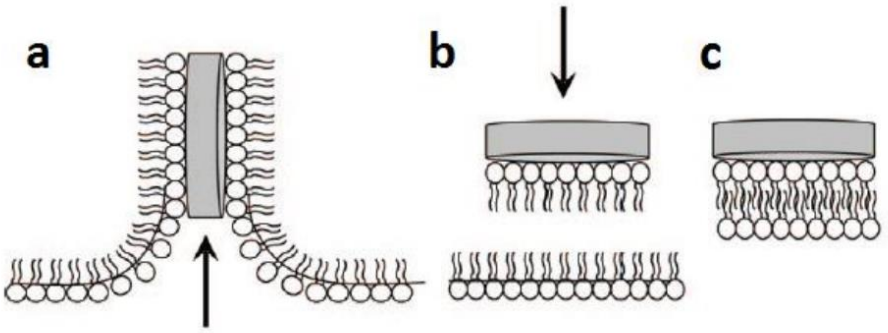

Figure 2.4-4. (a) Langmuir-Blodgett (LB) and (b) Langmuir-Schaefer (LS) deposition of monolayers and (c) the resulting solid-supported membrane.[85]

It has been observed that polymer bilayers were stable in air for approximately 2 hours, which is advantageous when comparing with solid-supported lipid membranes which are known to disrupt during the drying process. After 12 h of exposure to air polymer bilayers can disassemble and rearrange to form aggregates. LB method provides supported membranes with a defined architecture and fewer defects than those obtained with the vesicle fusion method. Unfortunately, this method shows some intrinsic difficulties, such as long time for performing the experiment and a high level of cleanliness required.[57,58]

2.4.4. Membrane prepared by solvent-assisted method

SALB's basic working principle is the deposition of lipids which are dissolved in an appropriate organic solvent. The following step involves the exchange of the organic solvent with an aqueous buffer, which induces the self-assembly of lipids into a supported bilayer membrane.[68] The SALB method can be successfully applied on a greater number of solid support, such as silicon dioxide, aluminum oxide and gold (Figure 2.4-5). In comparison to vesicle fusion method, it does not require lipid vesicles and it is simply based on the deposition of lipid molecules onto a surface.[272] Additionally, the SALB approach has the capability to prepare supported membranes containing high cholesterol concentrations compared to vesicle fusion method. This is of great interest for the understanding of how cholesterol affects the membrane biophysical properties, including membrane fluidity and organization into domain structures such as lipid rafts.[273] In principle, the approach should also enable characterization of

cholesterol bilayer domains This method has been extensively applied to prepare lipid bilayer membranes and could be applied with proper adaption also to polymer and polymer-lipid mixtures for the preparation of polymer and hybrid membranes. The further characterization of those membranes with surface-sensitive analytical techniques (e.g. QCM-D, AFM or SPR) allows to explore those artificial cell membranes by taking advantage of a robust experimental protocol. Overall, SALB is a fast and straightforward method, however it presents the limitation of a required solubility of the chemical compound in an organic solvent and sometimes produce porous membranes. [272]

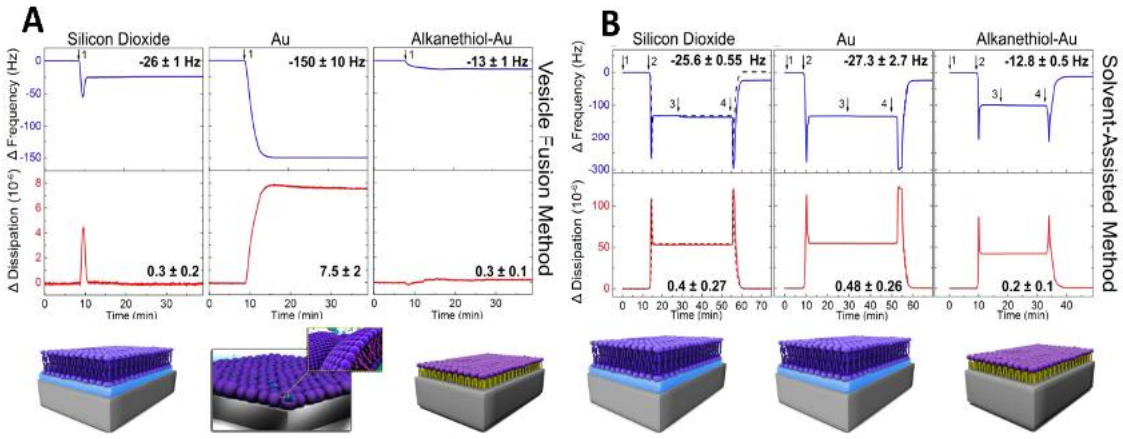

Figure 2.4-5. QCM-D monitoring of vesicle fusion and SALB methods on three different substrates: (A) vesicle fusion method; (B) SALB formation method. The dashed curve in figure B represents the control experiment in which lipid is not injected. The schematics show the proposed assembled lipid structures.[86]

2.5 Hybrid membranes

This chapter contains parts adapted from the review Agata Krywko-Cendrowska, **Stefano di Leone**, Maryame Bina, Saziye Yorulmaz-Avsar, Cornelia G. Palivanand Wolfgang Meier, "Recent Advances in Hybrid Biomimetic Polymer-Based Films: from Assembly to Applications", Polymers 2020, 12(5), 1003.

2.5.1. Hybrid polymer-lipid membranes

Hybrid materials are considered as another type of biomimetic platforms.[87] Membrane domains play an important role in the process of biomolecule-membrane combination, making hybrid membranes of great interest for understanding the mechanisms behind membrane related processes or for developing active platforms for several biomimetic applications. By combining amphiphilic block copolymers and phospholipids it is possible to obtain hybrid

membranes, which represent a promising class of materials to be employed for the preparation of artificial membranes. Those membranes have intermediate characteristics between pure copolymer and pure lipid membranes[16]. Through this combination it is possible to obtain either homogeneous or heterogeneous membranes, which depends on the miscibility of the two compounds. If they are not miscible, the membrane will undergo phase domain separation. By modulating the composition of the polymer-lipid mixtures, it is possible to obtain hybrid materials with desired properties and to control the interactions between these materials and biomolecules.[3] These interactions are strictly related to the hybrid composition in a way that it allows the control over the location and concentration of the proteins, in order to obtain biocompatible materials with specific properties and functions.[87,88] The most important application for hybrid membranes is the biomimicry of "lipid raft", namely membrane phase domains found in biological membranes, which are involved in important biological processes, such as lateral protein organization, cell signaling, membrane tension regulation, etc.[89] It was observed in previous works, that the polymer-lipid molar composition influences the morphology of hybrid membranes.[90–92] For example, by mixing PEG-g-PEO diblock copolymer with saturated DPPC and unsaturated POPC (Figure 2.5-1).[89] Phase domain separation could be observed, for a certain polymer content. When the polymer content was mixed with POPC and higher than 60%, lipid was homogeneously distributed within the vesicle, whereas when lipid content was higher, the hybrid vesicles underwent the formation of separated polymersomes and liposomes within few hours.

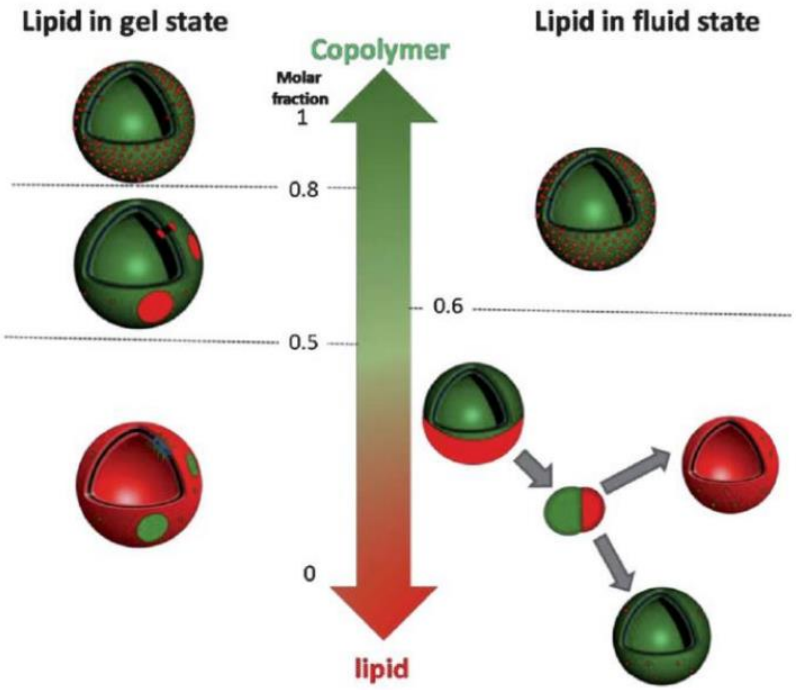

Figure 2.5-1. Schematic of hybrid vesicles, formed by PEG-g-PEO mixed with DPPC (gel state) or POPC (fluid state), according to the molar composition and fluidity of the lipid at room temperature.[89]

The mixture composition is fundamental for driving the binding of proteins to a hybrid membrane and can be used as a model for studying receptor/ligand recognition.[93] For example, the interactions between a binary mixture of PMOXA-b-PDMS-b-PMOXA and DPPC with the protein OmpF was investigated, showing its preferential distribution in the polymer-rich phase.[94] However no further systematic investigation was performed on this process.

2.5.2. Solid-supported membranes based on polymers and lipids

Copolymer-lipid-based hybrid supported membranes have been prepared in a membrane-like architecture (i.e., mono-, bi-, or multi-layers) using different deposition methods.[74,81,86,95–97] Regardless of the ratio of polymer and lipid in the mixture, it was possible to produce hybrid membranes which possess at the same time enhanced mechanical stability and mobility, when compared to one-component membranes,[98] possibly related to a synergic activity of both the polymer and the lipid within the membrane. The method employed to produce hybrid supported membranes can be the same used for lipid and polymer membranes with proper adaption: Langmuir transfer, vesicle fusion and solvent-assisted method.

Recently, by blending the PBD and DOPC in specific chemical composition (molar ratio 3:7) it was possible to obtain a hybrid membrane with improved viscoelastic properties and permeability onto a protein layer.[78] The hybrid membrane behaved as a barrier for the protein layer against the attack of an enzyme.[99] Polymer-lipid hybrid membranes can be characterized in terms of viscoelastic properties and membrane coverage by QCM-D, using its sensor chip as the solid support. Sessile droplet method and ellipsometry can be further employed to determine the hydrophobicity/hydrophilicity of the membrane and its thickness, respectively.

2.5.3. Properties of polymer-lipid membranes

The advantages provided by copolymers in terms of mechanical resistance,[3,100] together with the ones provided by lipids in terms of enhanced mobility and specific interaction with membrane proteins,[81] allows to design and develop hybrid platforms with advanced features.[87,101,102] It has been observed that the physical state of the hybrid components, either gel or liquid phase, influences the protein distribution within the membrane.[87] In fact, the combination of copolymers and lipids in hybrid membranes revealed cutting-edge properties, such as an improved membrane fluidity and an assisted insertion of biomolecules. Recently, PDMS-b-PMOXA diblock copolymers have been blended in different molar ratio with various phospholipids (i.e. DPPC, DOPC, and DPPE), for understanding how factors like surface pressure or the hydrophobic chain length mismatch affecting the domain separation in hybrid monolayers in terms of shape and size.[96,103] Also, the structure and the Tg of polymers, and the Tm of lipids influence the formation of heterogeneous membranes.[87,88,104,105] It must be specified that polymer-lipid phase separation is never complete, rather we refers to either a lipid- or polymer-enriched domain.[103] This domain enrichment, due to polymer/lipid diffusion within the membrane, was for example investigated in hybrid monolayers composed of PIB, PEO, and DMPC,[104] or PGMA-b-PPO-b-PGMA triblock copolymer with DPPC and DMPC.[106] It has been found that an efficient phase domain separation in polymer-lipid hybrid membranes resembles the lipid rafts found in cell membranes, where they are involved in crucial biological processes, such as protein lateral organization or signal transduction.[107] By controlling the phase domain separation it is possible to control the incorporation of biomolecules into the membrane to create platforms with desired functions.[103]

They can also be used for the reconstitution of biomolecules.[108–110] Biomolecules can be combined with a polymer-lipid membrane by specific binding (e.g., receptor/ligand recognition),[111] where the variety of functional groups for the polymers allows the covalent bonding of a chosen biomolecule with great versatility.[86] Alternatively, biomolecules can be

inserted,[93,112] as it is the case of the potassium channel from MloK1, which has been inserted into hybrid membranes composed of PDMS-b-PMOXA and different lipids (POPC, DPPC or POPE). According to the physical state of the combined lipid, the protein could be inserted spontaneous into a specific phase domain (Figure 2.5-2).[103] In another study has been observed that solid-supported hybrid membrane composed of diblock copolymer poly(butadiene-b-ethylene oxide) (PBD-b-PEO) and DPPC presents better permeability of a drug compared to single-component membranes.[113]

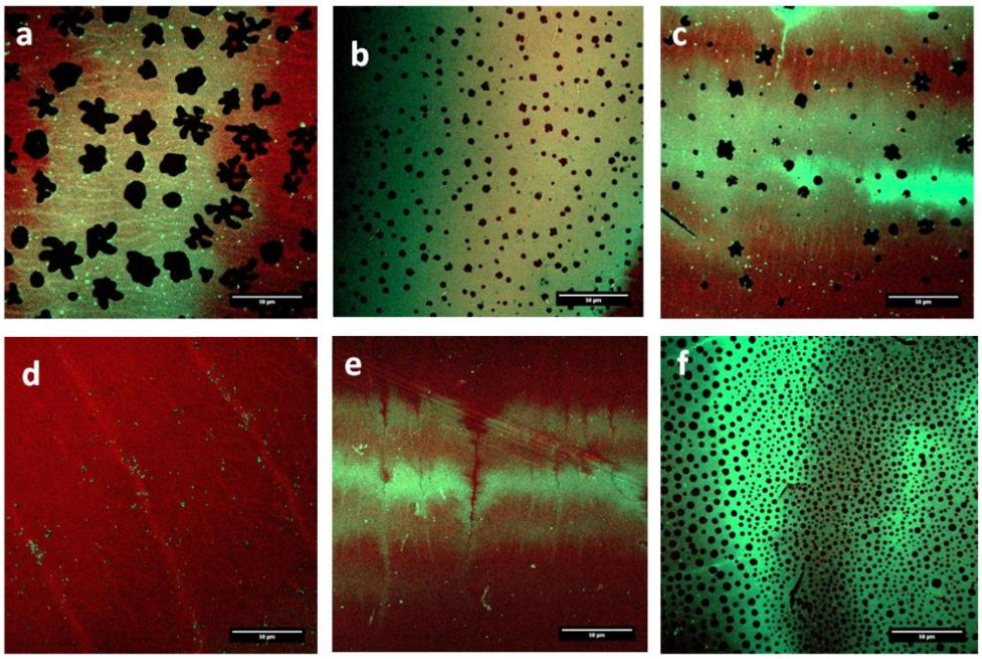

Figure 2.5-2. CLSM micrographs showing the protein distribution in films consisting of mixtures of $PDMS_{65}$-*b*-$PMOXA_{12}$ and (a) DPPC (xDPPC = 0.75), (b) DPPC (xDPPC = 0.5), (c) DPPE (xDPPE = 0.25), (d) DOPC (xDPPC = 0.25), and (e) POPE (xDPPC = 0.25). (f) PDMS37-b-PMOXA9 mixed with DPPE (xDPPE = 0.5).[103]

2.6. Combination of biomolecules into polymeric membranes

2.6.1. Polymersomes decorated with biomolecules

The choice of polymer composition and the decoration of the vesicle surface with specific biomolecules allows to tune the properties of the vesicles. For example, it was possible to encapsulate enzymes into the vesicles, this way allowing the development of nanoreactors for the production of active compounds in situ.[114] The advantage of this strategy involves in the production of the active compound in a controlled way and on demand.[24,115] Different membrane proteins have been successfully inserted into the membrane of polymeric vesicles,

such as Complex I,[23] OmpF,[24,116–118] or gramicidin.[119,120] For instance, vesicles formed with the triblock copolymer PMOXA-b-PDMS-b-PMOXA with incorporated OmpF were used to encapsulate a penicillin acylase enzyme. The presence of pores in the membranes allowed the substrates (7-ADCA and PGME) to enter the nanoreactors and to produce cephalexin.[24] When the PEO-b-PDMS-b-PMOXA triblock copolymer was used for preparing vesicles, it was possible to control the orientation of the two different hydrophilic block by tuning the chain length of PEO and PMOXA.[121] The asymmetry of the polymer membrane played a key role in the functionality of Aquaporin, which was able to insert with the desired orientation.[122] Another approach consisted in the covalent attachment of nanoreactors onto a solid support, resulting in antimicrobial surface (Figure 2.6-1).[120]

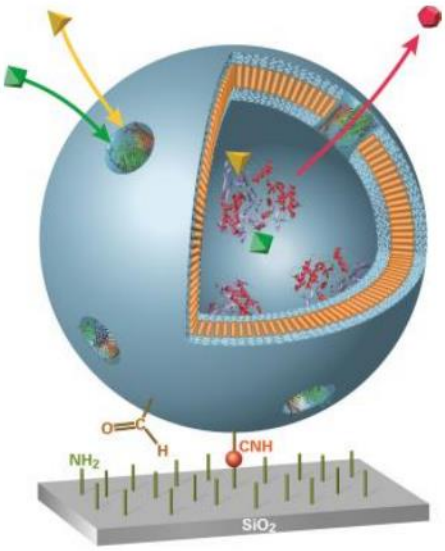

Figure 2.6-1. Scheme of enzymatically active, immobilized nanoreactors for the synthesis of antibiotics.[44]

2.6.2. Solid-supported planar membranes equipped with biomolecules

The main purpose of preparing artificial membranes is the mimetic of biological membranes in order to obtain functional surfaces. Enzyme's immobilization can be achieved with different methods: i) physical adsorption onto the membrane surface, ii) insertion into the membrane, iii) specific coupling with the membrane surface (e.g. biotin-streptavidin, metal-His-tag protein)[123] and iv) entrapment in matrices, such as polymer networks or channels.[14,42,124,125] The membrane should also possess appropriate composition and properties, namely thickness and fluidity, which will facilitate the combination with the biomolecules.[72] Immobilization of

biomolecules is a straightforward method for the development of active surfaces for applications in the field of medicine and bioengineering.[126–128] For example, immobilization of enzymes onto a membrane surfaces allows its continuous catalytic activity.[129–131] Among those, artificial metalloenzymes are hybrid molecules which combines the organometallic and enzymatic catalysys.[239-240] They hold many potential applications in the industrial field, such as asymmetric synthesis or chemomimetic biocatalysis.[240] In order to increase the quantity of enzyme combined, the immobilization is frequently performed on porous material,[132–134] which however suffer the main drawbacks of diffusional limitations. On the other side, non-porous materials present better diffusion, but low enzyme encapsulation efficiency. Additionally, there is the risk of protein denaturation when entering in contact with the solid support.[135] To avoid protein denaturation, the solid support has to be covered with lipid- or polymer-based soft layers.[125,136,137] The higher stability of polymer membranes compared to lipid ones, make them more reliable for potential applications as active surfaces. Among these combination approach, the biggest challenge remains the insertion of transmembrane proteins, in such a way that the protein keeps its native structure and functionality. To avoid the contact of the protein with the support and a consequent protein denaturation,[57,136] an ultra thin (nm range) polymer layer, called "cushion", has been introduced between the solid support and the artificial membrane (Figure 2.6-2). The cushion should be thermodynamically and mechanically stable, and need to interact in the repulsive way with the membrane.[123] Commonly used types of polymers employed as membrane cushions are: cellulose, dextran, chitosan, polyelectrolytes or lipo-polymers tethers.[136,138,139] Additionally, they have been frequently used for protein insertion, for example ATPase,[140] outer membrane proteins (OmpF and OmpA),[141] or α-He.[142] Alternatively, the adsorption and fusion of proteo-liposomes has been widely adopted as method for preparing solid-supported lipid membrane with inserted proteins.[143]

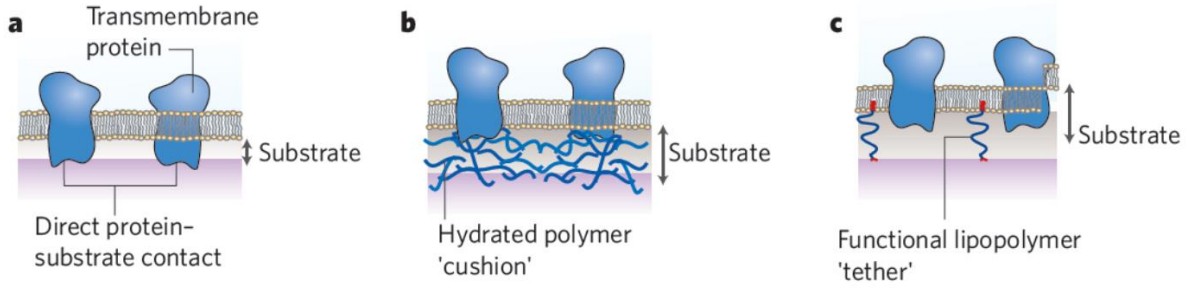

Figure 2.6-2. Transmembrane protein inserted into (a) lipid membrane deposited directly onto the solid support, (b) lipid membrane onto polymer cushion, and (c) lipopolymer-tethered membrane.[123]

Polymeric membrane possess higher thickness (3 – 40 nm) compared to lipid membranes (3 – 4 nm),[144] and this reduces the interactions between the incorporated protein and the solid support, which prevents the protein denaturation.[72] A successful attempt consisted in the insertion of α-He into a solid-supported PB-b-PEO membrane upon applied electrical current.[145] The protein was inserted successfully and it preserved its functions. However this method have some limitations, such as the need of a conductive material as solid support and the risk of protein denaturation or membrane disruption due to the current applied.

2.7. Applications of solid-supported membranes

2.7.1. Membranes composed of copolymers

Potential applications of solid-supported membranes as sensors, for example, may require the incorporation of membrane proteins. Membranes obtained either by vesicle spreading or by grafting method may hamper the functional incorporation of biomolecules, for reasons related to the surface charge or the chain packing density of the membrane. To control these properties and creating systems with improved performances in terms of protein-membrane combination, self-assembly of amphiphilic polymers was applied in place of surface chemistry or electrostatics. Additionally, polymers with various chemical compositions can be employed,[29] which allows a great versatility of the system, with application in the field of biophysical studies, sensor developments and nanotechnology. For example, it was found that the adsorption of cyt c on electrodes (e.g., Pt, Hg, Au, and Ag) induced large conformational changes and protein denaturation.[114,115,119,146] The attempt to use different electrodes based on nanomaterials (e.g., carbon nanotubes, graphene, and nanoparticles) might not be enough to preserve the cyt c functionality.[87,89,121,122,147,148] In this case, the formation of solid-supported polymer membrane as a mean of electrode surface modification, resulted in a biocompatible system for the cyt c−substrate interaction. Such a dynamic platform can be also used to host biomolecules and to develop efficient biosensors due to the enhanced protein−membrane−substrate communication achieved.[91,92]

2.7.2. Hybrid membranes composed of polymers and lipids

Hybrid polymer-lipid membranes have the property to rearrange their architectures in response to external stimuli, like the contact with a biomolecule or a cell membrane. That is why they

can serve as robust model for understanding bio-chemical processes within cells or investigating the interactions between cell membranes and biomolecules, such as the case of monolayers at air–water interface composed of PHA and DOPC, as a model to analyse the mixing properties between synthetic and biological membranes.[149] Due to their mimicry capability, polymer-lipid hybrid membranes can be used for a broad range of surface-specific applications in the field of biotechnology and nanomedicine.[103,108,150] In the field of bio-sensing, polymer-lipid hybrid membranes have been employed as taste sensors in substances,[151–154] for example by using a membrane composed of PVC and TDAB, with a lipid concentration chosen for the detection of a specific taste.[151,153,155]

3. Results and Discussion

In the first part of this chapter (3.1), we present how polymer-lipid hybrid membranes provide a favourable environment for the selective and functional attachment of a model redox protein, cyt c, with both covalent attachment and insertion. It was possible to selectively drive the insertion of cyt c into the lipid domain or the covalent conjugation onto the functionalized polymer domain of hybrid membranes. Moreover, we found that the protein accessibility and its functionality were dependent on the combination strategy: the conjugation promoted higher accessibility and supported higher peroxidase-like activity. This model system can be modulated for improving the accessibility of the biomolecules and their functionality after recombination with membranes for the development of novel active surfaces.

The SALB method has been recently used for the fabrication of lipid supported membranes. In the second part of this chapter (3.2), we applied for the first time this method on different di- and triblock copolymers. In this part of the thesis, we employed PDMS-b-PMOXA of different block ratios to create solid-supported polymer membranes to be employed for biomolecule reconstitution based on the biotin-SAV specific interaction. We chose a biotin-functionalized copolymer for preparing a solid supported polymer membrane. Two biomolecules were chosen as candidates for the membrane decoration: a DNA strand with its complementary strand and an artificial ADAse. Additionally, we quantified the catalytic activity of the ADAse after the membrane recombination. The systematic characterization of the solid supported polymer membranes obtained via SA method combined with the study of the interactions between the membranes and model biomolecules provides a useful insight on functional surfaces.

After a deep study on the characterization of lipid-polymer hybrid membranes and after we expanded the SA method for the preparation of polymer planar membranes, we combined the two concepts. The last part of this chapter (3.3) is a preliminary study concerning the formation, characterization and optimization of solid-supported hybrid membranes by SA method. Here we combined amphiphilic di-block copolymers such as PDMS-PMOXA and PEO-PG with various phospholipids commonly found in bio-membranes (e.g. DPPC, POPE, SM). The advantageous properties of hybrid materials, together with the application of the straightforward membrane deposition method is of great interest for medical and bio-engineer fields of application.

3.1. Hybrid Supported Membranes equipped with a model protein to enhance the protein activity

This chapter contains parts adapted from the paper **Stefano di Leone**, Saziye Yorulmaz Avsar, Andrea Belluati, Riccardo Wehr, Cornelia G. Palivan, and Wolfgang Meier, "Polymer- Lipid Hybrid Membranes as a Model Platform to Drive Membrane-Cytochrome c Interaction and Peroxidase-like Activity", J. Phys. Chem. B 2020, 124, 22, 4454-4465.

ABSTRACT

Controllable attachment of proteins to material surfaces is very attractive for many applications including biosensors, bioengineered scaffolds or drug screening. Especially, redox proteins have received considerable attention as a model system not only to understand the mechanism of electron transfer in biological systems, but also the development of novel biosensors. However, current research attempts suffer from denaturation of the protein after its attachment to solid substrates. Here, we present how lipid, polymer and hybrid membranes based on mixtures of lipids and copolymers on a solid support provide a more favorable environment to drive selective and functional attachment of a model redox protein, cytochrome c (cyt c). Polymer membranes provided chemical versatility to support covalent attachment of cyt c, whereas lipid membranes provided flexibility and biocompatibility to support insertion of cyt c through its hydrophobic part. Hybrid membranes combine the most promising characteristics of both lipids and polymers and allowed attachment of cyt c with both covalent attachment and insertion driven by hydrophobic interactions. We then investigated the effect of different attachment strategies on the accessibility and peroxidase-like activity of cyt c, in the presence of different membranes. The real-time combination of cyt c with the planar membranes was investigated by quartz crystal microbalance with dissipation. It was possible to selectively drive the insertion of cyt c into a specific lipid domain of hybrid membranes. In addition, protein accessibility and its functionality were dependent on the specificity of the combination strategy: covalent conjugation of cyt c to polymer and hybrid membranes promoted higher accessibility and supported higher peroxidase-like activity. Taking together, the combination of biomolecules with planar membranes can be modulated in such a way to improve the accessibility of the biomolecules and their resulting functionality for the development of efficient "active surfaces".

INTRODUCTION

Cell membranes consist of phospholipids, glycolipids, and a large variety of proteins responsible for active or passive transport and signalling.[156] One strategy to understand how biological membranes are associated with proteins, to support biological processes, is to utilize model membrane platforms. To date, naturally occurring or synthetic phospholipids and amphiphilic block copolymers have been used to create model membrane platforms[157–159] in combination with a variety of different biomolecules including proteins, peptides, and receptors. So far, synthetic membranes have been characterized in a three-dimensional assembly (e.g., liposomes, polymersomes, and giant vesicles), which has been not always straightforward because of the challenges associated with characterization of vesicular model systems. Therefore, supported membrane formation by a single component (e.g., lipids or polymers) emerged.[36,136,160–162] Deposition of the planar membrane on the solid support presents many advantages compared to vesicular membranes:[163] (i) a higher amenability for characterization by surface sensitive analytical tools (e.g., atomic force microscopy(AFM), quartz crystal microbalance with dissipation (QCM-D), and surface plasmon resonance), and thus, the investigation of protein-membrane interaction kinetics in real-time, in situ, and label-free format[164] and (ii) the possibility to pattern the surface to monitor membrane phase separation[103] and selective molecular binding.[165]

In addition to single component membrane platforms, phospholipids and block copolymers have been mixed to form hybrid membranes.[103,136,160] Within hybrid membranes, amphiphilic block copolymers provide improved mechanical and structural stability while phospholipids can provide a better environment for integration of biomolecules.[93,103,166,167] Depending on how lipid and polymer chains are distributed within hybrid membranes, an enhanced control of membrane functionalization with different biomolecules (e.g., proteins) can be achieved.[18,86,110,113] In fact, hybrid membranes can undergo phase domain separation when the fluid-phase polymer and gel-phase lipids are used to prepare them and this significantly affects protein–membrane interaction.[149] Additionally, phase domains in hybrid membranes have been created by changing the molar ratio of each component and molecular parameters of lipids and block copolymers, such as phase transition temperature and composition.[87,103,106,168] The control over the membrane–protein combination is essential for the development of "active surfaces" with desired properties. Although most of the hybrid membrane studies have been focused on the mixing of lipids and block copolymers in vesicles, only a few studies have explored the properties of the hybrid membranes on solid supports and their combinations with proteins (e.g., P-glycoprotein) and peptides (e.g. gramicidin A and valynomicyn).[55,149,169,170]

Planar membranes on the solid support are obtained either by substrate-mediated vesicle fusion[78,171] or Langmuir Blodgett transfer method,[86,171] while their characterization is achieved by a combination of surface methods including QCM-D, AFM, and ellipsometry.[103] Because of the capability of lipids and copolymers to re-arrange the membrane architecture and generate domains, hybrid membranes represent ideal candidates for understanding protein–membrane interactions.[172] These domains facilitate the interaction with proteins, in a way similar to the so-called "lipid-rafts" found in cell membranes.[167,172] For example, when the DPPC lipids (phase transition temperature of 41 °C) were mixed with the poly(dimethyl siloxane)90-block-poly(2-methyl-2-oxazoline)10 (PMOXA-PDMS) block copolymer at room temperature, proteins were selectively inserted only into the polymer domains because the lipid domains were in the gel phase, and they did not support insertion of the proteins.[103] The advantage of combining proteins with synthetic planar membranes is based on preserving protein activity, which can be prohibited when a protein is directly attached to a bare substrate surface, such as gold, silica, or glass.[173–177] Attachment of proteins with different solid substrates is mainly based on noncovalent interactions, such as ionic or hydrogen bonds and often induces protein denaturation. For example, it is well known that functional properties of cytochrome c (cyt c) were hampered because it adsorbed strongly on electrodes (e.g., Pt, Hg, Au, and Ag) because this adsorption caused large conformational changes and denaturation.[178–180] Moreover, direct electron transfer between cyt c and unmodified electrode surface is slow due to undesired contact between the prosthetic group and the electrode.[181] So far, in order to provide a better environment for cyt c to function, different electrodes which are mainly based on nanomaterials (e.g., carbon nanotubes, graphene, and nanoparticles) have been used.[182–187] Nevertheless, these attempts might not be sufficient to preserve the whole cyt c activity. By forming planar membranes on solid support as a mean of electrode surface modification, (i) a natural biocompatible means of cyt c–substrate interactions and (ii) effective, highly dynamic platform to host biomolecules can be achieved.[188,189] Such a system improves the protein–membrane–substrate communication for the development of highly sensitive and efficient biosensors.

Here, we combine different solid-supported membranes based on lipids, copolymers, and mixtures of lipids and copolymers with cyt c, a model protein in order to understand which molecular factors play a crucial role in its accessibility and functionality. We attached cyt c using two different approaches, one based on insertion mediated by hydrophobic interactions and a second one by covalent conjugation of cyt c with specific functional groups of the copolymer. More specifically, cyt c is a critical signaling molecule, leading to activation of

enzymes in the intrinsic pathway of apoptosis upon permeabilization of the upper layer of the mitochondrial membrane.[190–193] It has a relatively small size of 12 kDa with a globular shape, and it is known that its binding to the membranes can be driven by either ionic interactions or small hydrophobic domains which drives the spontaneous insertion.[193,194] Moreover, the presence of amine groups of two specific external lysines (Lys72 and Lys73) supports cyt c to be covalently conjugated to the carboxylic groups of the copolymer in the membranes. To date, the combination of cyt c with the biologic membranes mainly takes places through electrostatic interaction with negatively charged surfaces because of two residual lysines, partial insertion via hydrophobic interaction, or complete incorporation into the membrane.[194,195] Both electrostatic and hydrophobic interactions played a role on cyt c combination with membranes based on anionic lipids.[196–198] The contribution of the hydrophobic interaction on cyt c insertion has been studied using zwitterionic lipid membranes, and the results indicated that cyt c induced the disruption of the membrane.[199] To preserve membrane integrity, another approach to combine cyt c with membranes has to be taken into account. In this respect, the covalent conjugation of cyt c to carboxylated nanoparticles provides strong binding, leading to an improved stability for bio-sensing applications.[200] However, up to now, there is no report regarding the effect of combination strategies of cyt c with planar membranes to distinguish its accessibility and the resulting peroxidase-like activity at different membranes.

Toward this goal, we first explored the formation of lipid, polymer, and hybrid monolayers at the air–water interface to determine the surface pressure at which densely packed films were formed, before transferring them onto silica wafers with the Langmuir–Blodgett method. Then, we characterized integrity, topography, and morphology of the resulting supported membranes before and after the combination with cyt c by AFM and confocal laser scanning microscopy (CLSM), respectively. QCM-D was used to quantify the amount of cyt c combined with each type of planar membrane and how it affected the viscoelastic properties, thus providing insights into the accessibility of cyt c. After combination with different membranes, we assessed indirectly the peroxidase-like activity of cyt c by an Amplex red (AR)-based fluorimetric assay. These different approaches to combine a protein with planar membranes together with the differences in the composition, morphology, and properties of these planar membranes serve to indicate which are the essential factors for equipping different membranes with proteins in order to produce efficient “active surfaces”.

3.1.1. Polymer-Lipid Hybrid Membranes Preparation

We selected the functionalized diblock $PDMS_{90}$-b-$PMOXA_{10}$-COOH as copolymer and DPPC as phospholipid and we acquired the Langmuir isotherm of the single components and their mixture (weight ratio 50:50 wt. %) as a function of the mean molecular area occupied by a molecule to compare the differences between the monolayers at air-water interface (Figure 3.1-1). Above the surface pressure of 15 mN/m, all isotherms showed a transition from liquid expanded to liquid condensed phase, irrespective of the composition. Isotherm of PDMS-b-PMOXA-COOH copolymer showed a lift-off around 1750 Å, a larger plateau and a breaking point higher than 40 mN/m, indicating highly flexible monolayers at the air-water interface, already observed for other PMOXA-PDMS copolymers[183]. Isotherm of the DPPC lipid exhibited a lift-off at circa 100 Å with a steep slope and a breaking point at 60 mN/m. Isotherm of the mixture of the DPPC lipid and PDMS-b-PMOXA-COOH copolymer displayed an intermediate profile compared to the isotherms obtained from single components, with a lift-off lower than 1000 Å and a breaking point at 49 mN/m. During the recording of the Langmuir isotherms at air-water interface, the changes in morphology of the lipid, copolymer and hybrid monolayers were real-time monitored by BAM (Figure 3.1-1 B) for copolymers (a-c), lipids (d-f) and copolymer-lipid mixtures (g-i) at three representative surface pressure (0, 9 and 35 mN/m, respectively). Initially, when no surface pressure was applied, no film was observed. At the surface pressure of 15 mN/m, the copolymers formed micelles at the air-water interface and then they changed their micellar architecture to a homogenous copolymer monolayer at the surface pressure of 35 mN/m (b-c), in agreement to previous reports for block copolymersIn the case of lipids, flower like assemblies with sizes of approximately 10 µm were observed at a surface pressure of 9 mN/m, which transformed to planar lipid monolayers at air water interface for a surface pressure of 35 mN/m (e-f). The lipid-copolymer mixture did not show any assemblies at the intermediate surface pressure of 9 mN/m, and micron sized domains were observed at the surface pressure of 35 mN/m due to separation of lipids from the copolymers (h-i). It is important to mention that polymer-lipid phase separation does not completely occur, and each domain is not pure. The lipid domains were found to be embedded into the continuous polymer rich phase, as already observed elsewhere.[103]

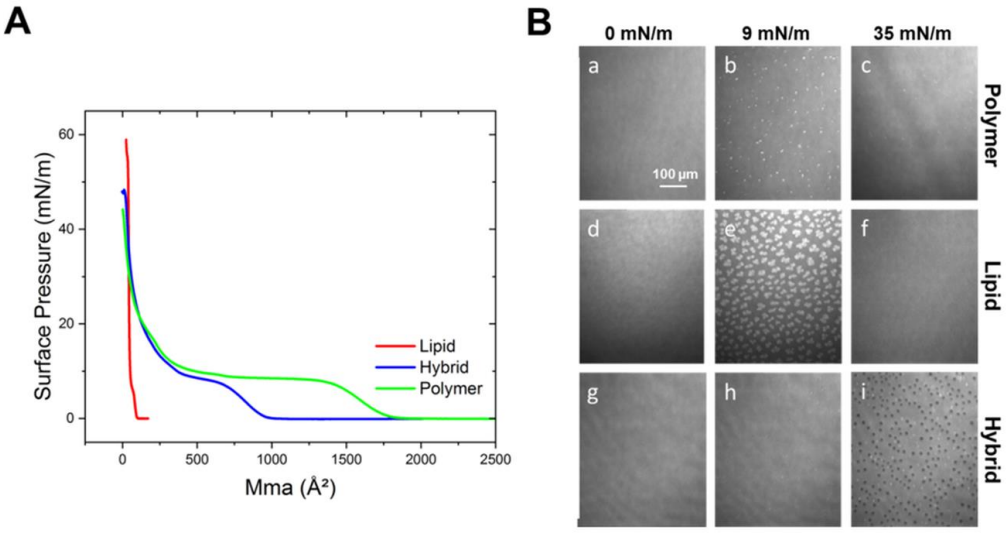

Figure 3.1-1. Langmuir isotherms of lipid, copolymer and hybrid (50:50 wt.%) (A) and BAM images of lipid, polymer and hybrid (B) at surface pressure of 0, 9 and 35 mN/m.

3.1.2. Formation of different model membranes on solid support

Monolayers of polymer, lipid and hybrid mixture were transferred to solid support using LB method, to create supported polymer, lipid and hybrid bilayer membranes, respectively. First, the monolayers at the air-water interface were deposited to the solid support through an upstroke at a constant surface pressure of 35 mN/m,[9,18,55,162] resulting in solid-supported monolayers. AFM images showed that the solid-supported polymer monolayer was not homogenous and self-assembled into micellar structures with sizes of 20 nm on solid support, which is in agreement with literature reports.[190,201] In contrast, the hybrid monolayer was uniform on solid support, with lipid and polymer domains, which had a height difference of 6-8 nm (Figure 3.1-2).

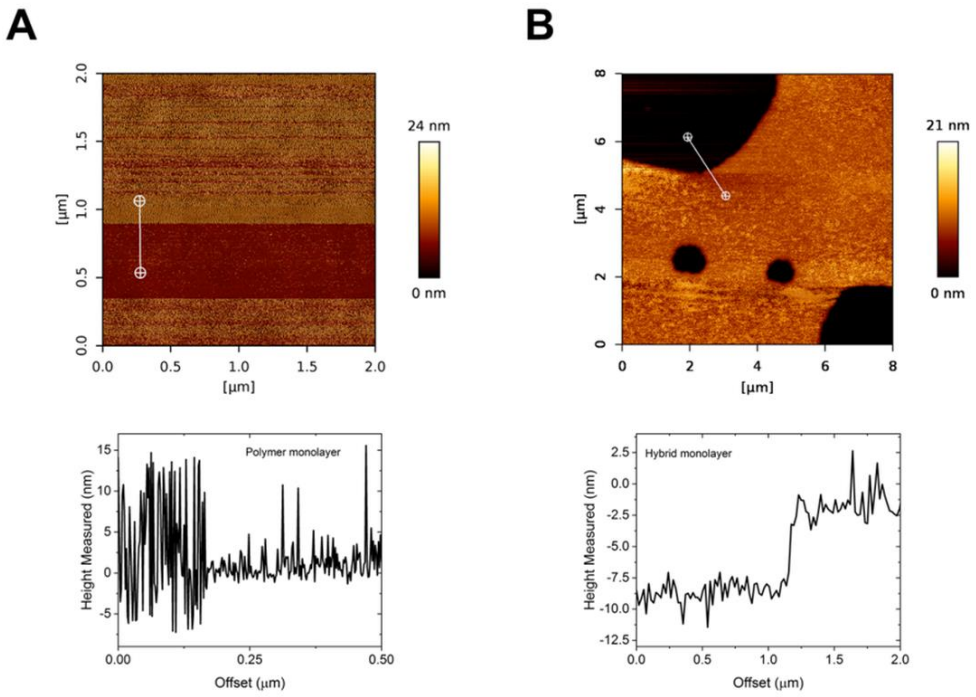

Figure 3.1-2. AFM height profile of polymer monolayer showing micelles 20 nm high (A) and height profile of hybrid monolayer (B).

This difference was caused by the molecular mismatch between lipids and block copolymers. The supported bilayer membranes were prepared by LB transferring, on a silica support, of two consecutive monolayers, one deposited via an upstroke and a following via a down-stroke.[100] The surface morphology and topography of the resulting bilayer membranes were analyzed by AFM height (Figure 3.1-3) and phase (Figure 3.1-4) imaging. Phase profile was necessary to observe the domain separation, whereas the height profile showed the mismatch between the polymer and the lipid phase domains in the hybrid membranes. Surface topography of supported polymer membrane was planar and homogenous, indicating that the deposition of a second layer induced the formation of a stable planar architecture.

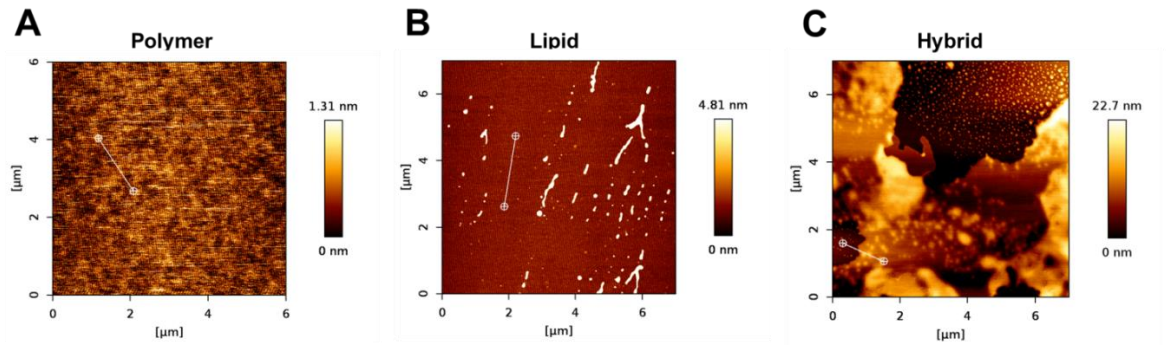

Figure 3.1-3. AFM characterization of solid supported bilayers. Height profiles of polymer (A), lipid (B) and hybrid (C).

After drying, there were no micellar structures on the supported polymer membranes, in contrast to the polymer monolayer. As confirmed by AFM profiles, the supported DPPC lipid membranes contained several defects (Figure 3.1-4 B), due to the possible overturning mechanism that occurred during the depositionMoreover, supported hybrid membranes showed clear separation of lipid and polymer domains (Figure 3.1-4 C).

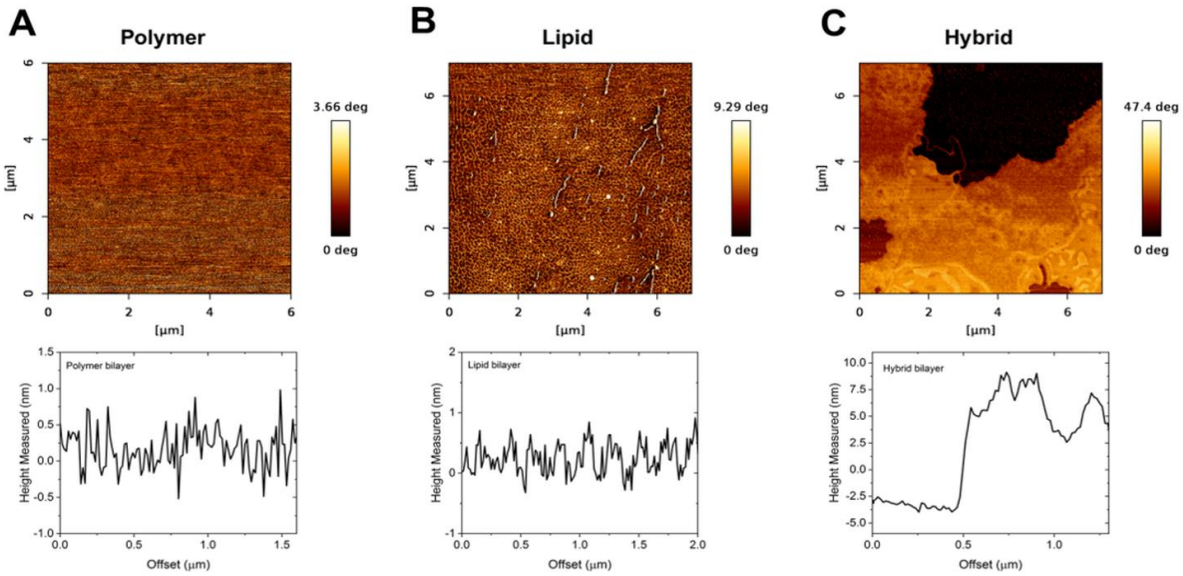

Figure 3.1-4. AFM characterization of solid-supported bilayers. Phase profile (up) and cross section (down) of polymer (A), lipid (B) and hybrid (C) membranes.

The height difference between lipid and polymer domains in hybrid membrane was approximately of 11 ± 1 nm. The AFM phase image shows dark that represent the lipid domains and bright spots that represent the polymer domains. Domain enrichment was also observed: small polymer clusters were present in lipid-rich phase while small lipid clusters were present in polymer-rich domains. As the size of the lipid or polymer domains are tens of micron, there is no limit for size of proteins, which are either inserted or conjugated to the membranes as long as they have specific characteristics (e.g. surface charge or hydrophobic part for insertion, functional group for conjugation). Therefore, any hydrophilic peripheral proteins can be inserted or conjugated to hybrid membranes after necessary adjustments of the membrane composition. For example, ECM proteins (e.g. collagen with molecular weight of approximately 300 kDa or fibronectin with molecular weight of approximately 220 kDa) have been attached to the polymer domains through covalent conjugation and their effect on cell adhesion, proliferation and function have been investigated for development of cell-based diagnostics, tissue engineering, medical implants and biosensors

3.1.3. Investigation of the supported membrane quality

We then investigated the presence of lipid-rich or polymer-rich domains in hybrid bilayers, by CLSM (Figure 3.1-5). 1,2-dipalmitoyl-sn-glycero-3-phosphoethanolamine-N-(lissamine rhodamine B sulfonyl) lipid was added (1 wt. %) into the solution of the hybrid mixture before deposition onto silica support. The Rhodamine B lipid diffused only into the polymer-rich domains, as indicated by red colour, because they are both in a fluid phase.

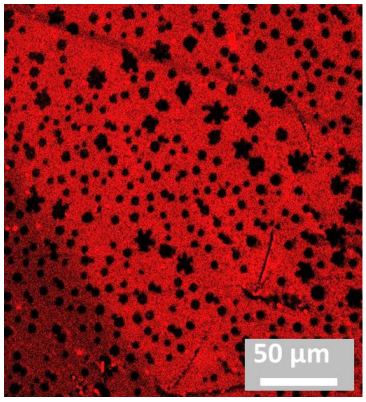

Figure 3.1-5. CLSM image of hybrid bilayer rinsed with PB buffer.

The blend of a small fraction of lipids with polymers into hybrid bilayers was due to similarity of the phases of the labelled lipid with the polymer. On the contrary, dark domains are specific for DPPC lipids, and are similar in shape and size when compared to BAM images.[100,104] To further explore the uniformity of supported model membranes, we evaluated the adsorption of BSA, a globular protein which has been previously used to determine membrane surface coverage[95,100,104,201] BSA adsorption was appreciable on silicon dioxide compared to the planar bilayer membranes made of DPPC lipids or PMOXA-PDMS copolymers.[95] In principle, BSA adsorption is expected to be negligible on the defect-free membranes deposited on silicon dioxide, whereas it increases with increasing amount of defects found in a membrane, e.g. the availability of bare silicon oxide for BSA. We quantified the BSA adsorption onto polymer, lipid and hybrid membranes by QCM-D and compared them with bare silicon dioxide support (Figure 3.1-6). A solution of BSA (C = 500 µg mL-1) was injected onto bare silica or supported membranes after baselines were established in PB. BSA adsorption on silicon dioxide led to a frequency shift of -24 ± 1 Hz whereas on supported polymer membrane of −2 ± 1 Hz which resulted in an appreciable reduction in amount of BSA adsorbed. We calculated a membrane surface coverage higher than 92 ± 4 %, indicating that the polymer membrane did not contain major defects. By contrast, the frequency shift was −6 ± 2 Hz for the BSA adsorption on supported lipid membranes, leading to a reduction of membrane coverage to 75 ± 3 %. Thus, there were more defects in supported lipid membranes compared to hybrid or polymer counterparts. These results were in agreement with AFM data. In the case of BSA adsorption onto supported hybrid membranes, the frequency shift to −4 ± 2 Hz, was associated with a membrane surface coverage of 83 ± 4 %. The presence of defects on the membranes on silica was also compensated by covering the defects with BSA adsorption, which is expected to prevent nonspecific interactions of cyt c with bare silicon oxide.

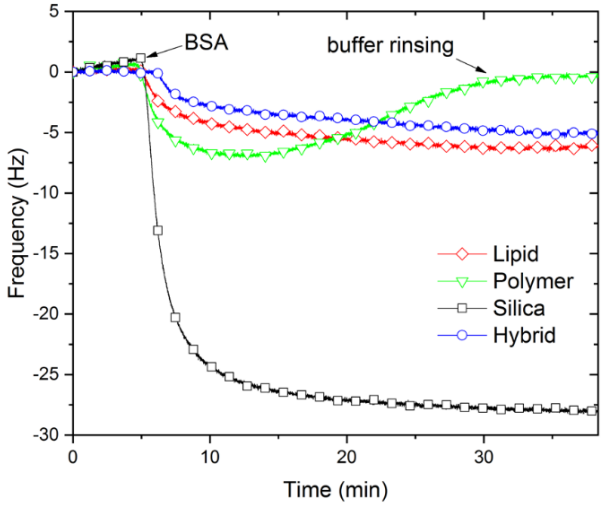

Figure 3.1-6. QCM-D of BSA adsorption comparison onto different membranes in order to evaluate major defects. Silicon oxide was used as control. BSA solution in PB has a concentration of 500 μg/ml.

3.1.4. Combination of cytochrome c with supported model membranes

After depositing the membranes, we monitored the real-time combination of cyt c with the lipid, polymer and hybrid membranes. We employed two different strategies: i) cyt c insertion into the membrane through hydrophobic interactions, and ii) covalent conjugation (Figure 3.1-7) of cyt c to the membranes by binding the accessible lysine of cyt c to COOH functionalized polymer through EDS/sNHS coupling chemistry.[194,202,203] The conjugation provides stability to cyt c, preventing the loss of its heme or denaturation. Because cyt c is normally found in the inner cell membranes, the covalent bond provides the needed stability for cyt c when located on the outer membrane. [203,204]

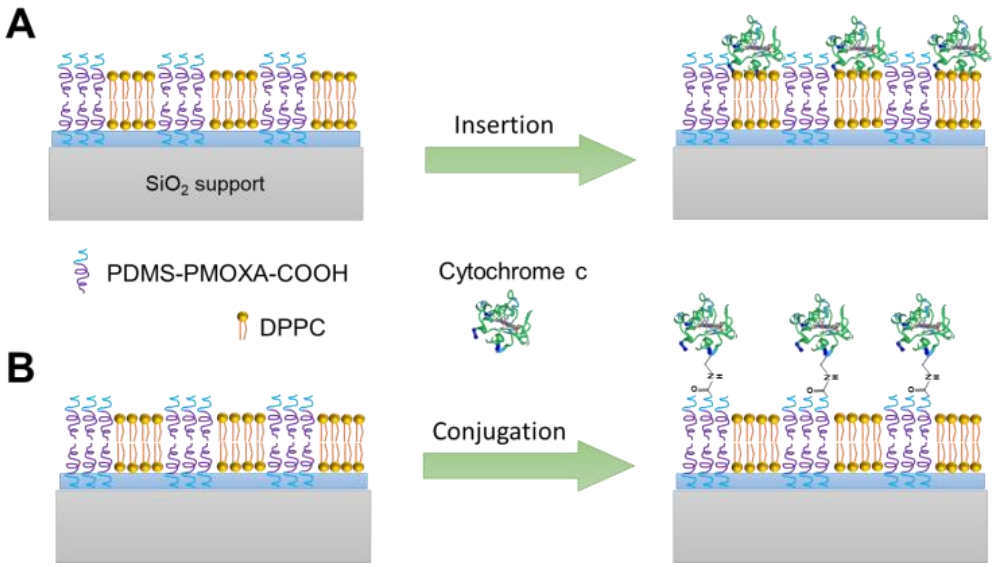

Figure 3.1-7. Schematic representation of hybrid supported bilayer and their combination with model protein cytochrome c through (A) insertion and (B) covalent conjugation by EDC/sNHS coupling.

We compared the insertion of cyt c into solid supported membranes by QCM-D. The QCM-D measurement baseline signals were stabilized in phosphate buffer. After 5 min of baseline stabilization, a solution of 500 µg/ml of cyt c was injected. First, we monitored cyt c combination onto silica surface (see Figure 7-2), resulting in a frequency shift of -16.4 ± 5.8 Hz and a cyt c mass of 290 ± 103 ng/cm^2. The combination here consisted in an irreversible and not selective process, since it was driven by either attractive electrostatic interaction between positively charged cyt c and negatively charged silica and, which could result in protein denaturation. Moreover, cyt c insertion into supported polymer and hybrid membranes led to a similar frequency shift of -8.0 ± 0.9 Hz and -7.5± 2.1 Hz, respectively, while it led to small frequency shift of -2.4± 2.3 Hz for the supported lipid membranes. The mass of the inserted cyt c was estimated by using the Sauerbrey equation (Table 3.1-1). The mass of inserted cyt c on the supported polymer bilayer was 142 ± 16 ng/cm^2, 133 ± 38 ng/cm^2 for hybrid bilayer and only 42 ± 40 ng/cm^2 for lipid bilayer. The frequency shifts obtained from cyt c adsorption in the presence of polymer-, lipid- and hybrid-based layers were lower than the one obtained from bare silica substrate because PMOXA-PDMS block copolymer has antifouling characteristics and cyt c combination was driven by specific interactions.[205]

To gain more insight into the viscoelastic properties of the combined cyt c on the different supported membranes, we used the correlation between dissipation and frequency (Figure 3.1-4), which can be linked to accessibility of the protein on the membrane surface.[206] The dissipation value for the lipid membrane was around $0.1*10^{-6}$ and lower than the value determined for the polymer and hybrid membranes ($0.7*10^{-6}$ and $0.5*10^{-6}$, respectively). The values for dissipation also indicate the difference in the overall flexibility of the different membranes: polymer and hybrid membranes present a higher degree of mobility due to their molecular structure and the resulting membrane packing, compared to lipid membrane.[103] This is in agreement with the fact that the lipid is in the gel phase. Secondly, the cyt c was covalently conjugated to supported polymer bilayer and hybrid bilayer, based on the formation of a peptidic bond between the ending functional group of the functionalized polymer and the outer lysine of the cyt c (see Figure 7-3).[194]

The conjugation reaction was performed before the addition of cyt c to the bilayers. The carboxylic groups of the polymers were activated by injecting EDC/sNHS solution (C = 10 mg/ml) (see Table 7-1) and then rinsed with buffer, before the injection of cyt c solution (C = 500 µg/ml). Nevertheless, during the conjugation reaction a small amount of cyt c may have also inserted into the membrane. The conjugation of cyt c to the supported polymer bilayer led to a frequency shift of -7.4 ± 0.8 resulting in a mass of 132 ± 18 ng/cm^2, while the conjugation of cyt c to the supported hybrid bilayer induced a frequency shift of -2.5 ± 0.7 Hz, resulting in a mass of 44 ± 13 ng/cm^2 (see Table 7-2). The lower amount of cyt c conjugated to the hybrid membrane is mainly due to the lower number of carboxylic groups available compared to the polymer membrane, according to the molar ratio of 50% in the hybrid. No conjugation was performed for the lipid membrane, due to the absence of the carboxylic functionalization. When we compared the two combination strategies of cyt c for the supported hybrid bilayers, the frequency shifts for the insertion method was higher than for the conjugation , while the dissipation shifts revealed to be higher for the conjugation, with the highest value of $1.0*10^{-6}$ (Figure 3.1-8). The differences in the frequency/dissipation ratio suggest that cyt c has a different conformation when it is combined with the hybrid bilayers by using different combination strategies. The explanation relies on the higher degree of freedom cyt c has when it is conjugated to the membrane, standing away from it, instead of partially penetrating it with its hydrophobic part. Moreover, cyt c preferred a combination with the hybrid membrane through insertion rather than conjugation. However, neutral DPPC lipid cannot establish a strong attractive electrostatic interaction with the positive-charged cyt c. Instead, the presence

of anionic lipids in the hybrid membrane may increase the insertion of the protein.[190,207–210] The isoelectric point (pI) of cyt c is in the range of 10.0-10.5 and in condition of neutrality it presents a positive charge,[194] so by increasing the pH over this value it would be possible to inhibit the spontaneous insertion due to repulsive interactions between the membrane and the protein.[194] We kept here the system at neutral pH condition.

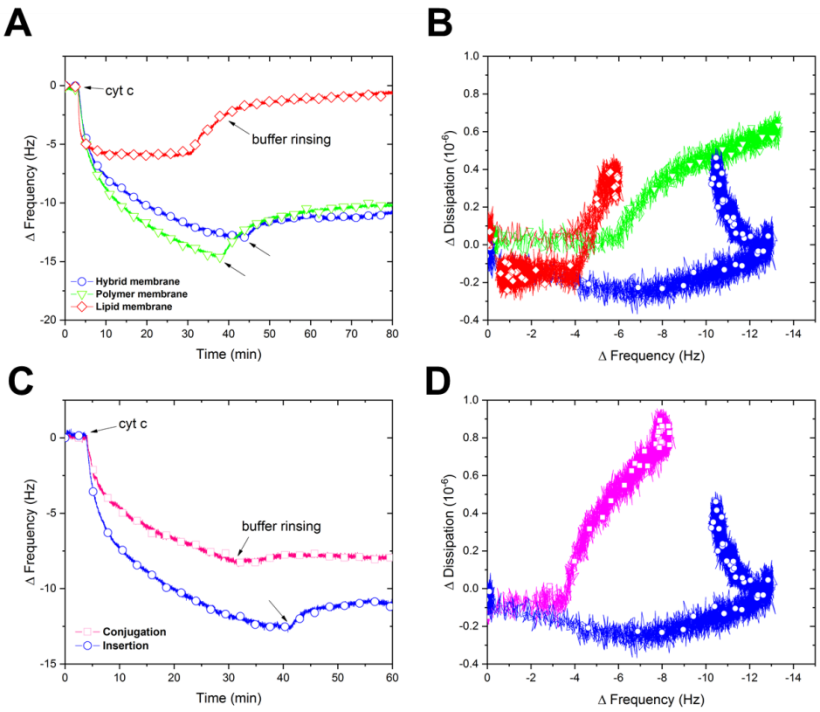

Figure 3.1-8. QCM-D plots of protein combination with supported membranes: protein insertion (A); comparison of protein combination methods with hybrid membrane (C) and their corresponding ΔD vs Δf plots (B and D). Solutions used are cytochrome c in PB (500 μg/ml) and pure PB for rinsing steps.

3.1.5. Membrane stability after the protein recombination

After insertion of cyt c within the different membranes, we also monitored the changes in membrane integrity by analysing AFM height and phase profiles. Because of the small size of cyt c (approximately 3 nm) compared to the domain sizes, we assume that each domain can accommodate more than one cyt c. After the protein insertion, we observed that, in general, the protein aggregates in clusters (white spots) of different sizes and average height of 5 ± 2 nm. No modification of the polymer membrane architecture was observed after cyt c insertion: the

synthetic membranes preserved their planarity and homogeneity, probably due to their robustness (see Figure 3.1-9).

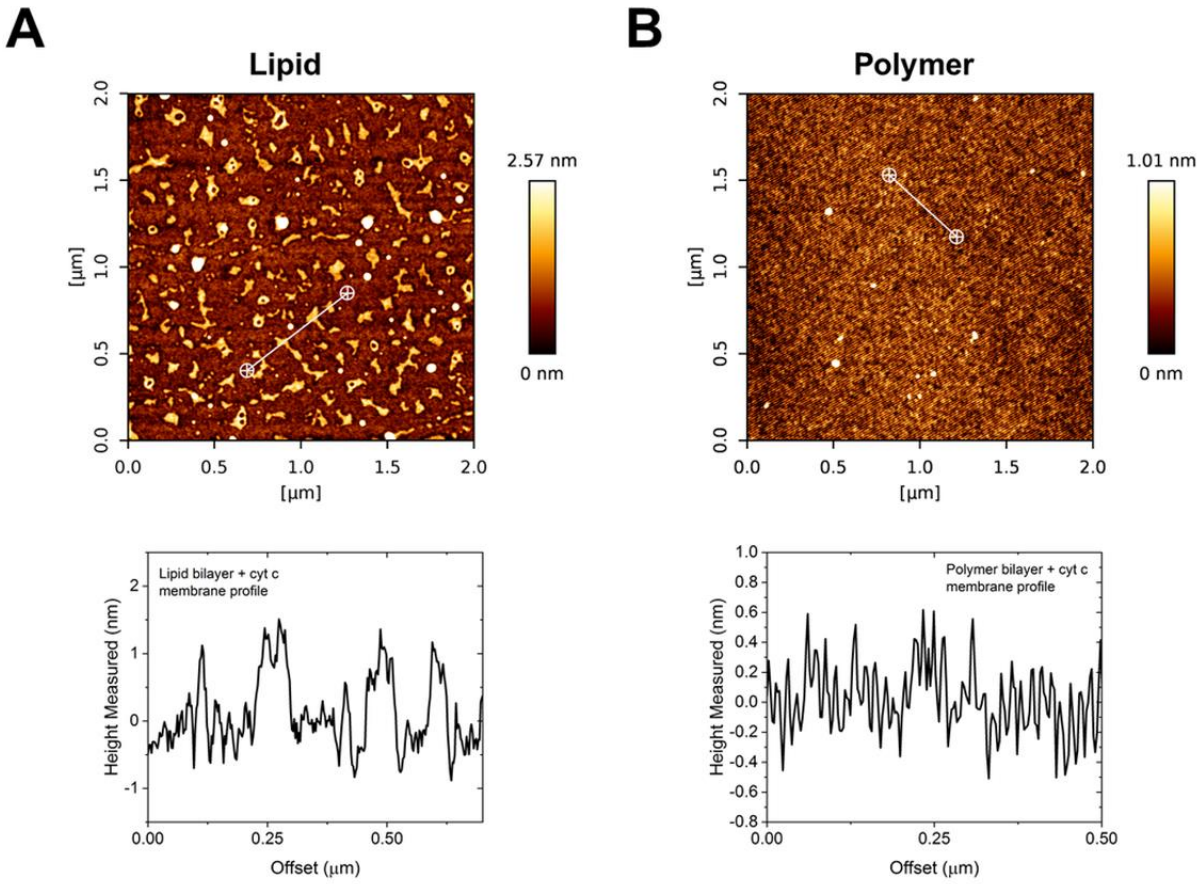

Figure 3.1-9. AFM height profile of different membranes after protein combination: lipid bilayer (A), showing membrane removal; polymer bilayers (B).

The low cyt c height (2 ± 1 nm) found in polymer membrane, might be due to a deeper penetration of the protein into the bilayer, as compared to lipid and hybrid membranes (Figure 3.1-10). As the lipid bilayer was removed from the silica support, similarly to other reports,[190,199] it resulted in a discontinuous membrane with cyt c clusters mainly located on the silica dark background. Desorption of lipid bilayers from the silica after addition of cyt c was also confirmed by QCM-D (see before): the decrease in mass observed before the buffer-rinsing step indicated the removal of the membrane from the support. Interestingly, the interaction of the cyt c with the hybrid bilayer indicated no bilayer removal, as expected for the lipid phase, rather a bilayer reorganization took place, where the lipids self-assembled in the polymer matrix and constituted rafts accommodating the protein (Figure 3.1-10 C and 3.1-

11 in detail). The copolymer preserved the bilayer integrity due to its mechanical resistance while the lipid phase allowed the cyt c to insert due to its fluidity.[106,211] Therefore, the hybrid bilayer was suitable for achieving a selective combination of the protein with a specific bilayer domain: the lipid domain allowed the insertion while the polymer one served for the conjugation.

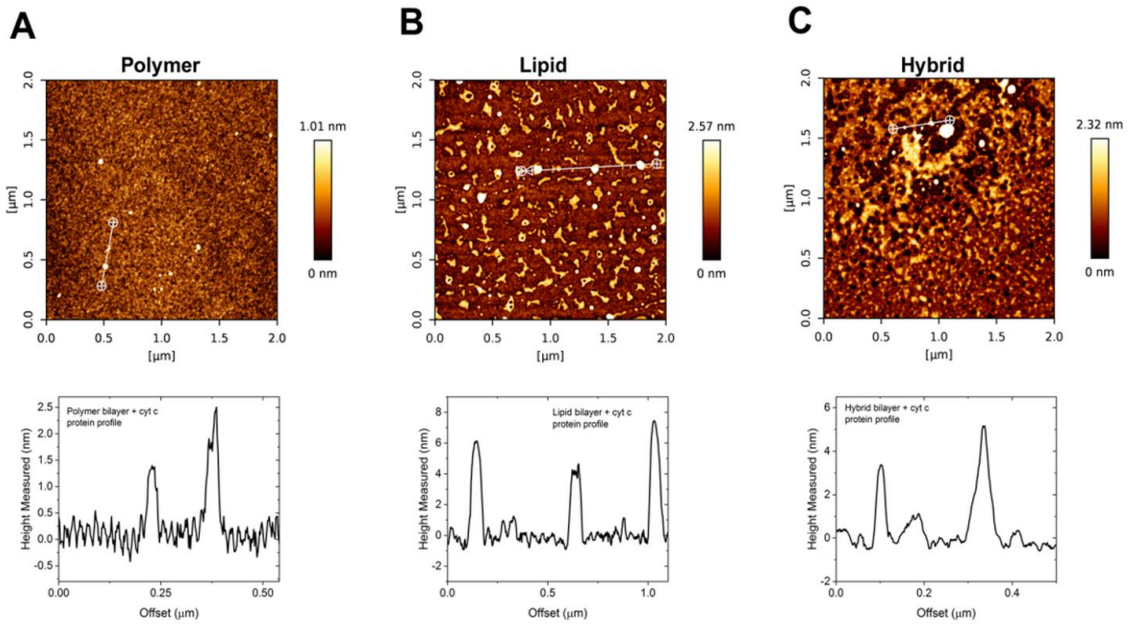

Figure 3.1-10. AFM height profile of different membranes after protein insertion: polymer (A), lipid (B) and hybrid bilayers (C).

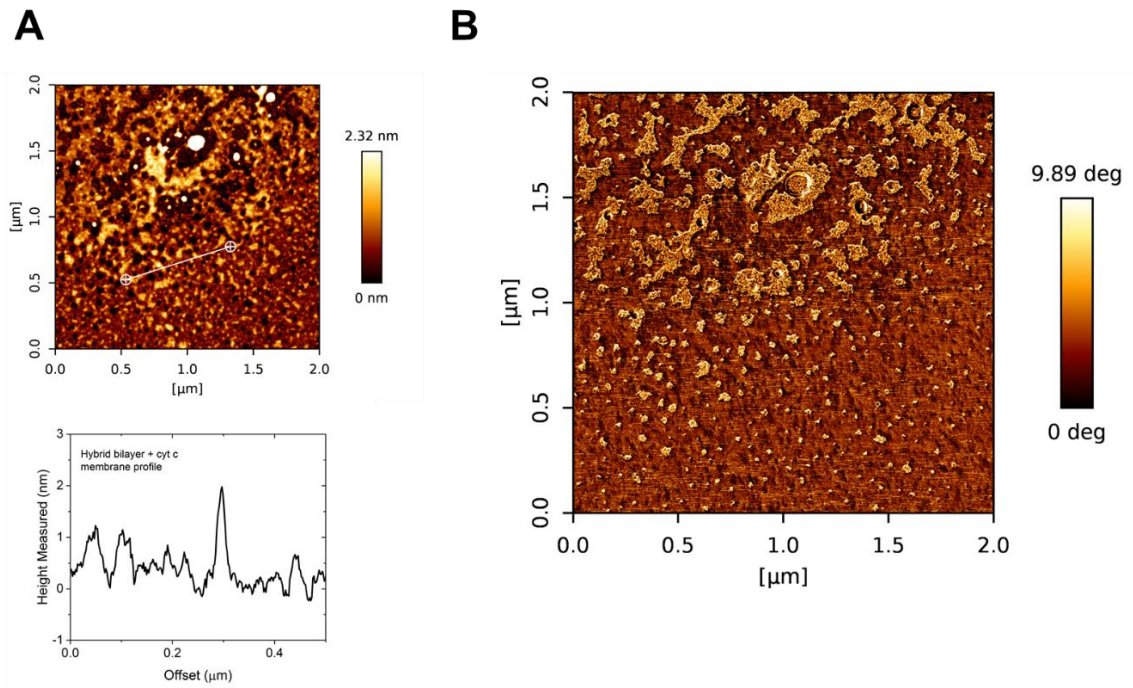

Figure 3.1-11. AFM images of hybrid membrane after protein combination: height (A) and phase profile (B) of hybrid membrane. Lipid rafts are clearly visible in the phase image.

3.1.6. Assessment of peroxidase-like activity of cyt c on supported hybrid membranes

Cyt c plays an important role in the elimination of hydrogen peroxide (H_2O_2) from mitochondria and respiratory chain, leading to exhibited peroxidise-like activity.[212] The activity of cyt c is based on the reaction of its iron (III) porphyrin, which, in the presence of a cofactor, turns to an oxo-iron species that rapidly oxidize different substrates.[213] We evaluated the peroxidase-like activity of cyt c when combined with supported polymer and hybrid bilayers either by two different combination approaches: i) insertion or ii) conjugation. We did not evaluated solid-supported lipid membranes due to their instability after insertion of cyt c. We assessed indirectly the cyt c activity in the presence of the cofactor H_2O_2, with an AR based fluorimetric assay. This colorless, non-fluorescent substrate can be oxidized by the $OH^{\cdot}$ radicals, produced by cyt c, to the colored and fluorescent resorufin. A first indication of a successful reaction was the color change of the solution (see Figure 7-4). Time-dependent kinetics of resorufin fluorescence intensity (in a.u.) induced by the addition of H_2O_2 to cyt c serves to evaluate the peroxidase-like activity of cyt c after its combination with supported polymer and hybrid membranes (Figure 3.1-12). In order to eliminate the effects of AR auto-oxidation from the spontaneous dissociation of H_2O_2 and avoid overestimating the peroxidase-

like activity of cyt c, we used the AR auto-oxidation for background correction. We did not expect a degradation of hybrid membranes by the presence of H_2O_2, as experiments in similar conditions have been already tested for PDMS-b-PMOXA polymers, resulting that no significant membrane disturbance by H_2O_2 were observed.[214,215] Moreover, a negligible oxidation of AR by H_2O_2 was observed by the fluorometric measurements and AR here served as a scavenger and prevented a possible degradation of lipid domains. The activity of cyt c when combined with polymer or hybrid membranes, was always preserved in different degrees as compared with the free protein (Figure 3.1-12 A), regardless from the combination method adopted. As expected, cyt c has a lower activity, which can be explained by two factors: i) a reduced conformational freedom of cyt c due to its interaction with the membrane, and ii) the fact that the enzyme only covers a bidimensional space, to which the substrates must diffuse, instead of occupying the entire volume, underlying that diffusion is a fundamental parameter.[215] Besides, the presence of molecules nearby the bilayer interface, might cause further oxidation of the produced resorufin, before it diffuses back into the bulk of the solution, to non-fluorescent dihydroresazurin,[216,217] inducing a drop in the fluorescence signal detected in the initial non-linear kinetics. When the cyt c was covalently bound to supported polymer or hybrid membranes, a higher peroxidase-like activity was determined, compared to cyt c inserted into the membranes. This is due to a higher accessibility of the protein for the substrates when it is conjugated. When cyt c is inserted, a greater density of cyt c on the membrane than the previous case (per QCM-D measurements) does not translate into higher activity, likely because such technique does not ensure an easy accessibility of the enzyme's active site, which can end up buried towards the membrane, whereas the anchoring of cyt c prevents it from inserting with a wrong orientation.[218] Moreover, QCM-D overestimates the density of cyt c on the membranes since bound water was also taken into account when calculating the protein density. Therefore, when the bound water is subtracted, actual density of cyt c on the membranes might be smaller and directly correlated with activity. In order to obtain a rough estimation of the average activity of the protein, inserted and conjugated into polymer and hybrid membranes, the intensity of fluorescence after 10 minutes was normalized by the number of cyt c molecules. It was found that cyt c inserted into the polymer membrane exhibits a low activity, with a fluorescence intensity of 30 a.u. The value slightly increased for the cyt c inserted into the hybrid membrane (50 a.u.). A high activity was instead found for the cyt c conjugated to the hybrid membrane, with the highest value of circa 300 a.u.. Remarkably, in both cases the activity was increased if the protein was associated to a hybrid membrane, rather than the purely polymeric one, in this case the presence of lipid rafts might play an

important role, increasing the flexibility of the protein and the mobility within the membrane and, consequently, improving its accessibility. To study the long-term activity of our hybrid membranes, we followed the enzymatic oxidation of AR for 12 h, for inserted and conjugated cyt c (Figure 3.1-12 B). Even though the intensity profile is similar within the first 200 minutes, afterwards the activity of the conjugated cyt c drifts to higher values than the inserted cyt c, confirming the sustained and long-lasting activity of the protein with a proper accessibility. Further studies will evaluate in more details cyt c after insertion or conjugation with the hybrid membrane.

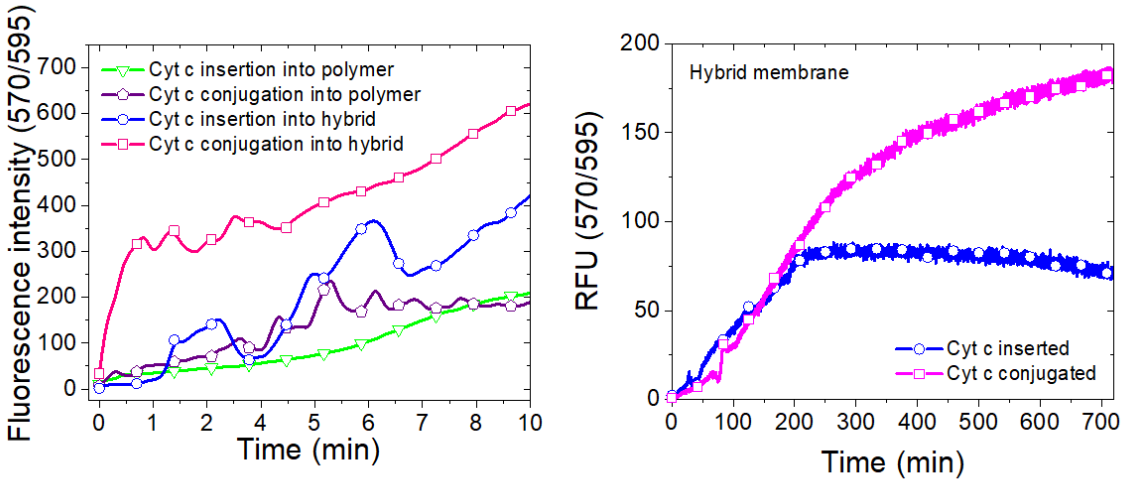

Figure 3.1-12. Qualitative comparison of protein activity by fluorimetric assay after the combination with different membranes for 10 minutes (A), and with hybrid membrane through different methods for 12 hours (B).

3.2. Expanding the Potential of Solvent-Assisted Membrane Preparation to Create Bio-Interfaces From Amphiphilic Block Copolymers

This chapter contains parts adapted from the paper Stefano di Leone, Jaicy Vallapurackal, Saziye Yorulmaz Avsar, Myrto Kyropolou, Thomas R. Ward, Cornelia G. Palivan, Wolfgang Meier, "Expanding the Potential of Solvent-Assisted Method to Create Bio-Interfaces From Amphiphilic Block Copolymers", Biomacromolecules 2021.

ABSTRACT

Artificial membranes, as materials with biomimetic properties, can be applied in various fields, such as drug screening or bio-sensing. The solvent-assisted method (SA) represents a straightforward method to prepare lipid solid-supported membranes. It overcomes the main limitations of established membrane preparation methods, such as Langmuir-Blodgett (LB) or vesicle fusion. However, it has not yet been applied to create artificial membranes based on amphiphilic block-copolymers, despite their enhanced mechanical stability compared to lipid-based membranes and bio-compatible properties. Here, we applied the SA method on different amphiphilic di- and triblock poly(dimethylsiloxane)-block-poly(2-methyl-2-oxazoline) (PDMS-b-PMOXA) copolymers and optimized the conditions to prepare artificial membranes on a solid support. The real-time membrane formation, the morphology and the mechanical properties have been evaluated by a combination of atomic force microscopy and quartz crystal microbalance. Then selected biomolecules including complementary DNA strands and an artificial deallylase metalloenzyme (ADAse), were incorporated to these membranes relying on the biotin-streptavidin technology. DNA anchoring onto membranes is of great interest for applications such as drug delivery, development of biosensors and assembly of materials. In this specific case, the anchoring of DNA strands served to establish the capability of these synthetic membranes to interact with biomolecules by preserving their correct conformation. The catalytic activity of the ADAse following its membrane anchoring induced the functionality of the biomimetic platform. Polymer membranes on solid support as prepared by the SA method open new opportunities for the creation of artificial membranes with tailored biomimetic properties and functionality.

INTRODUCTION

Amphiphilic block copolymers and phospholipids that self-assemble into membranes in aqueous conditions are utilized as models for natural biological membranes.[86,219] Those membranes can synthetically reproduce natural processes and reveal details about the interactions between a membrane and biomolecules (e.g. enzymes,[215,220] proteins,[163,221] pore-forming peptides[163]). Moreover, they can also be applied as fundamental component of biosensors,[222] water purification systems,[223] bio-screening and surface coating.[224–226] In particular, planar membranes based on amphihilic copolymers are robust when fixed or adsorbed on a solid substrate (e.g. silica[97,100,227,228] or gold[229]), which make them attractive candidates for biomedical and industrial applications.[227,230] Additionally, the polymer chemical functionalization make them versatile and attractive candidates for biomedical and industrial applications.[86,219,227,230] So far, the preparation of solid-supported polymer membranes is achieved via Langmuir Blodgett (LB) and Langmuir Schaeffer (LS)[100,161–163] or by vesicle fusion.[80,231] However, these methods have important drawbacks, such as: i) they can be applied to limited copolymer types and solid supports[232] ii) require long optimization conditions[219,230] and iii) the insertion of biomolecules in a synthetic membrane is a delicate task because it is difficult to reproduce the physiological environment necessary for the preservation of the biomolecule's functionality.[233]

Recently, a new method called solvent-assisted lipid bilayer formation (SA) was introduced for phospholipid-based systems as an alternative to the previously mentioned methods.[232] The SA method involves three basic steps: i) the deposition of lipid molecules dissolved in a water-miscible organic solvent (e.g. ethanol, isopropanol) onto a solid surface, ii) the exchange of the organic phase into aqueous phase, which triggers the self-assembly process and iii) the planar membrane formation once the system reaches equilibrium. This method is fast and the lipid membrane formation can be monitored in real-time. In addition, this method is also versatile as it allows the use of a wide range of lipid membrane-types and various substrates.[233,234] However, the SA method has not yet been used to generate polymer solid-supported planar membranes as well as scrutinize the conditions which promote their formation.

Here we introduce the SA method for the development of polymer solid-supported membranes and combine the resulting membranes with biomolecules to explore whether such hybrid interfaces allow biomolecules to be accessible and fulfill their bio-functionality. In this work we use for simplicity the term 'membrane' to describe and include all the 'membrane-like' solid-supported polymer assemblies we obtained by SA.

First, we systematically evaluated the formation of solid-supported polymer membranes and optimized the conditions for the solvent assisted method (SA). We selected a small library of three PMOXA-PDMS diblock copolymers and one PMOXA-PDMS-PMOXA triblock copolymer, proven to allow functional insertion of biomolecules, to test and optimize the planar membrane formation by SA method.

Second, we used the diblock copolymer which formed the most uniform and defect-free planar membrane and mixed it with biotinylated PDMS-PMOXA in various weight ratios in order obtain solid supported planar membranes exposing increasing amounts of biotin. Accessible biotin molecules serve for attachment of avidin- or streptavidin-bearing molecules. The biotin-streptavidin25 or biotin-avidin[235,236] couples are well known molecular recognition pairs forming strong and highly specific noncovalent bonds. These remain functional under various environmental conditions. We evaluated the biotin content of the resulting planar membranes and the accessibility for binding avidin- or streptavidin- bound biomolecules by biotin-avidin and biotin-streptavidin coupling assays.[235,237]

Planar polymer membranes obtained with the SA method have been characterized by quartz crystal microbalance with dissipation monitoring (QCM-D) to detect the real-time membranes formation and the quality in terms of membrane coverage. In addition, Atomic force microscopy (AFM) and force spectroscopy were used to investigate the membranes' morphology and mechanical properties. Finally, we evaluated the noncovalent attachment of bioactive molecules to the biotinylated planar polymer membranes. Functional insertion or attachment of bio-active molecules within polymer membranes is a delicate task because it requires special conditions which allow the biomolecules to maintain their intrinsic functionality.[220] As a model biomolecule, we first selected biotinylated DNA strands for verifying their attachment in the correct conformation. We then explored the attachment of an artificial metalloenzyme to the biotinylated synthetic membranes on solid support. Created by the combination of an active organometallic complex and a selective host protein, artificial metalloenzymes display great potential for synthetic biology (e.g. *in vivo* catalysis), nanotechnology (e.g. proteins with customized properties) and biotechnology (e.g. enantioselective catalysis).[238–240] Specifically, we studied the interaction of biotinylated planar polymer membranes formed by the SA method with an artificial deallylase (ADAse).[241] The ADAse was obtained by the anchoring of a biotinylated ruthenium complex into the binding pocket of Sav31. We investigated whether the functionalized polymer membrane exposes the

biotin groups properly to facilitate the attachment of the ADAse. An essential point was to find out the differences in terms of activity and functionality between the ADAse free in solution and when anchored to the synthetic membrane. In particular, we determined whether the binding between the ADAse and the polymer membrane affects its catalytic activity QCM-D was used to monitor and quantify the attachment of DNA and ADAse on the planar polymer membranes. The activity and functionality of free ADAse in solution and when coupled to the membrane was evaluated by fluorescence spectroscopy thanks to the generation of a fluorescent product as result of ADAse activity. The functional attachment of DNA, and most importantly, ADAse to polymer membranes produced by the SA method opens up new perspectives on biohybrid membranes for the development of synthetic membrane-based biosensors and biocatalytic platforms.

3.2.1. Solid-supported polymer membrane formation by SA method

While the SA method has been employed for preparing lipid planar membranes onto silica or gold solid supports,[95,242–246] here we aim to use it for amphiphilic copolymers. We used $PDMS_m$-b-$PMOXA_n$ diblock copolymers with different hydrophobic block lengths (roughly n = 10, m = 30, 60 and 90) and a $PMOXA_6$-*b*-$PDMS_{36}$-*b*-$PMOXA_6$ triblock copolymers (Figure 3.2-1). First, we investigated the real-time membrane formation onto a silica solid substrate at different hydrophilic/hydrophobic block ratios of the copolymers. Next, we evaluated how the molecular structure of the copolymers affected the membrane-assembly process. We monitored the membrane formation by using QCM-D (Figure 3.2-1 C and D).

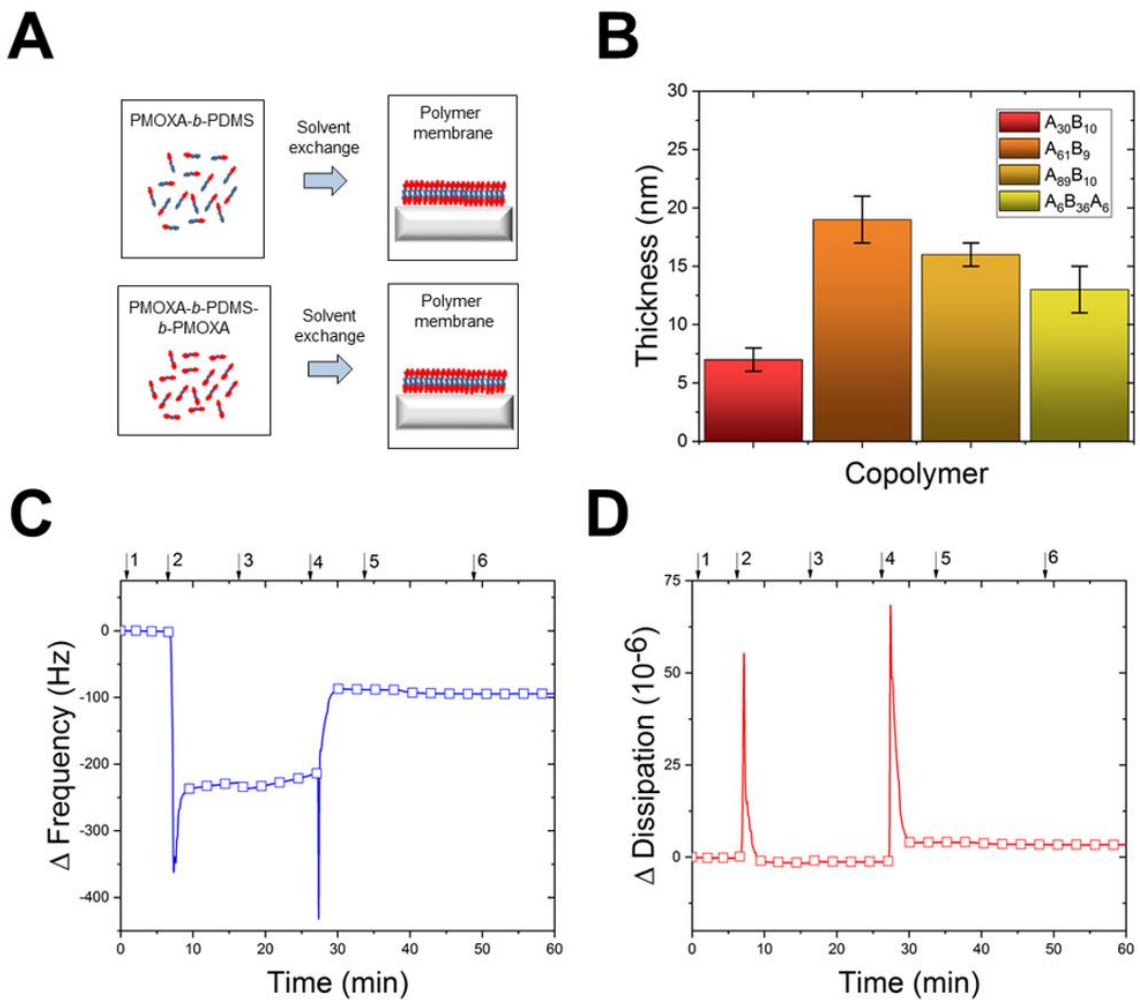

Figure 3.2-1 Polymer membrane formation for different di- and tri-block copolymers: schematic representation (A); bar chart of membrane thicknesses (B); QCM-D generic frequency (C) and dissipation (D) profiles for polymer membrane-formation: buffer (1), solvent exchange (2), polymer solution (3) buffer rinsing (4), BSA (5), buffer rinsing (6).

The frequency and dissipation values obtained with the QCM-D measurements for the different polymer membranes were used to calculate their thickness (Figure 1B and Table 7.3). The thickness calculated for the different polymer membranes varied between 7 ± 1 and 19 ± 2 nm for the diblock copolymers (30 up to 89 PDMS units) and it was of 13 ± 2 nm for $B_6A_{36}B_6$ triblock. In general, the thickness of the membranes increased proportionally with the increase in the PDMS block length, in accordance with previous reports for PDMS-PMOXA membranes as reported by Itel and coworkers41. In contrast, it was not possible to obtain a homogeneous membrane for $A_{89}B_{10}$ polymer.

In order to evaluate the quality of the solid-supported polymer membranes, we used the BSA protein established assay: BSA adsorbs onto silica substrates, minimizing interactions with the membrane[95,201,247] and thus highlighting the uniformity of the formed membrane. A frequency shift in QCM-D indicates an adsorption of BSA onto the silica substrate is associated to defects in the polymer membranes. It reveals a direct interaction between the BSA and the substrate (Table 7.3). The values of the frequency shift between −4 and -6 Hz indicates a degree of defects comparable to that resulting when polymer membranes were produced via the Langmuir-Blodgett method.[241] The calculated membrane coverage was of 80 ± 6% for the monolayer obtained with the $B_6A_{36}B_6$. For this membrane we expected a monolayer assembly, according to the triblock polymer structure.[104,201,247,248] In the case of bilayers obtained with the PDMS-*b*-PMOXA diblocks (respectively of 30, 61 and 89 PDMS units), the calculated membrane coverage was 84 ± 4%, 76 ± 6% and of 48 ± 5%. As expected, planar membranes were easier to form by the SA method for lower hydrophilic/hydrophobic polymer chain ratio. Apparently, due to its long PDMS chain, diblock $A_{89}B_{10}$ did not form a homogeneous membrane. Instead of a planar assembly, this polymer favored the formation of structures with hydrophobic properties (e.g. inverted micelles, according to the packing parameter[249]) that detached from the hydrophilic silica.

As all the membranes obtained by the SA method showed good membrane coverage with minor defects. The use of SA method provides membranes with good quality in terms of homogeneity together with a rapid preparation procedure.

3.2.2. Morphology and characterization of solid-supported membranes

The morphology of the solid-supported polymer membranes and their mechanical properties were evaluated by a combination of AFM and force spectroscopy. AFM phase and height imaging modes in air were used to characterize the polymer membranes in terms of surface morphology. By comparing polymer membranes obtained with different PDMS-b-PMOXA copolymers, it was possible to observe the formation of protrusions with an island shape (Figure 3.2-2). We consider that these islands presumably derive from polymer self-assembling into vesicles during the SA process and their incomplete fusion onto the silica surface. The length of the PDMS block plays a key role in the island formation regardless of the polymer functionalization. Islands with diameter in the range of few nm were found for the membranes based on PMOXA-PDMS copolymer with the hydrophobic block of 30 and 35 repeating units (Figure 3.2-2 A and B). The diameter of these islands increased up to hundreds of nm for the membranes resulting from the copolymer with a PDMS block of 61 repeating units (Figure 3.2-

2 C). The presence of such islands significantly increases the surface area and therefore will favour the interaction with biomolecules. The different phase contrast for the islands and the membrane is representative of a different interaction with the AFM tip. This different interaction is related to higher elasticity of the islands compared to planar polymer membrane. When the copolymer with the highest number of PDMS units (i.e. 89) was scrutinized, no formation of polymer islands was visible. Instead, a planar assembly was observed and confirmed by the difference in the phase of only 2 deg (Figure 3.2-2 D). Nevertheless, the membrane presented high non-homogeneity due to the long hydrophobic block length of this polymer in accordance to the performed BSA test. When the solvent-exchange method was applied to the triblock $B_6A_{36}B_6$, only few vesicles (or vesicle-like architectures) were found onto the silica support. The drying process for this triblock copolymer apparently resulted in the polymer detachment from the support. Triblock copolymers have been reported to form solid supported monolayers and adopt the 'U' shape conformation.[250] This is related to the low stability of the planar assembly based on the triblock copolymer tested in this study. Consequently, this leads to the polymer's detachment from the solid substrate. A table to summarize the polymer membrane characteristics is here reported (Table 3.2-1).

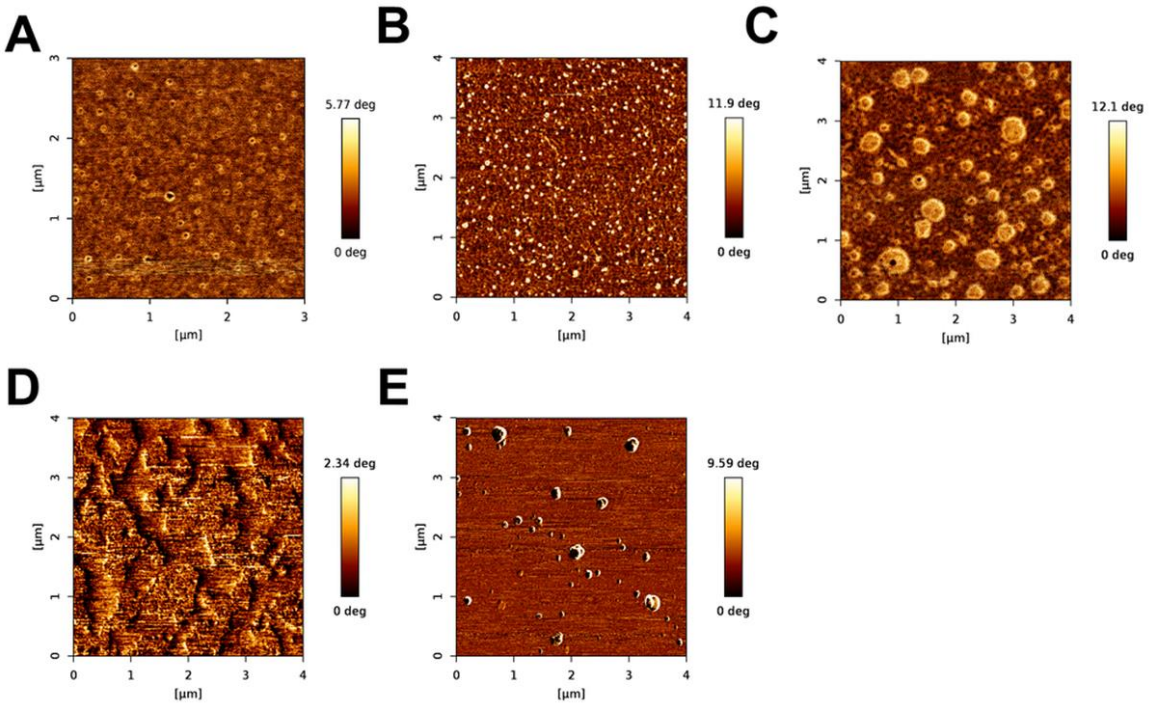

Figure 3.2-2 AFM phase images of different polymer membranes obtained from diblock copolymers: biotin-$A_{35}B_{12}$ (A), $A_{30}B_{10}$ (B), $A_{61}B_9$ (C), $A_{89}B_{10}$ (D), and triblock copolymer $B_6A_{36}B_6$ (E).

	Polymer membranes			
Polymer	Thickness (nm)	Membrane coverage (%)	Roughness (nm)	Elasticity (nN/µm)
$A_{30}B_{10}$	7 ± 1	84	1.75	3.16
$A_{61}B_{9}$	19 ± 2	76	1.76	8.85
$A_{89}B_{10}$	16 ± 1	48	n.a.	n.a.
$A_{6}B_{36}A_{6}$	13 ± 2	80	n.a.	n.a.

Table 3.2-1. Polymer membranes characteristics: thickness and membrane coverage obtained by QCM-D in liquid; roughness and elasticity obtained by AFM in air.

3.2.3. Biotinylated polymer membranes on solid support: formation by SA method

To enable coupling of biomolecules with the solid-supported planar membranes, we mixed the copolymer $A_{61}B_{9}$ with biotin-$A_{35}B_{12}$ copolymers and then used the SA method to assemble the membranes (Figure 3.2-3 A). The biotin-functionalized diblock copolymer facilitated the selective and strong avidin-biotin assembly[251] and consequently enabled the selective anchoring of biomolecules to the membrane. We were interested in studying how the membrane composition affects the biotin-accessibility for the targeting avidin attachment. With QCM-D, we monitored the membrane formation for different weight ratio $A_{61}B_{9}$/ biotin-$A_{35}B_{12}$ composition: 100:0, 80:20, 50:50, 20:80 and 0:100 (Figure 3.2-3 C and D). The calculated thicknesses of the polymer membranes were in a range varying between 19 ± 1 and 14 ± 1 nm depending of the ratio between the two copolymers in the mixtures (see Appendix). Additionally, we determined the masses of different membranes (Figure 3.2-3 B) providing a more detailed comparison of the membranes for different polymer compositions relying on the Composite Sauerbrey model. These values are in agreement with those obtained for other PDMS-b-PMOXA planar polymer membranes.[163]

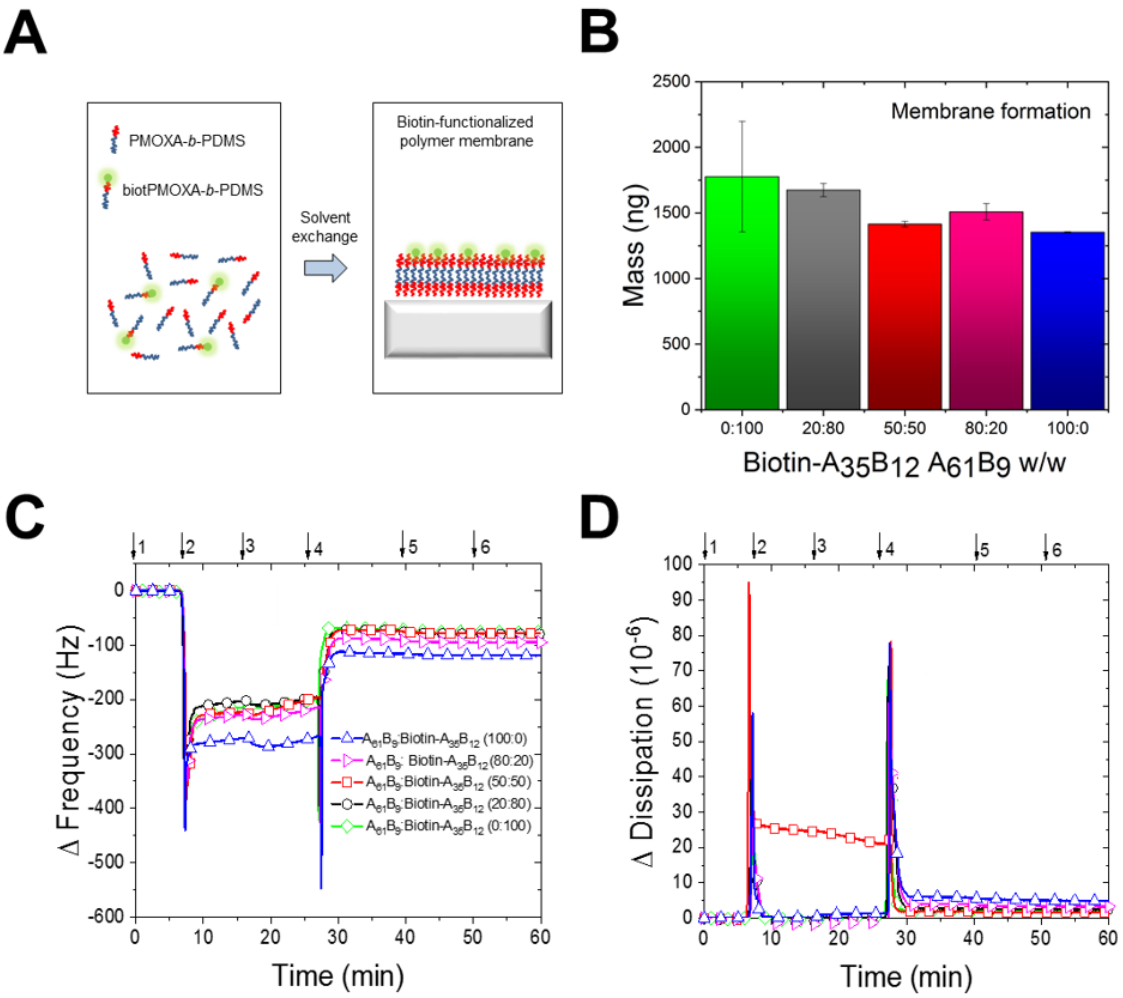

Figure 3.2-3 Functionalized polymer membrane formation for biotin-$A_{35}B_{12}$ and $A_{61}B_9$ polymers: schematic representation of membrane formation (A); bar chart of thicknesses for membranes at different polymer composition (B); QCM-D frequency (C) and dissipation (D) plots for membrane formation, buffer (1), solvent exchange (2), polymer solution (3) buffer rinsing (4), BSA (5), buffer rinsing (6).

The membrane quality was evaluated with BSA in terms of percentage of membrane coverage as described above. The frequency shift observed by QCM-D varied between -5 and -6 Hz (Table 7.4) which is representative of a low amount of membrane defects with a calculated average membrane coverage over all membranes of 75 %.

To determine the influence of different PDMS block lengths on biotin-exposing polymer membranes, we mixed $A_{30}B_{10}$ instead of $A_{61}B_9$ with biotin-$A_{35}B_{12}$ (80:20 w/w ratio). We relied on QCM-D to characterize the formation of a membrane from copolymers with almost no PDMS length mismatch (Figure 3.2-4 and Table 7.5). An average membrane thickness of 12 ±

4 nm was observed as expected for a shorter polymer length. We expect a higher accessibility to the biotin functional groups of the membrane when composed of copolymers with comparable block length.

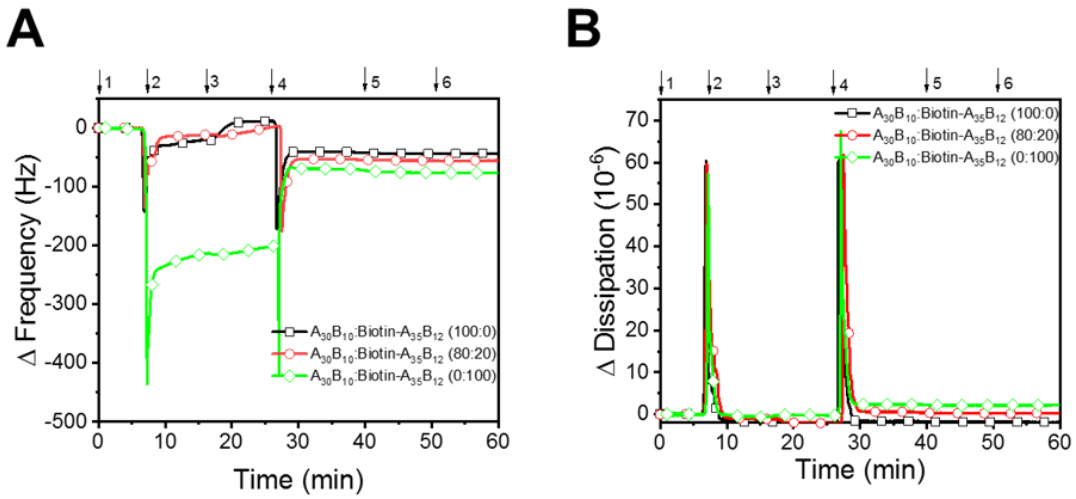

Figure 3.2-4. QCM-D plots of a SAPB experiment for biotin-$A_{35}B_{12}$ and $A_{30}B_{10}$ polymers at different weight/ratio: buffer (1), solvent exchange (2), polymer solution (3) buffer rinsing (4), BSA step (5), buffer rinsing (6). Frequency (A) and Dissipation (B) graphs are reported.

Additionally, the conditions were optimized in terms of copolymer concentration to obtain reproducible and robust polymer membranes. A concentration of 0.5 mg/ml provided the best membrane coverage without forming additional structures (Figure 3.2-5 and Table 7.6).

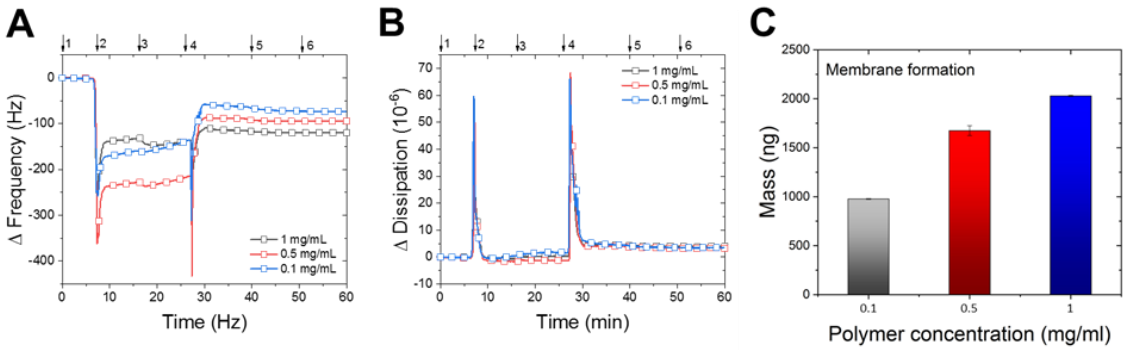

Figure 3.2-5. QCM-D plots of a SAPB experiment for biotin-$A_{35}B_{12}$ and $A_{61}B_9$ polymers (20:80 w/w) at different concentrations: buffer (1), solvent exchange (2), polymer solution (3) buffer rinsing (4), BSA (5), buffer rinsing (6). Frequency (A) and Dissipation (B) graphs are reported. Bar chart of two-component membranes for different polymer concentration is reported (C).

3.2.4. Physico-chemical properties of biotinylated membranes

We used the functionalized polymer biotin-$A_{35}B_{12}$ mixed with two non-functionalized polymers of different PDMS length ($A_{61}B_9$ and $A_{30}B_{10}$) and formed functionalized polymer membranes by the SA method. We used AFM to characterize the mechanical properties and morphology of membranes based on biotin-$A_{35}B_{12}$/$A_{61}B_9$ and biotin-$A_{35}B_{12}$/$A_{30}B_{10}$ copolymer mixtures (20:80 weight ratio). The AFM height profile revealed main differences in dimensions of the islands and on the membrane elasticity. The roughness of the surface was comparable to that of the polymer membranes (Figure 3.2-6 and Table 7.7). The cross-section revealed a height of 20 ± 1 nm for big islands, compared to 8 ± 2 nm obtained for small islands (Figure 3.2-6 A and B respectively). These are related to the polymer PDMS block lengths. In general, these islands have the shape of semi-fused vesicles (Figure 3.2-6 C), as reported for lipid membranes prepared with the SA method46 and for similar PDMS-b-PMOXA membranes obtained with the film hydration method.[252]

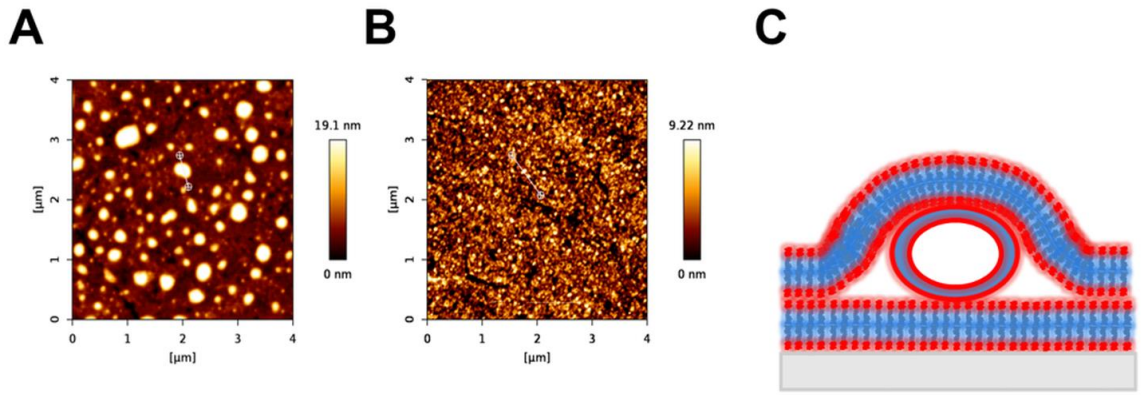

Figure 3.2-6. AFM height profile of two component polymeric membranes (20:80 w/w) composed of biotin-$A_{35}B_{12}$/$A_{61}B_9$ (A) and biotin-$A_{35}B_{12}$/$A_{30}B_{10}$ (B). Schematic representation of $A_{61}B_9$ polymer islands (C).

Force spectroscopy measurements provided information about the mechanical properties of the biotin-exposing polymer membranes. Phase, Young´s modulus and adhesion images (Figures 3.2-7 and 3.2-8) together with force-distance curves (Figure 3.2-9) were used for the characterization of the functionalized polymer biotin-$A_{35}B_{12}$/ $A_{61}B_9$ and biotin-$A_{35}B_{12}$/ $A_{30}B_{10}$ membranes (20:80 weight ratio). Young´s modulus provided information about the stiffness of the membrane with an average value of 24 MPa. This is in the range of what was reported for similar PDMS-b-PMOXA membranes with solution spreading.[252] The values of the Young modulus indicate that different PDMS block lengths do not affect the overall membrane stiffness. Inside islands there is a lower stiffness than the planar membrane bulk assembly, in

accordance with what is expected for a vesicle-like structure (black spots in Figure 3.2-7 B).[253] The Young´s modulus obtained for polymer membrane was not remarkably different from what found for gel phase lipid membranes: functional polymer membranes composed of biotin-$A_{35}B_{12}$-$A_{30}B_{10}$ and biotin-$A_{35}B_{12}$-$A_{61}B_9$ showed an average value of 24 MPa, compared to a value of 28 MPa found for pure DPPC membranes.[254] The adhesion image of the biotin-$A_{35}B_{12}$/$A_{61}B_9$ membrane allows the calculation of a maximum value of 185 pN (Figure 3.2-7 C). This is slightly higher than that of the biotin-$A_{35}B_{12}$/ $A_{30}B_{10}$ membrane (Figure 3.2-8 C) where a value of 164 pN has been obtained.[255] The higher adhesion value for the biotin-$A_{35}B_{12}$/$A_{61}B_9$ membrane indicates a higher elasticity for membranes composed of polymers with longer chains and bigger islands. The polymer mixture formed a worm-like assembly within the islands, visible in the adhesion image (Figure 3.2-7 C).

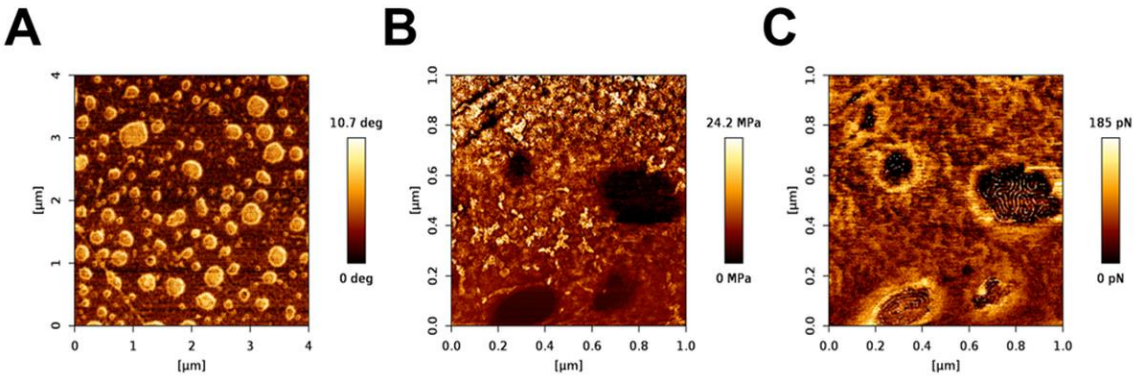

Figure 3.2-7. AFM characterization of membrane composed of biotin-$A_{35}B_{12}$ and $A_{61}B_9$ polymers (20:80 w/w): phase image (A), Young´s modulus (B) and adhesion (C).

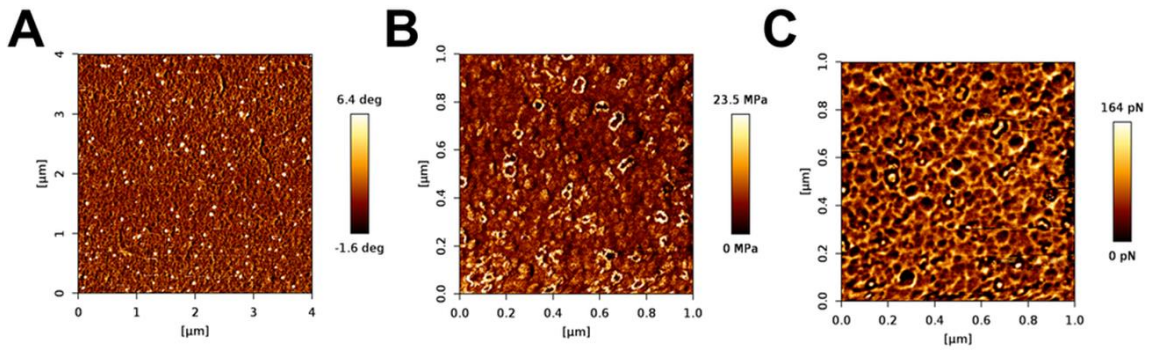

Figure 3.2-8. AFM characterization of membrane composed of biotin-$A_{35}B_{12}$ and $A_{30}B_{10}$ polymers (20:80 w/w): phase image (A), Young´s modulus (B) and adhesion (C).

Roughness and elasticity values of all polymer membranes were compared (Table 7-7). The average roughness was similar for all the polymers and the functionalized polymer membranes

ranging from 1.23 to 1.61 nm, whereas the bare silica measured a roughness of 120 pm. We compared the force-distance curves of both biotin-exposing membranes biotin-$A_{35}B_{12}$/ $A_{61}B_9$ and biotin-$A_{35}B_{12}/A_{30}B_{10}$ respectively (20:80 w/w) with a silica substrate (Figure 3.2-9). A narrow slope in the curve is typical of a stiff material whereas a broad slope represents stronger interaction between the tip and the material, which is characteristic of an elastic material.[256] As expected, the silica support (Figure 3.2-9 C) had higher stiffness compared to the polymer membranes. Biotin-$A_{35}B_{12}/A_{61}B_9$ (Figure 3.2-9 A) revealed even higher elasticity than biotin-$A_{35}B_{12}/A_{30}B_{10}$ (Figure 3.2-9 B). None of the biotin-exposing membranes presented a discontinuity point in the curve, which indicates membrane breaking. As expected, the synthetic membranes have a higher membrane resistance when compared to lipid membranes.[253] The almost complete overlap of the "approach" and "retract" curves for the biotin-$A_{35}B_{12}/A_{61}B_9$ membrane (Figure 3.2-9 A) revealed that there is no change in volume of the investigated polymer islands when they enter into contact with the tip.[252] Therefore, the biotin-exposing membranes preserved their initial structure. Polymer islands in both biotin-exposing membranes revealed a value of the bending modulus higher than gel phase lipids, presumably due to their significantly higher thickness of polymer membrane (18-20 nm) compared to lipid membranes (4-5 nm).[252]

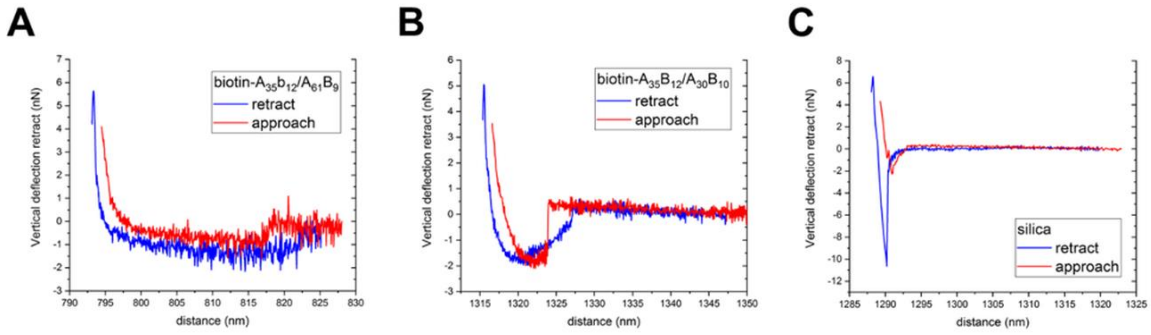

Figure 3.2-9. Comparisons of force-distance curves obtained from the biotin-$A_{35}B_{12}/A_{61}B_9$ mixture (20:80 w/w) (A), biotin-$A_{35}B_{12}/A_{30}B_{10}$ (20:80 w/w) (B) and silica substrate (C).

The SA method applied for the first time on polymers can compete with established methods frequently employed for preparing lipid and polymer-based supported membranes(refs). The main advantages of this strategy are: i) It does not requirethe preliminary formation of vesicles, as for vesicle fusion, ii) it is fast and user friendly without requiring special equipment in contrast to LB. However, the optimization of SA for polymer membranes still remains a challenge.

To establish that the SA method drove the polymer self-assembly into a membrane-like architecture suitable for attaching biomolecules (e.g protein, enzymes), an important aspect is the accessibility of biotin for interaction with biomolecules by biotin-avidin and biotin-streptavidin interactions respectively. Avidin and streptavidin are tetrameric proteins: after binding one of the four pockets of either protein, two-to-three biotin-binding sites remain available for the attachment of other biotinylated biomolecules (Figure 3.2-10 A).

By combining biotin-$A_{35}B_{12}$ and $A_{61}B_9$ copolymers at different weight ratios, we created biotinylated-supported membranes. Next, we added avidin and quantified its attachment by QCM-D (Figure 3.2-10 C and D). In the absence of the biotinylated polymer in the mixture, a small amount of avidin weakly adsorbed onto the membrane and was removed in the rinsing step. By increasing the percentage of biotin-$A_{35}B_{12}$, a higher quantity of avidin attached to the membrane (Figure 3.2-10 B). The highest observed frequency shift was -29 ± 1 Hz for the biotin-$A_{35}B_{12}$/$A_{61}B_9$ 80:20 composition corresponding to a mass of 513 ± 18 ng (Table 7-8). The membrane composed of 100% of biotin-$A_{35}B_{12}$ presented a frequency shift of only -26 ± 2 Hz, which is a lower value compared to what was obtained from the biotin-exposing membranes. This low value for the membrane composed only of the biotin-functionalized copolymer biotin-$A_{35}B_{12}$ can be related in this specific case to a better accessibility of the biotin displayed on the surface. Therefore, this involves the binding of more than one biotin-binding site present in homotetrameric avidin. By comparing the dissipation values before and after the avidin attachment (Figure 3.2-10 B), the values displayed negligible differences (Table 7-8). This suggests that no significant change in the viscoelastic properties of membranes after the protein attachment occurs. A table to summarize the functional polymer membrane characteristics and the amount of attached avidin is below reported (Table 3.2-2).

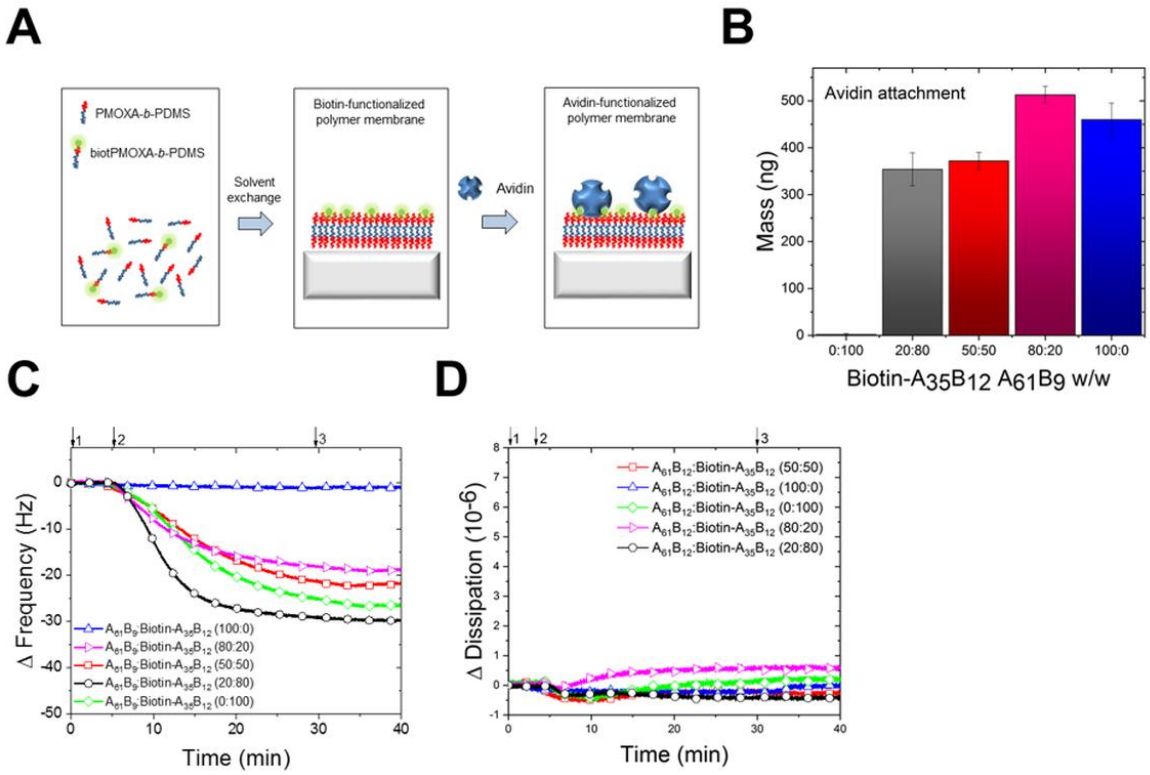

Figure 3.2-10. Avidin attachment onto functionalized membrane formed by biotin-$A_{35}B_{12}$ and $A_{61}B_9$ polymers at different weight ratio: schematic representation (A); bar chart of quantified attachment (B); QCM-D frequency (C) and dissipation (D) plots, buffer (1), avidin (2) and buffer rinsing (3).

	Functional polymer membrane		Avidin attachment
Biotin-$A_{35}B_{12}$ $A_{61}B_9$ w/w	Thickness (nm)	Membrane coverage (%)	Mass (ng/cm^2)
0:100	19 ± 1	75	0
20:80	17 ± 1	79	354 ± 35
50:50	15 ± 2	75	372 ± 18
80:20	15 ± 2	75	513 ± 18
100:0	14 ± 1	75	460 ± 35

Table 3.2-2. Functional polymer membranes characteristics obtained by QCM-D in liquid (thickness, membrane coverage and amount of avidin attached).

Based on the results obtained so far, we selected the ratio of biotin-copolymer/non-functionalized copolymer 20:80 w/w as best composition in terms of protein attached/ratio of functionalized polymer. Next, we investigated the effect of the hydrophobic block length mismatch on the membrane-protein attachment. We added avidin to biotin-$A_{35}B_{12}/A_{30}B_{10}$ 20:80 w:w membranes (Figure 3.2-11 and Table 7-9). Since only 247 ± 35 ng of avidin was anchored, we conclude that biotin-$A_{35}B_{12}/A_{61}B_9$ is a more efficient membrane than biotin-$A_{35}B_{12}/A_{30}B_{10}$ to anchor avidin. Our results suggest that bigger islands, observed when the $A_{61}B_9$ polymer was used, affect the membrane capability to bind biomolecules since they provide a greater surface area available for the attachment without limiting the biomolecule's accessibility.

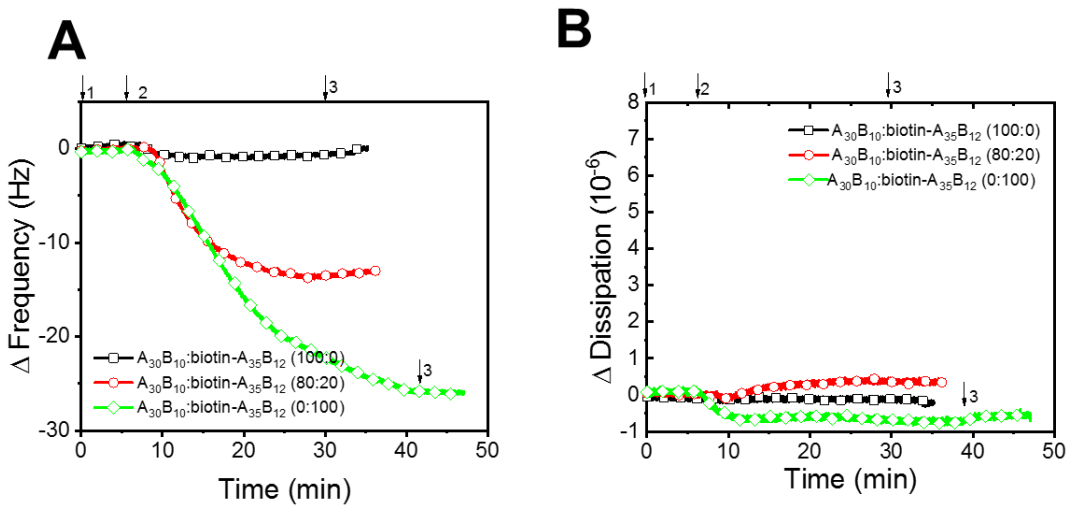

Figure 3.2-11. QCM-D plots of avidin attachment onto membrane formed by biotin-$A_{35}B_{12}$ and $A_{30}B_{10}$ polymers at different weight ratio: buffer (1), avidin (2) and buffer rinsing (3). Frequency (A) and Dissipation (B) graphs are reported.

We also evaluated the quantity of avidin anchore on polymer membranes with different biotin-$A_{35}B_{12}/A_{61}B_9$ (20:80 w:w) concentrations. The optimal biotin-$A_{35}B_{12}/A_{61}B_9$ concentration for forming a complete membrane suitable for the higher avidin attachment was found to be 0.5 mg/ml with an amount of avidin of 354 ± 25 ng (Figure 3.2-12 and Table 7-9).

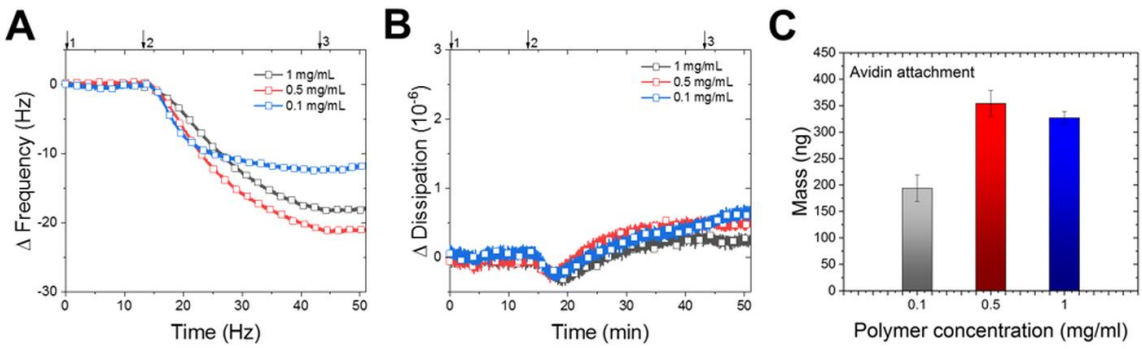

Figure 3.2-12. QCM-D plots of avidin attachment onto membrane formed by biotin-$A_{35}B_{12}$ and $A_{61}B_9$ polymers (20:80 w/w) at different concentrations: buffer (1), avidin (2)and buffer rinsing (3). Frequency (A) and Dissipation (B) graphs, together with the bar chart of mass of avidin attached (C) are reported.

We also monitored the attachment of steptavidin (Sav) to biotin-exposing membranes generated by the SA method.[251] QCM-D experiments revealed a frequency shift of -18 ± 3 Hz and a mass of 310 ± 47 ng for the biotin-$A_{35}B_{12}$/$A_{61}B_9$ 20:80 w:w mixture (Table 7-10).

Both avidin and Sav binding to biotin-exposing membranes highlight the accessibility of biotin for molecular recognition interactions even in different conditions (weight ratio of the mixture, chain mismatch, concentration). Moreover, these conditions were optimized for obtaining the best protein attachment and limiting the hindrance: $A_{61}B_9$ membranes provided higher attachment than $A_{30}B_{10}$ both for avidin and Sav attachment.

3.2.5. Bio-active molecules anchoring on polymer membrane

The functionalized biotin-$A_{35}B_{12}$/$A_{61}B_9$ membrane was selected for binding of two biomolecules: i) DNA strand and its complementary strand; ii) the artificial metalloenzyme ADAse (Figure 3.2-13 A and Table 7-10). The attachment of biomolecules was monitored by QCM-D (Figures 3.2-13 B and C) and quantified in terms of mass of biomolecules attached (Figure 3.2-13 D).

In the first case, we set out to demonstrate that the biotin-exposing polymer membrane allows the attachment of biotinylated DNA strands in the proper conformation (biotDNA). For this, the first strand has to bind the membrane and remain accessible for the complementary strand (DNAcs). First, the biotin-equipped polymer membrane was functionalized with Sav. Then the biotDNA was added. The selective biotin-Sav chemistry led to the attachment of 110 ± 15 ng of biotinylated DNA in the presence of 310 ± 47 ng of Sav previously attached to the polymer membrane. Finally, 44 ± 10 ng of the complementary strand were attached (Table 7-10).

Despite the attachment being successful, as confirmed by the frequency values, we observed a drop of the biomolecule quantity in the course of this step-by-step procedure. We hypothesize that roughly half of the available biotin-binding sites are accessible to bind to biotDNA strand. In addition, only a fraction of the bound biotDNA retains a proper conformation allowing the attachment of its complementary strand.

The last part of our study dealt with the anchoring of the biotin-exposing polymer membrane with the artificial metalloenzyme ADAse which catalyzes a deallylation reaction. This study is important to understand the enzyme-membrane interaction and for the preparation of an active biomimetic platform. This is the first time that the ADAse was combined with a polymer membrane onto a solid support. The structure of the ADAse consists of ruthenium coordinated to a biotinylated cofactor (**1**) bound to Sav31. We evaluated both polymer membranes biotin-$A_{35}B_{12}/A_{61}B_9$ and biotin-$A_{35}B_{12}/A_{30}B_{10}$ (80:20 composition) towards their ability to bind the ADAse (Figure 3.2-13 C). To anchor the ADAse onto the membrane, it was first combined with homotetrameric Sav in solution, in a 1:1 molar ratio, thus leaving on average 3 three free biotin binding sites per Sav. By comparing the attachment of ADAse complex on biotin-$A_{35}B_{12}/A_{61}B_9$ and biotin-$A_{35}B_{12}/A_{30}B_{10}$ membranes, we observed a small difference in the amount of protein attached, 301 ± 47 ng and 283 ± 47 ng respectively (Table 7-10). A larger hydrophobic block length lead to an increase in the amount of ADAse anchored to the membrane (i.e. 20 ng). This highlights again the enhanced capability of hosting biomolecules due to higher membrane greater porosity and surface area. By maintaining a membrane-like architecture with the biotin end group exposed, its accessibility towards biomolecule attachment was at the same time preserved.

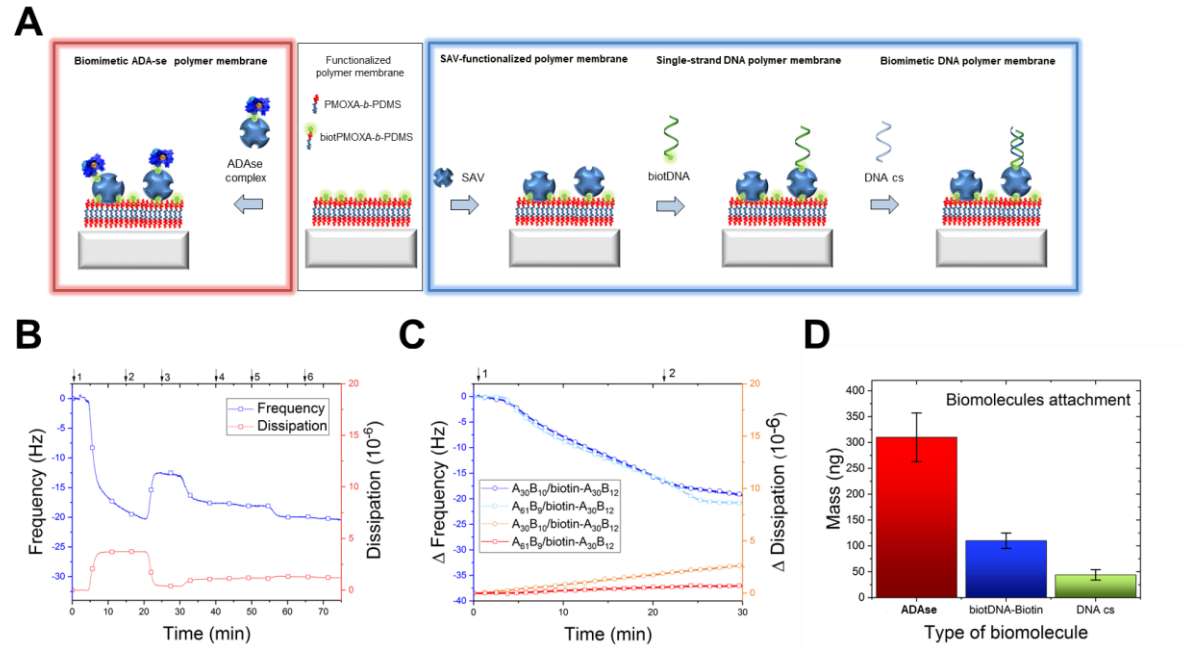

Figure 3.2-13. Schematic representation of biomimetic membrane formation (A); QCM-D plots of biomolecules combination with functionalized polymer membranes: DNA strands (B), Sav (1), buffer rinsing (2, 4, 6), biotDNA (3) DNAcs (5); ADAse (C), ADAse (1), buffer rinsing (2); bar chart of quantified attachment (D).

3.2.6. Evaluation of ADAse functionality within the polymer membrane

We monitored the catalytic activity of the artificial metalloenzyme following the attachment to the biotin-exposing polymer $A_{35}B_{12}/A_{61}B_9$ membrane. ADAse based on Sav and the biotinylated cofactor (**1**) [CpRu(Biot-Quinoline)(H_2O)] catalyzes the deallylation of an alloc-protected coumarin (**2**) converting it into aminocoumarin (**3**) (Figure 3.2-14 A and B). The latter product is readily detected by fluorescence spectroscopy.[241] Prior work by Heinisch and Schwizer et al[241] revealed that ADAse activity is maintained when Sav was displayed on the surface of *E. coli*. This strategy was used to genetically optimize the ADAse activity. The double mutant Sav S112Y-K121R was identified as a significantly improved variant compared to WT Sav. Based on this work, we selected these two variants (wild-type (WT) and S112Y-K121R (YR)) for immobilization studies. An essential point was to find out the differences in terms of activity and functionality between the ADAse free in solution and when anchored to the synthetic membrane. In particular, we determined whether the binding between the ADAse and the polymer membrane affects its catalytic activity. The QCM-D sensor coated with the biotin-$A_{35}B_{12}/A_{61}B_9$ membrane-ADAse was treated with a solution of the *N*-

(allyloxycarbonyl)-aminocoumarin (**2**, 20 μM in PBS). Catalysis was monitored by fluorescence spectroscopy over two days. In this specific case, we evaluated and compared the activity of two different ADAses: the wild type (WT) and the mutant (YR). Although it proved challenging to determine the amount of ADAse immobilized on the polymeric membrane, the fluorescence that was detected for either WT or YR correlated well with the trends observed in solution.[241] ADAse bearing the double mutation S112Y-K121R had significantly higher activity in solution compared to the wild type enzyme (Figure 7-12). We compared the activity of the enzyme in solution and when attached to the biotin-exposing membranes for both ADAses (Figure 3.2-14 C and D). YR displayed a higher catalytic activity compared to wild type both in solution and when attached to the membrane. The values of the converted substrate (in ng) after 48 hours for the experiments reported was estimated at 5 and 7 ng for the YR mutant (for the membrane- and in solution-ADAse respectively) compared to 2 and 4 ng for the wild type ADAse (Table 7-11). The enzyme had a higher activity in solution compared to the membrane-anchored ADAse. That may be traced back to substrate diffusion as well as to the limited amount of ADAse attached to the membrane compared to the solution-phase ADAse. In general, we observed slower reaction rates for the membrane-bound ADAses resulting in overall lower yields after 48 hours. Figure 3.2-14 D represents the trend of the enzyme activity over time, which showed an increase of the product formation for all the samples evaluated, with the reaching of a plateau in the specific case of the YR mutant in bulk, whereas Figure 6C shows the same values in a bar chart for better visualization. The accessibility to the active site of the ADAse after the membrane attachment is crucial for the enzyme to perform its catalysis. Here the catalytic activity for both variants revealed that the accessibility was preserved after the enzyme immobilization, thus highlighting the assembly of a functional biomimetic platform.

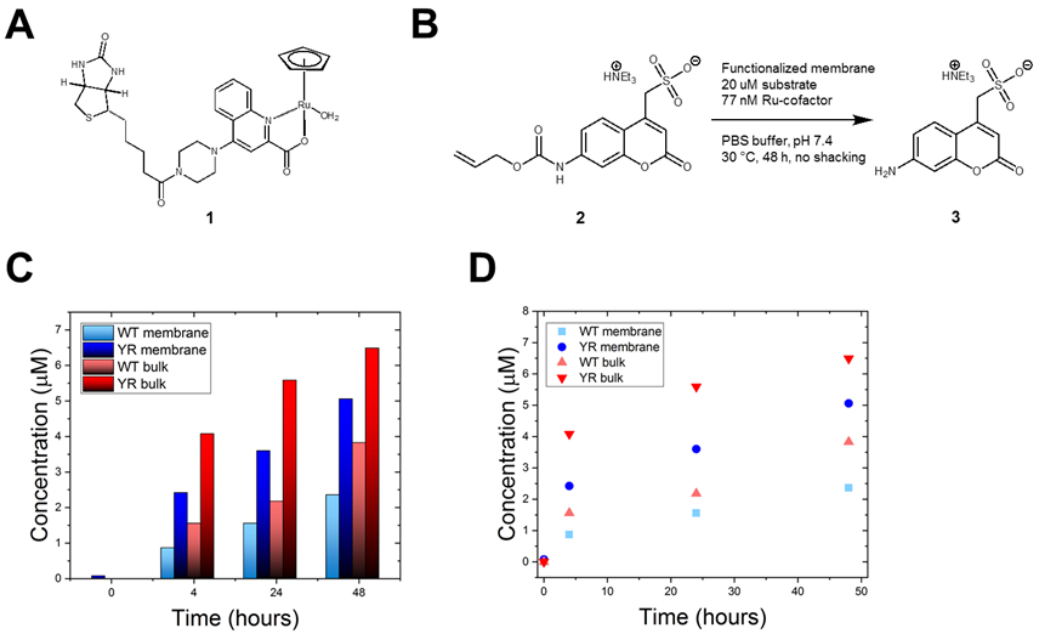

Figure 3.2-14. Schematic representation of the ruthenium-cofactor (A) and deallylation reaction (B); bar chart of the substrate converted with the catalysis performed by the ADAse. Wild type (WT) and mutant (YR) ADAse over time comparison in bulk or attached onto functional membrane (C and D).

3.3. Tailoring solvent assisted method for solid-supported lipid-polymer hybrid membranes

ABSTRACT

The combination of amphiphilic block copolymers and phospholipids opens new perspectives for the preparation of artificial membranes. The chemical versatility and mechanical resistance of the polymers, together with the fluidity and bio-compatibility of the lipids provides hybrid membranes with unique properties, which are of great interest in the field of bio-engineering. So far, hybrid membranes have usually been deposited onto solid support with established preparation methods such as Langmuir-Blodgett or vesicle fusion. In general, the preparation of this kind of platforms is time consuming and requires high precision and extreme clean conditions. The solvent-assisted method (SA) represents an easy and quick alternative to prepare solid-supported membranes. Initially developed for lipids, it has recently been extended with proper adaption to amphiphilic block copolymers. Here we applied for the first time the SA method to prepare polymer-lipid hybrid membranes. A small library of amphiphilic diblock copolymers was chosen: poly(dimethyl siloxane)-block-poly(2-methyl-2-oxazoline) (PDMS-b-PMOXA) and poly(butylene oxide)-block-poly(glycidol) (PBO-b-PG). We combined those polymers with phospholipids commonly found in cell membranes. While optimizing the conditions to prepare hybrid membranes, their real-time formation and morphology were evaluated by using a combination of atomic force micros-copy and quartz crystal microbalance. Significant differences regarding membrane coverage, formation of domains and the quality of the membranes were found depending on the type of polymer-lipid combination was used. This preliminary study on solid-supported hybrid membranes prepared by an optimized SA method put the basis for the development of a new and straightforward way to prepare artificial membranes.

INTRODUCTION

The design of synthetic membranes which are able to mimic the structure and function of natural cell membranes has become the subject of multidisciplinary research during the last decade.[40,72,257,258] This is due to the fact that such membranes have a great potential for both research and nanotechnology;[5,259] some of the most important application fields are molecular recognition and sequencing,[93,260] biosensing,[257,257] surface coating[261] and microelectronics.[262,263] Among the various types of synthetic membranes, the hybrid ones,

consisting of amphiphilic block copolymers and phospholipids are particularly attractive.[87,89,111] They combine the key advantages of each component: the chemical stability and versatility of block copolymers[19,252,264] and the bio-functionality of lipids.[265] Especially when the amphiphilic membrane is fixed on a solid substrate (e.g. solid supported hybrid membranes) the system obtains enhanced stability.[57,79,136] When polymer-based part of the membrane interacts with lipid-based part, the final morphology is governed by the charge, size, and molar ratio of the involved components.[87,89,103,266] In general, a mixture of polymers with lipids represents a hybrid structure where (im)miscibility effects are present: polymer with polymer and polymer with the hydrophobic lipid tail or with the hydrophilic lipid head group.[103,267,268] All those interactions together with the method of formation of such hybrid membranes determine the final structure.[87,89]

There are three main methods to create solid supported (polymer, lipid or hybrid) membranes: i) Langmuir-Blodgett,[9] ii) vesicle fusion[269–271] and iii) the recently reported solvent assisted (SA) method.[68,95,243] With all of them having their particular advantages and limitations, SA has emerged because it is quick, efficient and it requires no particular equipment or sophisticated sample preparation conditions.[95,272,273] The main step is to dissolve the amphiphilic molecules in an organic solvent and then expose it to an aqueous phase: the latter triggers the self-assembly process and the membrane formation. SA is therefore ideal for creating membranes in a fast and reproducible manner.

In our study we used SA to form solid supported hybrid membranes (Figure 3.3-1). Our aim is to further understand and ultimately optimize hybrid systems for future biomedical applications by testing various polymer-lipid compositions. For lipids, we chose among those commonly found in cell membranes and are established components of synthetic solid supported lipid membranes reported in literature:[274] DPPC, POPC, POPE, SM, DOPE and N-GPE. For polymers, together with PDMS-*b*-PMOXA of different PDMS block lengths, we also included (PBO-*b*-PG) (NMR in Appendix). We investigated how hydrophobic/hydrophilic effects influences the different hybrid membrane assembly. The asymmetry between phospholipids and copolymers, called hydrophobic mismatch, could induce a rearrangement to optimize the membrane structure, influencing properties such us thickness.[275] PBO-b-PG can be used as an alternative for the well-established PDMS-b-PMOXA.[276] Both copolymers are biocompatible and non-toxic.[277] They form highly flexible and fluid membranes because of their low glass transition temperatures and fully amorphous character and have been shown to self-assemble into planar membranes in high control and reproducibility.[100,224,260] In contrast to PDMS-b-

PMOXA, PBO-b-PG can be easily functionalized within the backbone of the hydrophilic block because of the hydroxy moieties throughout. Because of the reduced hydrophobility of PBO compared to PDMS, membranes composed of PBO-b-PG are more likely to be permeable for specific hydrophilic compounds.

First, we monitored the real-time formation of different hybrid membranes at different polymer-lipid weight ratio composition via QCM-D. Average thickness, mass and homogeneity were quantified for each hybrid membrane (see Table 7-12 in Appendix). Emphasis was put on their morphology characterization and the specific interaction between the polymer and lipid part, with a focus on their capability to phase separate: the morphology of diverse hybrid membranes and the presence of lipid rafts was characterized by atomic force microscopy (AFM). In this way, we could evaluate how the SA method affects the membrane self-assembly, the physicochemical properties and the phase domain separation. Moreover, by systematically testing various polymer-lipid compositions we were able to optimize hybrid membrane formation by adjusting the concentration and the sample composition.

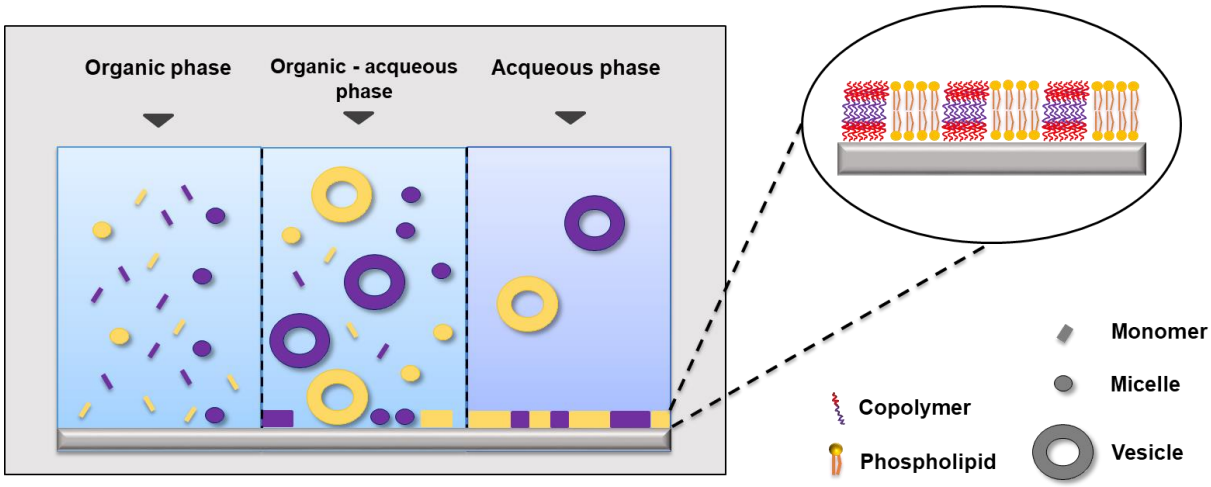

Figure 3.3-1. Schematic representation of a polymer-lipid hybrid membrane assembly induced by solved - assisted method.

3.3.1. Real-time membrane formation monitoring

As first step, we evaluated the polymer to lipid weight ratio which leads to the hybrid membrane with negligible defects and well-defined phase separation between the polymer and the lipid domain. We based this optimization step on combining PDMS-b-PMOXA polymer

with a PDMS block length of 61 repeating units ($A_{61}B_9$) and DPPC (Figure 3.3-2). We compared three different polymer-lipid compositions: i) $A_{61}B_9$-DPPC 20:80, ii) $A_{61}B_9$-DPPC 50:50 and iii) $A_{61}B_9$-DPPC 80:20. The membrane thickness calculated and reported here is an average value of the polymer and lipid thicknesses, since they have a remarkable length mismatch. By increasing the amount of polymer, the average thickness showed an increment from 9 nm, measured for the polymer-lipid 20:80, to 15 nm for the 50:50, up to 18 nm for the 80:20. After determining the mass and thickness for each deposited membrane, we evaluated their quality in terms of membrane coverage via BSA test.[266] BSA is an established method which enables the determination of the relative area of the QCM silica sensor covered by the membrane. In particular, BSA undergoes an unspecific adsorption onto the silica substrate. Therefore, the higher the amount of BSA we detect on the substrate the larger the area where our membrane failed to cover the substrate. The membrane coverage calculation was performed by comparing the BSA attachment onto a bare silica sensor and onto the deposited membranes. As the values for the membrane coverage were more than 80% for different polymer-lipid compositions, a good membrane quality was achieved, as reported in previous studies.[95,266] Specifically, for the latter case, the great amount of polymer in the mixture resulted in a coverage of 113±12%. In general, an amount higher than 100% stands for the full coverage of the QCM sensor and the formation of a complete monolayer with the partial formation of an additional layer, which increased the membrane porosity. The 50:50 composition was in most of the cases optimal for providing membranes with clear phase domain separation and consistent thickness. Thus, for the other polymers used we kept the polymer to lipid ratio 50:50 as constant. As a comparison to the established PDMS-*b*-PMOXA membranes, we combined also PBO-*b*-PG and DPPC at 50:50 weight/ratio (Figure 2) with the established protocol, which resulted in a hybrid membrane with an average thickness of 8 nm and a membrane coverage of 83±12%. The membrane thickness was affected by the mean molecular area occupied by the copolymer and by the membrane coverage. We found that a membrane coverage lower than 50% could significantly bias the membrane thickness with an error up to 2 nm, as observed for the NGPE lipid.

The hybrid membrane formation was expanded to the following phospholipids in combination with A61B9 and PBO-b-PG: POPC, SM, DOPE, POPE and NGPE. Those lipids belongs to the class of choline and ethanolamine and have been chosen for their different charge of the hydrophilic head and the different length and saturation of the hydrophobic chains. By varying

the polymer-lipid combinations we aim to a deeper understanding of the conditions that govern the hybrid planar membrane formation.

We combined PBO-PG copolymer and DPPC lipid at 50:50 weight/ratio (Figure 3.3-2) with the established protocol, which resulted in a hybrid membrane with an average thickness of 8 nm and a membrane coverage of 83±12%. The membrane thickness is affected by the mean molecular area occupied by the copolymer and by the membrane coverage. We found that a membrane coverage lower than 50% could significantly bias the membrane thickness with an error up to 2 nm, as observed for the NGPE lipid (see below).

The hybrid membrane formation was expanded to the following phospholipid in combination with $A_{61}B_9$ and PBO-PG polymers: POPC (Figure 3.3-3), SM (Figure 3.3-4), DOPE (Figure 3.3-5), POPE (Figure 3.3-6) and NGPE (Figure 3.3-7). POPE lipid was combined with different PDMS-PMOXA: $A_{89}B_{10}$, $A_{61}B_9$ and $A_{30}B_{12}$, hydrophobic block length respectively of 89, 61 and 30. By systematically varying the length of the hydrophobic block we opt for important information about the influence of hydrophobicity on the planar membrane assemblies[275]. In this specific case, the low hydrophobic mismatch between the $A_{30}B_{12}$ polymer and the lipid allowed the best membrane coverage of 96%, with the lowest standard deviation (below 1%) and an average thickness comparable to other membranes obtained with this lipid (10 nm against 12 nm). The low standard deviation can also be dependent from the polymer dispersity and is representative of higher reproducibility in the membrane formation.

DOPE and NGPE provided in both case defected membranes when combined with PBO_{50}-*b*-PG_{18} (Figure 3.3-6 and 3.3-7) whit a coverage of only 8±0% and 50±2% respectively, as also confirmed by AFM in the latter case.

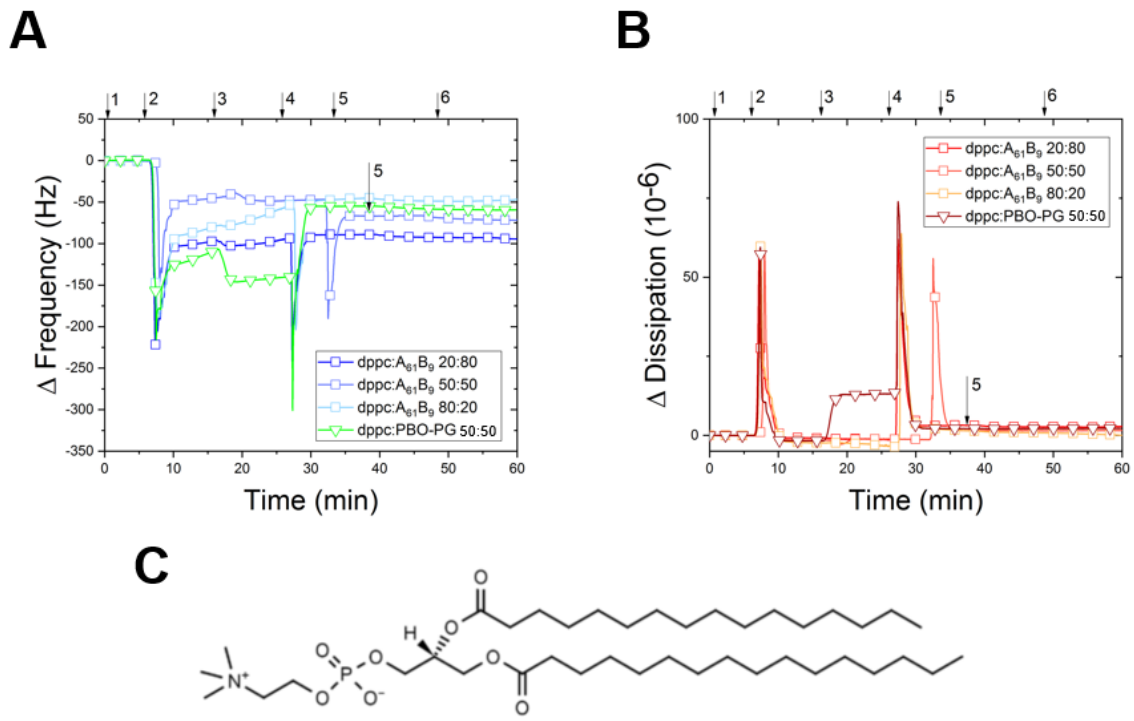

Figure 3.3-2. QCM-D plots of hybrid membrane formation: frequency (A) and dissipation (B) comparisons for different $A_{61}B_9$-DPPC mixtures and PBO_{50}-PG_{18}-DPPC at 50:50 weight ratio (↓1,4,6 = PBS, ↓2 = EtOH, ↓3 = polymer-DPPC solution, ↓5 =BSA); schematic representation of DPPC lipid.

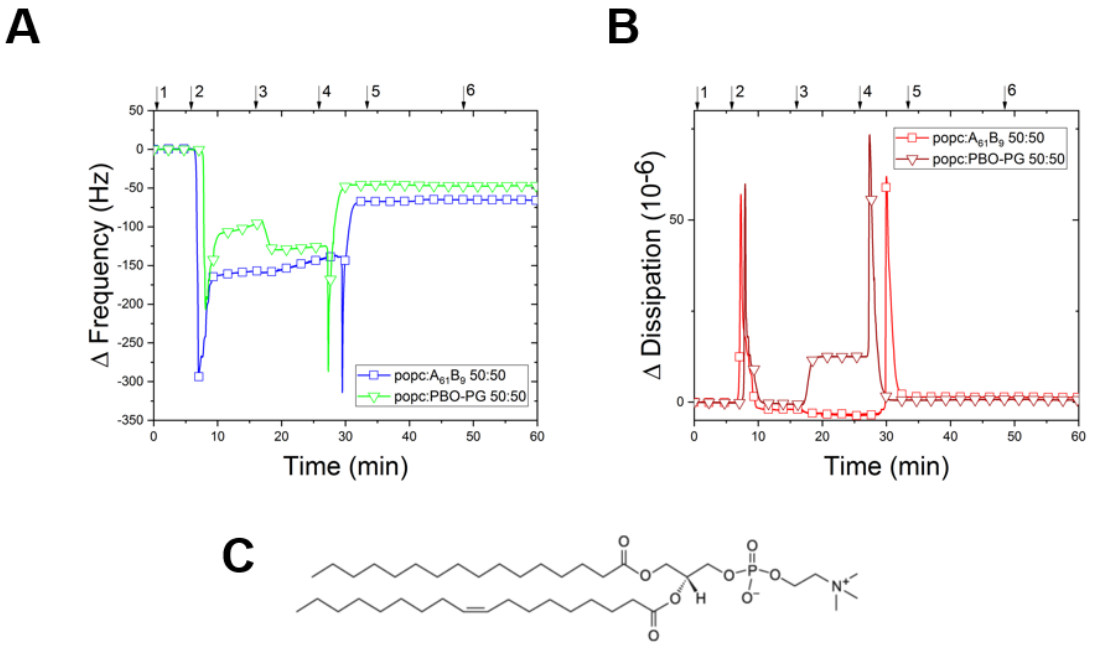

Figure 3.3-3. QCM-D plots of hybrid membrane formation: frequency (A) and dissipation (B) comparisons for $A_{61}B_9$-POPC and PBO_{50}-PG_{18} -POPC mixtures at 50:50 weight ratios (↓1,4,6 = PBS, ↓2 = EtOH, ↓3 = polymer-POPC solution, ↓5 =BSA); schematic representation of POPC lipid.

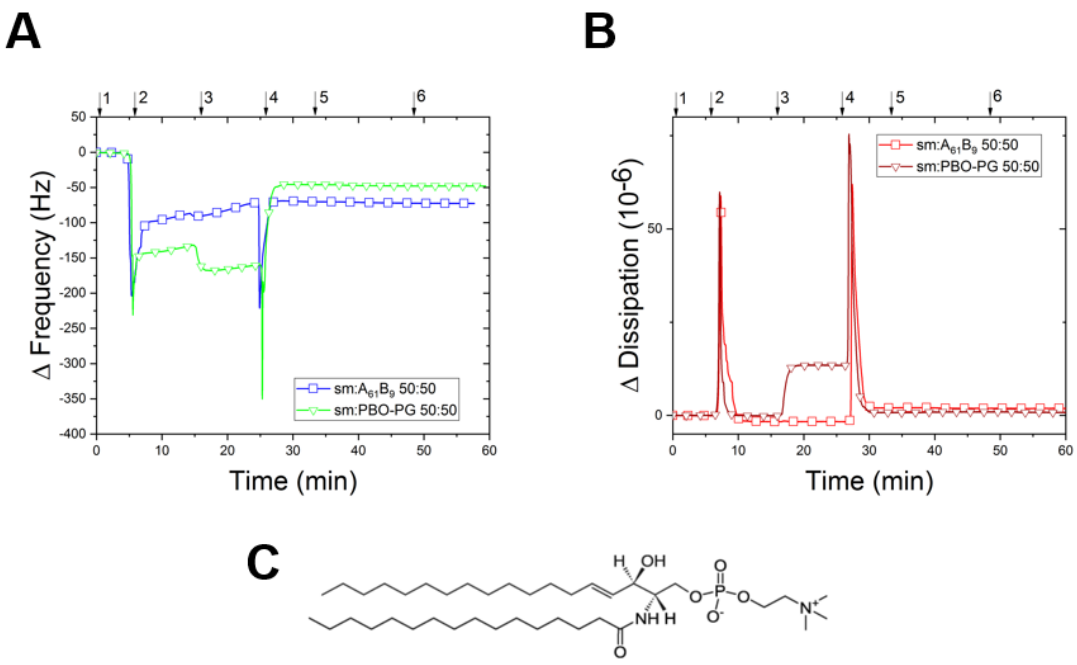

Figure 3.3-4. QCM-D plots of hybrid membrane formation: frequency (A) and dissipation (B) comparisons for $A_{61}B_9$-SM and PBO_{50}-PG_{18} -SM mixtures at 50:50 weight ratios (↓1,4,6 = PBS, ↓2 = EtOH, ↓3 = polymer-SM solution, ↓5 =BSA); schematic representation of SM lipid.

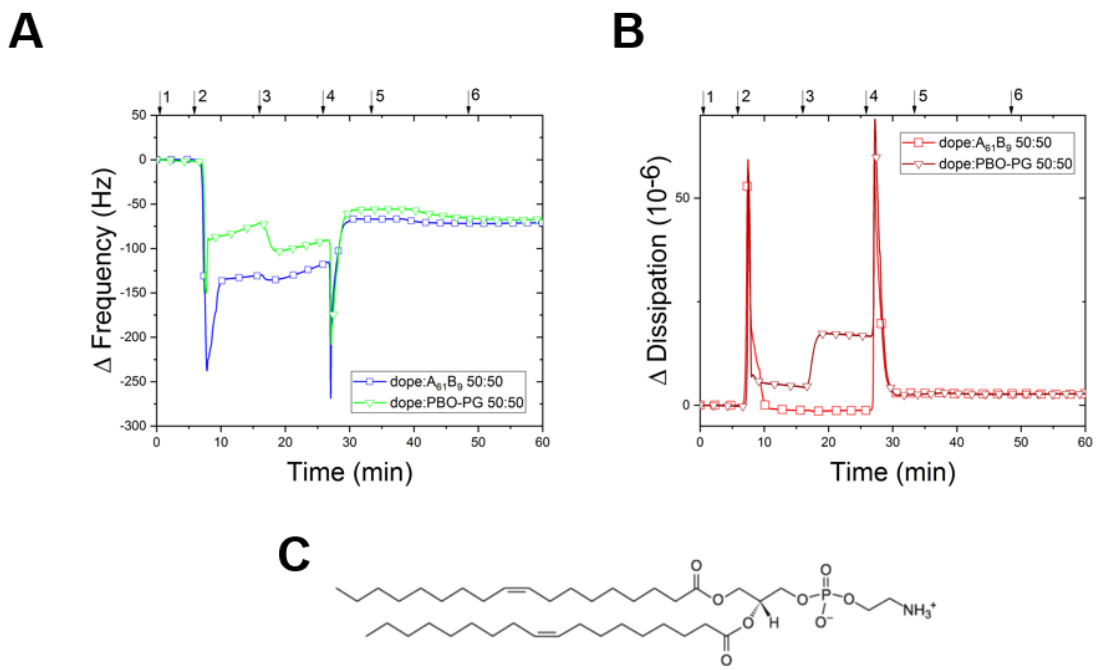

Figure 3.3-5. QCM-D plots of hybrid membrane formation: frequency (A) and dissipation (B) comparisons for $A_{61}B_9$-DOPE and PBO_{50}-PG_{18} -DOPE mixtures at 50:50 weight ratios (↓1,4,6 = PBS, ↓2 = EtOH, ↓3 = polymer-DOPE solution, ↓5 =BSA); schematic representation of DOPE lipid.

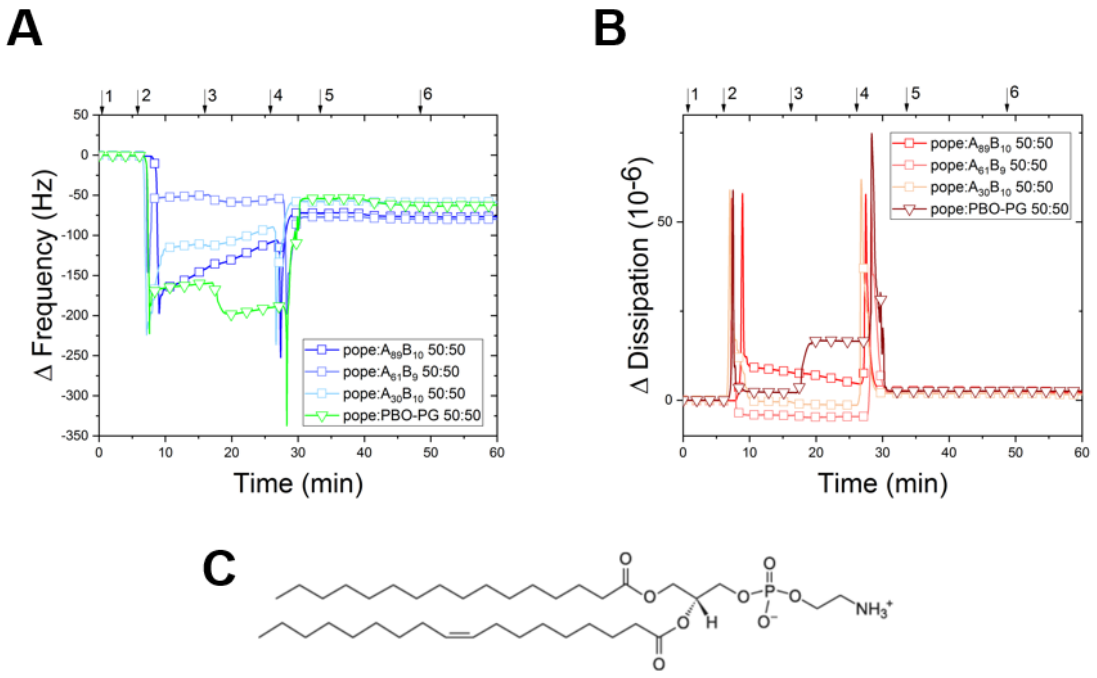

Figure 3.3-6. QCM-D plots of hybrid membrane formation: frequency (A) and dissipation (B) comparisons for A_xB_y-POPE at different PDMS block length and PBO_{50}-PG_{18} -POPE

mixtures at 50:50 weight ratios (↓1,4,6 = PBS, ↓2 = EtOH, ↓3 = polymer-POPE solution, ↓5 =BSA); schematic representation of POPE lipid.

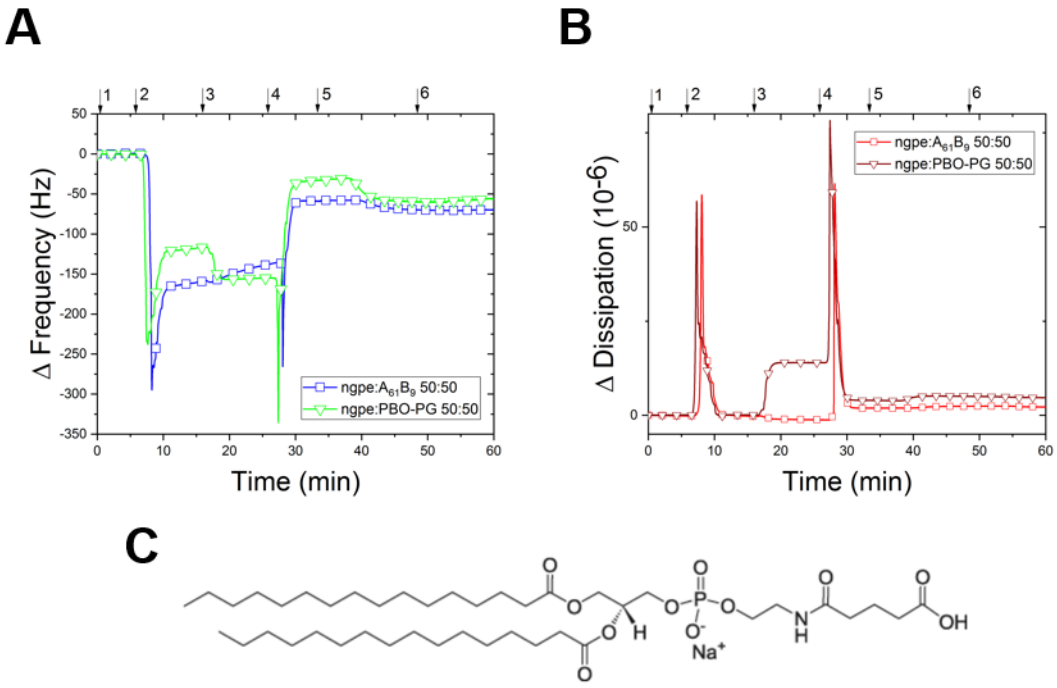

Figure 3.3-7. QCM-D plots of hybrid membrane formation: frequency (A) and dissipation (B) comparisons for $A_{61}B_9$-NGPE and PBO_{50}-PG_{18} -NGPE mixtures at 50:50 weight ratios (↓1,4,6 = PBS, ↓2 = EtOH, ↓3 = polymer-NGPE solution, ↓5 =BSA); schematic representation of NGPE lipid.

Frequency shifts for membrane formation and BSA step obtained with QCM-D experiments, together with calculated average thickness and membrane coverage, are reported in Table 7-11 (see Appendix). Overall, we observed that the higher length of the polymer block compared to lipid, was a determining factor for the membrane thickness and the influence of the lipids was negligible in this regard.[278]

To analyse the influence of the polymer-lipid composition on the quality of the obtained solid-supported membrane we, we compared the membrane coverage for the different lipids when combined with PDMS-PMOXA polymers (Figure 3.3-8 A and B). Moreover, we constructed a contour plot to associatetthe hydrophobicity, provided both by the polymer and lipid chains (Figure 3.3-8 C), to the membrane coverage. As observed, a longer lipid chain decreases the

chain mismatch and contributes to the formation of a planar assembly with better membrane coverage.[258] On the other side, a long hydrophobic polymer blocks may have favoured different membrane assembly according to the curvature and packing parameter, which resulted in the formation of inverted micelles instead of a planar membrane, or in the rearrangement of the membrane architecture when the membrane was dried.[279–281] The best membrane quality for the membrane obtained by this library of polymer was found for intermediate values of hydrophobic block length (circa 60 units)..[258] On the other side, a high hydrophobic polymer block length may have favoured a three dimensional rather than a bi-dimensional assembly according to the curvature and packing parameter.[279–281] The best membrane quality for the membrane obtained by this library of polymer was found for intermediate values of hydrophobic block length (circa 60 units). The average thickness of hybrid membrane is reported in function of lipid and PDMS-PMOXA polymer (Figure 7-14 A in Appendix): the higher values found for middle length polymer chain are supported by the membrane coverage data, which clarifies that the lower average thickness is related to the incomplete membrane formation rather than a mere polymer assembly. When PDMS-*b*-PMOXA was used, the hgher membrane thickness was recorded when 60 PDMS units and 36 chain units were combined. When PEO-*b*-PG was used, we obtained in general membranes with lower quality. The coverage resulted high for the longest lipid chain. In the latter case polymer hydrophobicity was kept constant (50 PEO block units). A different lipid hydrophobic tails drastically affected the membrane thickness. We believe this is not the only factor affecting the membrane architecture, which can be the aim of complementary study for the optimization of the membrane formation (Figure 7-14 B in Appendix). Higher hydrophilicity of PEO-PG when compared to PDMS-PMOXA, was a second parameter to take in account for the membrane assembly, and we would expected a better coverage for a shorter lipid chain. Nevertheless, the length mismatch between and polymers was a more determining factor in this regard: a longer lipid tails lead to the formation of membranes with higher coverage.

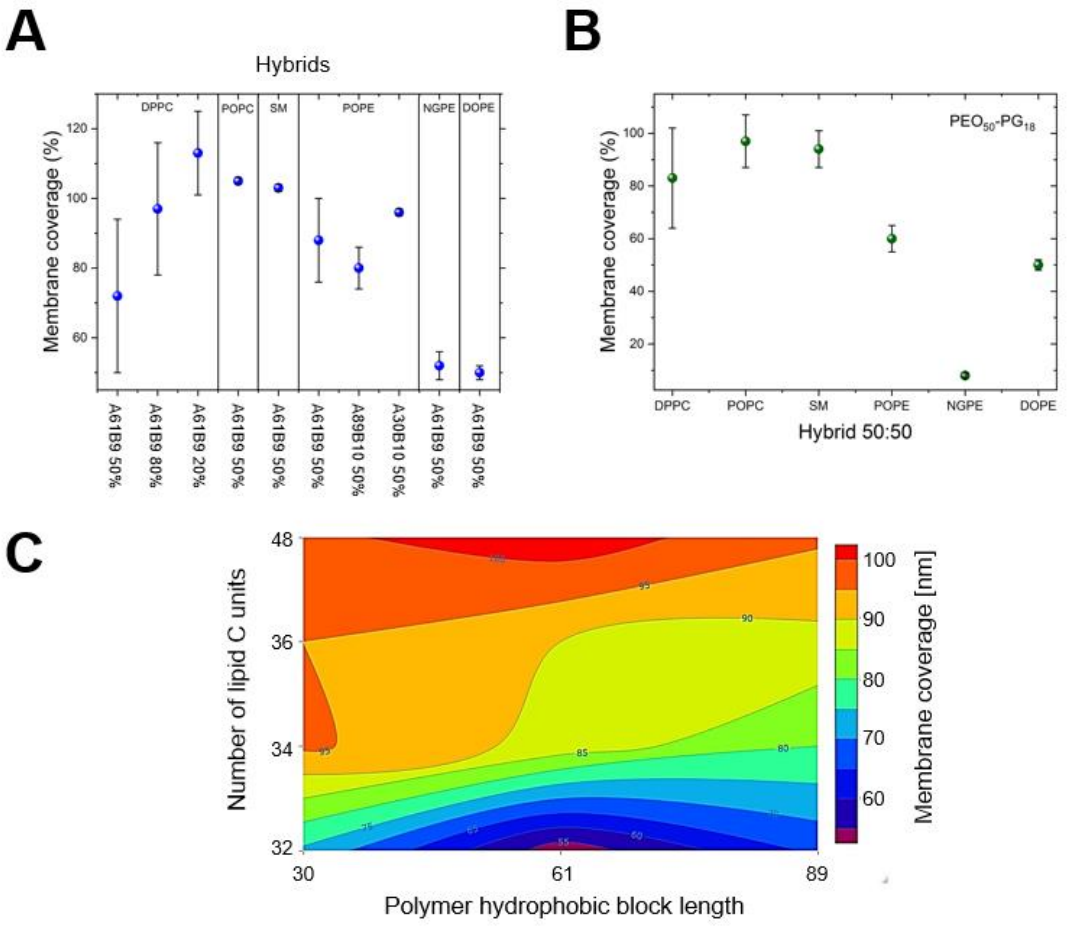

Figure 3.3-8. Scatter plot for different hybrid membranes composed of lipids and PDMS-PMOXA (A) or PEO-PG (B) polymers; contour plot reporting the membrane coverage in function of PDMS-PMOXA polymers and lipids hydrophobicity (C).

Despite the different lipid or polymer used, the SA method facilitated the successful preparation of hybrid membranes deposited onto silica support. The membrane coverage of polymer-lipid hybrid membranes obtained in this way was slightly lower than the one obtained with LB method.[266] This is due to the difference in the forces applied to induce the planar architecture that is the compression in LB method, instead of a self-assembly induced my the solvent exchange in SA method. This finding is of crucial importance for the application of SA method, considering the remarkable saving in time and quantity of sample gained at the expense of a small reduction of the membrane quality. Other structural and chemical parameters, such as glass transition temperature of the polymers[276,282] and melting temperature

and saturation of the lipids[283] may have influenced the polymer attachment onto the silica surface.

3.3.2. Characterization of membrane morphology

To obtain information about the hybrid membrane morphology, we analysed the hybrid membraned by AFM. Height and phase images of hybrid membranes were acquired with the purpose of: i) observe the phase domain separation; ii) evaluate the thickness mismatch between the membrane domains; iii) measure the height of polymer islands formed with SA method. Phase domain separation in polymer-lipid hybrid membranes is the key to create biomimetic materials, which replicates the functions of lipid rafts in cell membranes. The selective anchoring of biomolecules onto the lipid or polymer domain allows the development of versatile membranes with specific properties.[103,266]

First, we investigated the representative hybrid membranes previously obtained and monitored by QCM-D. Then, we expanded this study to other hybrid membranes obtained with a homemade device. This device was composed of two chambers and allowed the simultaneous preparation of two membranes per experiment, under the established SA protocol. We combined DPPC lipid with PDMS-*b*-PMOXA polymer of different hydrophobic chain lengths. When 89 PDMS repeating units were used, the hybrid membrane presented a planar assembly and a clear phase domain separation. The AFM height mismatch observed for the phase domains was of 4-6 nm (Figure 3.3-9). Additionally, the domain separation obtained in dry conditions was very similar to the one of the same hybrid membrane obtained with a different preparation method.[266] The presence of polymer islands typical of membranes obtained with SA method, were found only in the dry membrane. This suggested a partial reassemble of the hybrid membrane in dry conditions. Additionally, the domain separation obtained in dry conditions was very similar to the one of the same hybrid membrane obtained with a different preparation method (LB, see chapter 3.1).

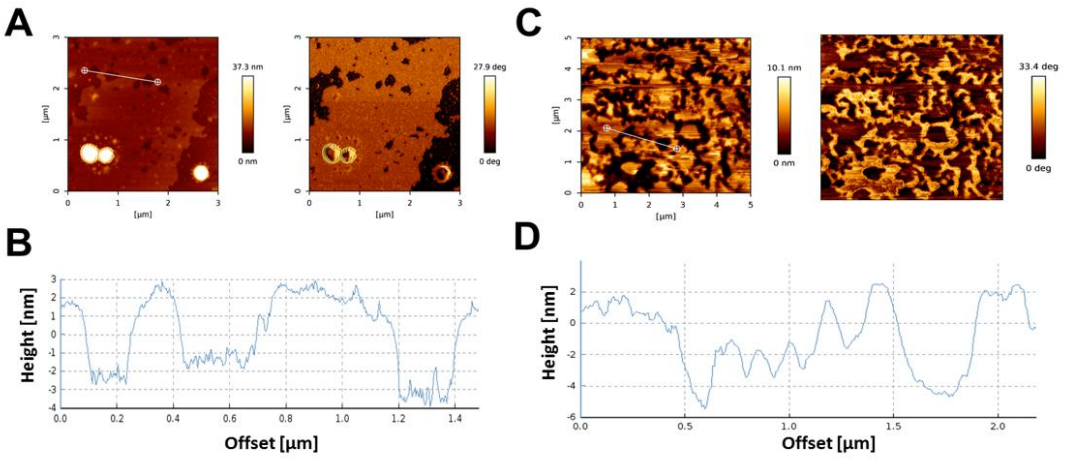

Figure 3.3-9. AFM characterization of membrane composed of $A_{89}B_{10}$ polymer and DPPC lipid (50:50 w/w): height image and phase image (A in air, C in water); cross section (B in air, D in water).

The combination of DPPC with PDMS-*b*-PMOXA (PDMS of 61 repeating units) and PBO_{50}-*b*-PG_{18} copolymers resulted in hybrid membranes with a defined phase membrane separation (Figure 7-15 in Appendix), and this facilitates a further biomolecule combination toward a specific membrane domain. The membrane architecture was found here also planar with the presence in both cases of polymer islands. According to the polymer conformation and hydrophobic/hydrophilic properties, the domain mismatch was different: 7±3 nm for PDMS-b-PMOXA, less than 1 nm for PBO-*b*-PG, a smooth membrane in the latter case.

SM was blended to PDMS-*b*-PMOXA at different PDMS block length, and PBO-*b*-PG, successfully forming planar membranes with phase domain separation (Figure 7-17, 7-18 and 7-19 in Appendix). The domain thickness mismatch measured was of 6±2 nm when $A_{61}B_9$ polymer was used, with defined lipid domains (Figure 3.3-10).

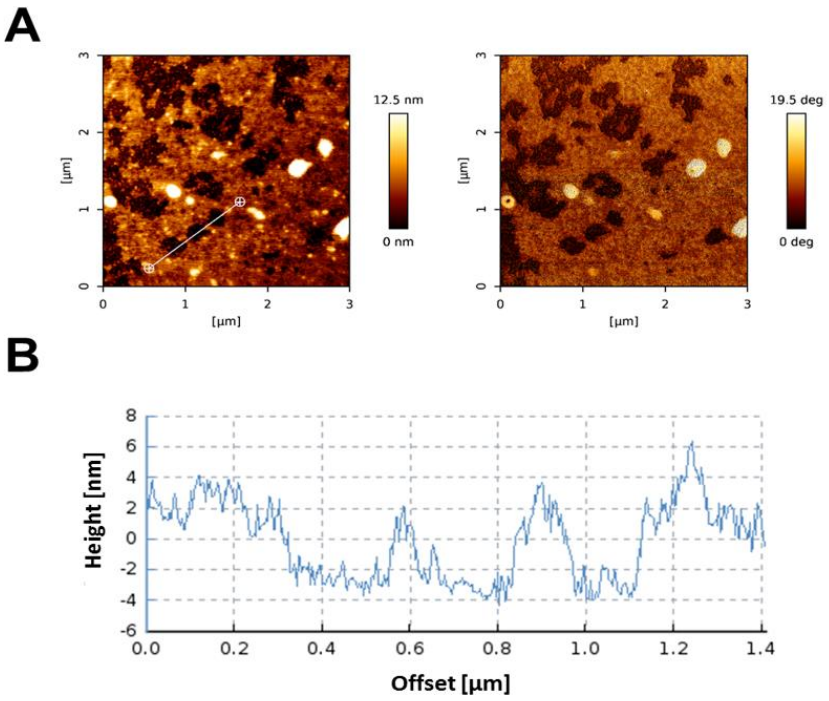

Figure 3.3-10. AFM characterization of membrane composed of $A_{61}B_9$ polymer and SM lipid (50:50 w/w): height image and phase image (A); cross section (B).

Hybrid membranes were also obtained for other mixture of PDMS-PMOXA and PBO-PG copolymer and SM, and showed phase domain separation in most cases, except for the polymer $A_{89}B_{10}$ (Figure 7-16 Appendix). We found out that also for hybrid mixtures, the number of polymer hydrophobic repeating units influences the membrane architecture and the domain mismatch is useful for predicting the behaviour of lipid domains. These domains are embedded into a polymer matrix, as the darker colour in the height profile showed. According to the hydrophobic/hydrophilic ratio of the polymer, the lipid inserts at different depths into the polymer bulk, determining the mismatch. We found out that also for hybrid mixtures, the number of polymer hydrophobic repeating units influences the membrane architecture

SA method applied on PDMS-*b*-PMOXA (PDMS blocks of 89 and 61) and NGPE lipid resulted also to be successful in terms of hybrid membrane formation and phase domain separation, with greater islands formation for shorter hydrophobic polymer chain (Figure 3.3-11). Instead, when NGPE was blended with PBO-PG, the images provided by dry AFM showed no membrane formation, rather the attachment of 3-4 nm height micelles onto the silica support (Figure 7-20 Appendix).

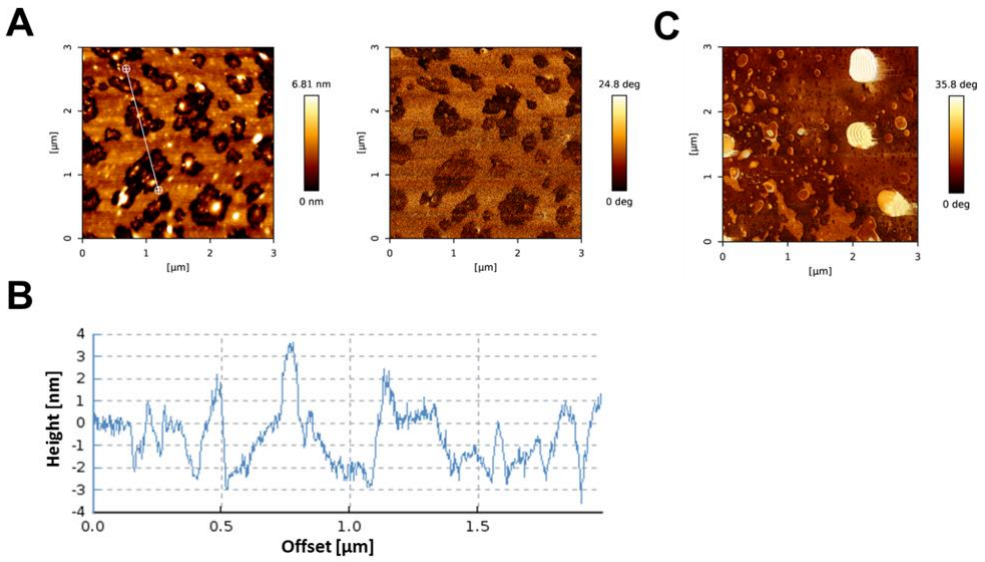

Figure 3.3-11. AFM characterization of membrane composed of $A_{89}B_{10}$ polymer and NGPE lipid (50:50 w/w): height image and phase image (A); cross section (B); phase image of $A_{61}B_{9}$-NGPE membrane (50:50 w/w) (C).

A limitation has been observed when POPE phospholipid was chosen for the hybrid mixture: the formation of membranes composed of POPE and both PDMS-PMOXA or PBO-PG copolymers was in both cases not possible (Figure 3.3-12 and Figure 7-21). The reason behind this could be related to the combination of factor such as the charge and saturation of the lipid,[284,285] in addition to the asymmetry derived from the polymer-lipid hydrophobic mismatch.[275] Characterized by AFM, phase and height images acquired showed that, regardless the length of the PDMS block (89, 61 and 30), the drying process lead to incomplete membrane formation and to the presence of several islands or fused vesicles with height values between 15 and 30 nm. The absence of phase domain separation together with the instability in air of hybrid membranes formed with POPE, made this lipid not a good candidate for the preparation of biomimetic platforms via SA method.

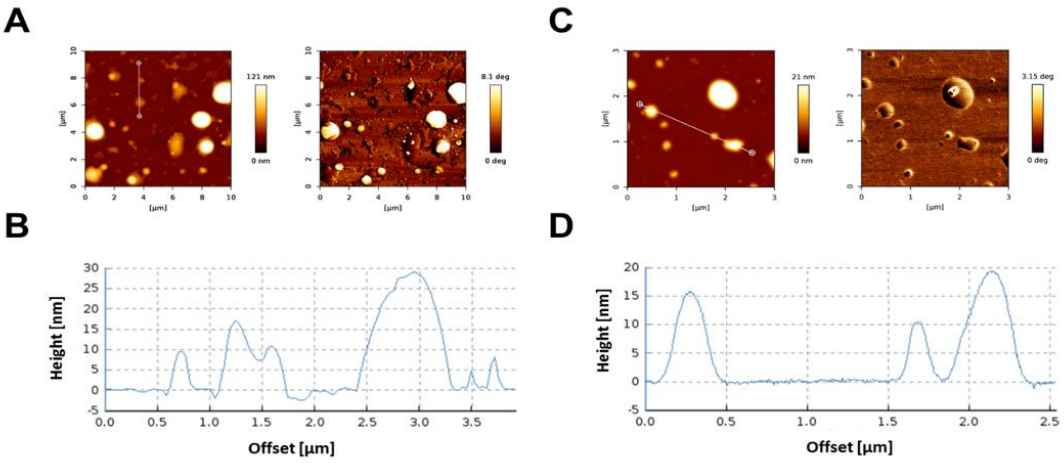

Figure 3.3-12. AFM characterization of membrane composed of $A_{30}B_{10}$-POPE (A and B) and $A_{89}B_{10}$-POPE (C and D) at 50:50 w/w. Height image and phase image are reported.

The morphology information regarding the phase domain separation and island formation are reported for the different hybrid membranes obtained and characterized by AFM (Figure 3.3-1). AFM images confirmed the formation of island, which were found as a probable consequence of the drying process and assumed different sizes according to the lipid used. DPPC and POPE formed big islands, whereas SM and NGPE small ones. We obtained a clear phase domain separation for all the polymer-lipid combination except for the POPE lipid. It is well known that the asymmetric distribution of lipids between the leaflets of biological membranes contributes to their curvature stress, and we believe that the same principle applies for polymer-lipid hybrid membranes. Accordingly, this can be extended to our study: for the membrane that could not keep a planar assembly resulting in a membrane detachment from the support (poor coverage, defected) as well as in the formation of island.[286–288]

An AFM comparison between a good quality membrane (high membrane coverage) and a poor quality, defective membrane are reported in Figure 3.3-13. There are major differences in the morphological characteristics and assembly for the two polymer-lipid mixtures: in $A_{89}B_{10}$-NGPE hybrid (Figure 3.3-13 A) a clear phase domain separation is visible, where the darker "stains" represents clusters of lipids entrapped in a polymer matrix, as observed for other hybrid membranes deposited with LB method.[266] The planar assembly is also clear for this combination, with a domain mismatch of 4-6 nm, in opposition to the 15-30 nm high vesicles

assembly found for the hybrid $A_{30}B_{10}$-POPE (Figure 3.3-13 B). No phase separation was observed for this hybrid combination.

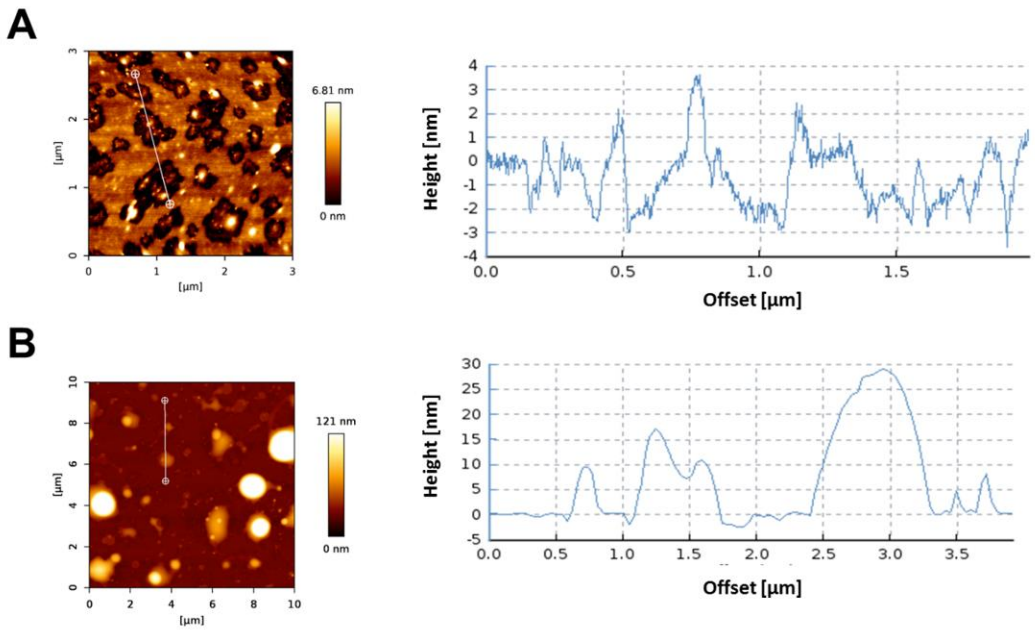

Figure 3.3-13. AFM height image comparisons between membranes with good and bad quality in terms of coverage and phase separation (A) and defected membranes (B) obtained with SA method.

Hybrid mixture (50:50 w/w)	Membrane coverage (%)	Phase domain separation	Islands presence
DPPC-$A_{89}B_{10}$	n.a.	yes	big
DPPC-$A_{89}B_{10}$ (in water)	n.a.	yes	no
DPPC-$A_{61}B_{9}$	72 ± 22	yes	big
DPPC-$PBO_{50}PG_{18}$	83 ± 19	yes	small
POPE-$A_{61}B_{9}$	88 ± 12	no	big
POPE-$A_{89}B_{10}$	80 ± 6	no	big
POPE-$A_{30}B_{10}$	96 ± 0	no	big
POPE-$PBO_{50}PG_{18}$	60 ± 5	not clear	big

SM-$A_{61}B_9$	103 ± 0	yes	small
SM-$A_{89}B_{10}$	n.a.	no	small
SM-$A_{30}B_{10}$	n.a.	yes	small
SM-$PBO_{50}PG_{18}$	94 ± 7	yes	small
NGPE-$A_{89}B_{10}$	n.a.	yes	no
NGPE-$A_{61}B_9$	52 ± 4	not clear	small
NGPE-$PBO_{50}PG_{18}$	8 ± 0	no	small

Table 3.3-1. Evaluation of the morphology properties of different polymer-lipid membranes obtained by AFM height and phase characterization and comparison with the membrane coverage.

Information regarding the stability of hybrid membranes in dry conditions are reported in Appendix (Figure 7-13). Due to the mechanical resistance of polymers, the membranes were in most cases able to preserve their planar assembly in dry conditions, except when the POPE lipid was used in the hybrid mixture. Despite the different lipid or polymer used, the SA method facilitated the successful preparation of hybrid membranes deposited onto silica support.

In this part of the thesis we demonstrated that SA method applied on hybrid mixtures of polymer and lipids was in most of the cases successful for creating hybrid membranes onto solid support with a planar assembly, a good membrane coverage with a low amount of defects, and an evident phase domain separation.

4. Conclusions and outlooks

The combination of artificial membranes with biomolecules has high potential for the development of bio-interfaces with desired properties, given by the specificity of the biomolecules. In the first part of this thesis, we used two strategies (insertion and conjugation) for the selective combination of cyt c with a hybrid membrane composed of PDMS-*b*-PMOXA copolymers and DPPC lipid. It was possible to control the protein recombination into a specific phase membrane domain of hybrid membrane: by behaving similarly to rafts in cell membranes, lipid domains in the hybrid preferentially induced the cyt c insertion into themselves, whereas the carboxylic functionalization promoted the cyt c conjugation onto polymer domains. It was also found that the protein activity was higher in hybrid membranes because of the synergic properties of lipids and polymers. Moreover, the conjugation strategy revealed to be the best approach for increasing the cyt c accessibility, and thus its activity.

In the second part of this thesis, we applied for the first time the solvent-assisted method to PDMS-b-PMOXA diblock and triblock copolymers to form polymer porous membranes highly reproducible, regardless of the hydrophobic block length or the structure of the polymer used. Polymer membranes obtained in this way present biocompatibility and good mechanical resistance, and can be employed as biomimetic platforms in different fields of application. In this specific case, the biotin functionalization of the polymer increased the versatility of the system. We investigated the interaction between our polymer membranes and DNA strands and the ADAse throught the well established biotin-streptavidin chemistry. Also in this case, biomolecules were able to perform their activity after the recombination with the membrane.

In the third part of the thesis, we studied the creation of multiple solid supported hybrid membranes, based on the advantages that SA offers (e.g. straightforward, versatility, low costs and small quantity of sample needed). Various compositions of polymers and lipids have been tested, and the hybrid membrane formation conditions were optimized. The physico-chemical membrane characteristics were studied by a combination of QCM-D and AFM. The goal of this study was to reveal the influence of physical characteristics such as: lipid to polymer ratio, hydrophobic to hydrophilic block polymer ratio and length of polymer and lipid chains on the resulting quality and morphology of hybrid membranes. Particularly, we looked at lipid-polymer domain separation, average thickness and characteristic assemblies (such as “vesicle-like” structures or “islands”) of the hybrid membrane. This takes us one-step further towards the understanding of the molecular parameters and the appropriate conditions for the

fabrication of solid supported hybrid membranes matching the current requirements of biomedical applications regarding nano-sized materials. Our main findings suggest that SA method is a valid alternative to other preparation methods for the development of solid-supported membranes. This work puts the basis for the development of novel polymer-lipid hybrid platforms benefitting from the best properties of both components: mechanical resistance from the polymers and enhanced fluidity from lipids. A possible next step requires more information about mechanical and viscoelastic properties for hybrid membranes. By expanding the libraries of copolymer and lipid employed and by changing the experimental conditions (e.g. pH, temperature), a prediction model for the preparation of planar hybrid supported membranes free o major defects can be established.

To summarize, the main goals of the thesis achieved were the following: i) self-assembly of polymers and hybrids into membranes with exposed functional groups, accessible for further biomolecule combination, ii) optimization of the novel solvent-assisted method to be applied onto polymer and hybrid membranes, iii) control over the biomolecule-membrane combination through spontaneous insertion or covalent bond formation and iv) evaluation of the preserved functionality of the biomolecules after the membrane recombination.

Taken together, these results support further development of the complex and versatile polymer and hybrid bio-interfaces by indicating the molecular factors that are relevant when biomolecules are combined with artificial membranes, especially when they are hybrid, containing lipid and polymer domains. Moreover, the use of the novel solvent-assisted approach opens the possibility for an easy and quick pathway to produce solid-supported membranes and to combine them with several different biomolecules.

5. Materials and Methods

5.1. Materials

Phospholipids POPE, SM, NGPE, DOPE POPE, DPPC, Liss Rhod DOPE and Rhodamine B-labeled DPPC were purchased from Avanti Polar Lipids (Alabaster, AL). Cyt *c* from bovine heart (≥95%) was obtained from Sigma-Aldrich and reconstituted to a concentration of 500 μg/mL with PB solution. PB was prepared using Na2HPO4·7H2O and NaH2PO4 which were purchased from Sigma-Aldrich. The phosphate buffer saline (PBS), BSA and ethanol were purchased from Sigma-Aldrich. EDC, sNHS, and all reported organic solvents were obtained from Sigma-Aldrich. Sav and avidin were purchased from Sigma and DNA strands from IDT. The silica slides (Ultrapak 100 mm thin wafer box) were purchased from Entegris Inc. (Germany) and used for layer deposition. All the diblock and triblock copolymers were provided by this group.

5.2. Preparation

5.2.1. Polymer Synthesis

PDMS-OH was activated with trifluoromethanesulfonic anhydride and chain-extended by cationic ring-opening polymerization with the 2-methyl-2-oxazoline monomer and quenched with triethylamine/water in order to obtain hydroxy-functionalized PDMS-b-PMOXA-OH.

The amphiphilic diblock copolymer PDMS-*b*-PMOXA-COOH was synthesized according to the following protocol: PDMS-OH was activated with trifluoromethanesulfonic anhydride and chain-extended by cationic ring-opening polymerization with the MOXA monomer. Quenching with triethylamine/water in order to obtain hydroxy-functionalized PDMS-*b*-PMOXA-OH was followed by end-group modification with succinic anhydride, leading to the final carboxy-functionalized PDMS-*b*-PMOXA-COOH. The dispersity of the copolymer was 2.09 according to gel permeation chromatography (GPC). In order to confirm the presence of the COOH end groups, FTIR was performed.

The amphiphilic triblock copolymer PMOXA-PDMS-PMOXA was synthesized according to an established protocol:[289] Potassium tert-butoxide solution (KOtBu, 0.25 mol L−1 in 1,4-dioxane, 6.44 mL, 1.61 mmol, 1 eq.) was transferred into a 20 mL microwave vial with a magnetic stirrer in a glovebox. Then, 1,4-dioxane (0.66 mL) and a solution of 18-crown-6 (0.50

mol L−1 in dioxane, 1.61 mL, 0.804 mmol, 0.5 eq.) was added. The vial was closed and unloaded together with a syringe filled with 1,2-butylene oxide (BO, 7.00 mL, 80.4 mmol, 50 eq.). BO was added to the reaction mixture through the septum of the lid and the microwave-assisted reaction was immediately started. The first heating step for two minutes at 50 °C was followed by the second step of two minutes at 60 °C and finally 30 min at 70 °C. After cooling to room temperature, the polymerisation was quenched by adding methanol (2 mL). After stirring overnight, the solvents and unreacted monomer were evaporated using a rotary evaporator. The crude polymer was dissolved in n-hexane (100 mL) and washed with methanol (100 mL) in order to remove all polar side products. The bottom methanol enriched phase was extracted three times with n-hexane (each 100 mL), the four hexane phases were combined and the solvent evaporated on a rotary evaporator. After drying overnight in high vacuum (0.05 mbar) the polymer was stored in a glovebox under argon. 4.69 g (Mn(NMR) = 3100 g mol−1, 1.51 mmol, Đ(SEC) = 1.05) of colourless, viscous poly(butylene oxide)$_{42}$ (PBO$_{42}$) were obtained.

PBO-PG was synthesized according to an established protocol:[276] potassium tert-butoxide solution was transferred into a 20 mL microwave vial with a magnetic stirrer in a glovebox. Then, 1,4-dioxane and a solution of 18-crown-6 was added. The vial was closed and unloaded together with a syringe filled with 1,2-butylene oxide. BO was added to the reaction mixture and the microwave-assisted reaction was immediately started. After the heating step and cooling to room temperature, the polymerization was quenched by adding methanol. After stirring overnight, the solvents and unreacted monomer were evaporated using a rotary evaporator. The crude polymer was dissolved in n-hexane and washed with methanol in order to remove all polar side products. The bottom methanol enriched phase was extracted three times with n-hexane, the four hexane phases were combined and the solvent evaporated on a rotary evaporator. After drying overnight in high vacuum the polymer was stored in a glovebox under argon. PBO$_{42}$ was obtained. PBO$_{42}$ was transferred into a microwave vial with a magnetic stirrer. 1,4-Dioxane was added and the vial was closed. A solution of potassium naphthalenide was added to the solution dropwise under shaking through the septum of the lid, until the equivalent point was reached. Then was added to quench the reaction. After stirring, and solvents evaporation, the cleavage of the protecting groups was performed. The copolymer solution was then dialysed for two days and PBO$_{42}$-*b*-PG$_{21}$ was obtained.

All the polymers used were characterized by NMR (see Appendix).

5.2.2. Activation of the carboxylic end group of copolymers in the membranes by EDC/sNHS

For the covalent combination of cyt *c* to the copolymers in the solid-supported membranes, the functional carboxylic end groups were first activated to amine-reactive sNHS esters by submerging the membranes in 3 mL of EDC solution (10 mg/mL in PB) for 10 min under gentle agitation. After washing with PB for 30 min to remove the unbound molecules, the membranes were submerged into sNHS solution (10 mg/mL in PB) for 10 min and washed again with buffer.

5.2.3. Preparation of ADAse

Catalyst precursor [CpRu(CH3CN)3]PF6 (4 mM in DMF) and ligand (4 mM in DMF) were mixed in a 1:1 ration to afford the ADAse stock solution (2 mM in DMF). 1.20 uL of ADAse solution (77 nM final concentration; 1 eq. to SAV) was added to the SAV solution (5 ug/mL = 77 nM final concentration in PBS).

5.2.4. Catalysis on the membrane using ADAse

The Ru-SAV complex was directly bound to the membrane with the same procedure: a solution of Ru-SAV in PBS (C = 77 nM) was injected for 15 minutes at a flow rate of 25 uL/min. After a rinsing step with PBS, the QCM sensor was submerged in fresh PBS (2 mL) and the fluorescent substrate (20 μM final concentration) was added for the fluorimetry measurement. The reaction was incubated at 30 °C and measurements were taken at time 0, 4, 24 and 48 hours. To determine the background fluorescence, PBS and a substrate solution (20 μM in PBS) were also measured. Additionally the free artificial metalloenzyme in solution (77 nM, non-membrane bound) was also analysed by adding it to a substrate solution (20 μM).

5.2.5. Preparation of silica wafers

Silica wafers were cut into slides of 1 cm2 that were rinsed with ethanol and dried. Before using, slides were placed in a UV ozone cleaner (Jelight Company Inc, Irvine, USA) for 20 min to remove contaminants from the surface. The cleaned slides were immediately used for layer deposition.

5.2.6. Membrane preparation with the solvent-assisted polymer bilayer method

The formation of the polymer membrane was performed directly onto QCM silica sensors and monitored using a QCM-D device. The QCM sensors were rinsed with water and ethanol and placed in a UV ozone cleaner (Jelight Company Inc, Irvine, USA) for 20 min to remove contaminants from the surface. The resulting sensors were immediately used for layer deposition: i) water was used for the baseline for 5 min; ii) ethanol was injected for 10 min, till the new stabilization of the baseline; the sample solution was added for 15 min; water was used for 10 min to induce the membrane assembly. For evaluating the membrane quality, a BSA solution (C = 0.5 mg/L) was added for 15 min, directly after the membrane formation , followed by the water rinsing for 10 min. All the biomolecules anchoring were performed after the BSA test by injecting the solution for 15-20 min; then, the water rinsing was performed to remove the molecules adsorbed. Solutions of polymer and of lipid-polymer hybrid mixture at different molar ratios were prepared by dissolving the samples in ethanol (C = 0.5 mg/L). The flow rate was kept at a constant value of 100 μL/min during the SAPB experiment or 50 μL/min during the protein attachment.

5.2.7. Polymer membrane decoration with biomolecules

The avidin attachment was performed according to the following procedure: PBS rinsing of the membrane (step 1); injection of the avidin solution (C = 50 ug/ml in PBS) for 20 minutes at a constant flow rate of 50 μl/min (step 2); final PBS rinsing for an additional 10 minutes to remove the unbound avidin (step 3).

Streptavidin (Sav) was bound to the membrane as follows: a solution of Sav in PBS (C = 5 μg/mL) was injected for 15 minutes at a flow rate of 50 uL/min.

A solution of a biotinylated DNA strand with the sequence 5BiosG/TTTTTTTTTTTTAACAGGATTAGCAGAGCGAGG (C = 100 nM) followd by its complementary sequence CCTCGCTCTGCTAATCCTGTT (C = 100 nM) were attached to the membrane Sav through the biotin/Sav chemistry. The DNA solutions were injected for 15 minutes at a flow rate of 50 uL/min. The rinsing step with PBS was performed at 50 uL/min for 10 minutes after each attachment in order to remove the unbound biomolecules. The attachment of each biomolecule was performed in the QCM device and monitored in situ.

5.2.8. Catalysis on the membrane using the ADAse

The ADAse was bound to the functionalized membrane as follows: a solution of ADAse in PBS (C = 80 nM) was injected for 15 minutes at a flow rate of 25 uL/min. After a rinsing step

with PBS, the QCM sensor was dipped into fresh PBS (2 mL) and the fluorescent substrate N-(allyloxycarbonyl)-aminocoumarin (2, 20 μM final concentration) was added for the fluorimetry measurement. The reaction was incubated at 30 °C and the measurements were performed at the following times: 0h (hours), 4h, 24h and 48h. To determine the background fluorescence, PBS and solution of the coumarin substrate (2, 20 μM in PBS) were also measured. Additionally, the free artificial metalloenzyme in solution (77 nM, non-membrane bound) was also analysed by adding it to a substrate solution (20 μM).

The fluorescence was determined by analysing 200 μL of each sample at λex = 395 nm and λem = 470 nm. All measurements were carried out in triplicate. The conversion was determined by fluorescence using a calibration curve, which was prepared using aqueous solutions.

5.2.9. AFM Sample preparation

All the hybrid membranes for AFM measurements were obtained with a homemade device. The device consisted of a chamber with two compartments (1 cm2 each) for hosting the cut silica wafer and allowed the simultaneous preparation of two membranes per experiment, under the established SA protocol. The chamber was connected to a digital peristaltic pump (Ismatec, Glattbrugg, Switzerland) and sealed. The solutions were injected at constant flow, following the same procedures adopted for the QCM-D measurements.

5.3. Methods

5.3.1. Area-surface pressure isotherms

The area-dependent surface pressure isotherms of lipid, copolymer, and mixtures of lipid and copolymer were measured by Langmuir Teflon mini-trough (KSV Instruments, Finland). The trough was equipped with two movable computer-controlled Delrin barriers for variation of the area per molecule and a Wilhelmy plate made of filter paper for measuring the surface pressure. The trough and barriers were cleaned with high-purity chloroform (HPLC grade, Sigma-Aldrich) and ethanol (≤99.8%, Fluka) before each measurement, and the trough was filled with ultrapure water. A fresh Wilhelmy paper was mounted and fully wetted with ultrapure water every time. The copolymer, lipid, and hybrid mixtures in chloroform were diluted with chloroform to a concentration of 1 mg/mL. An aliquot was spread onto the ultraclean water subphase with a glass Hamilton microsyringe and left untouched for 10 min to allow for

chloroform evaporation. Then, the lipid, copolymer, or hybrid monolayers at the air–water interface were compressed with a constant rate of 10 mm min^{-1}. During all measurements, a constant temperature of 23 °C was maintained. All reported data represent triplicate measurements.

5.3.2. Brewster angle microscopy

BAM experiments were performed with the EP3SW system (Nanofilm Technologie GmbH, Göttingen, Germany) equipped with a Nd:YAG laser (λ = 532 nm), a long distance objective (Nikon, 20×), and a monochrome CCD camera. The size of the BAM image corresponds to 220 × 250 μm2, with a resolution of 1 μm. The microscope was installed over the KSV Langmuir trough equipped with two movable barriers that lead to symmetrical compression. The BAM measurements were done in triplicate in order to obtain the best representation of the images.

5.3.3. Langmuir–Blodgett transfer

The Langmuir monolayers formed at the air–water interface were deposited on the solid substrate (silica wafer or silicon dioxide sensor QSX 303 SiO2) using a vertical dipping method. The dipping speed was 0.5 mm/min for downstroke and upstroke, maintaining the surface pressure at 35 mN/m. The bilayer films were transferred to the silica substrate by immersing the dipper downstroke for deposition of the first layer and lifting it upstroke for deposition of the second layer.

5.3.4. Confocal laser scanning microscopy

For CLSM, 1–2 volume % of Liss Rhod PE was added to the lipid/copolymer mixture before the LB transfer to the solid support. The supported hybrid bilayer was transferred to a glass slide and imaged within 1 h after the LB deposition. CLSM images were recorded on a Zeiss 880 LSM equipped with a 40x water-immersion objective (C-Apochromat 40×/1.2 W Korr FCS M27). A DBSS 561–10 laser (λ = 561 nm) with laser power at 2% was used for the excitation of Liss Rhod PE. The fluorescence intensities of the images were analyzed by ImageJ (v. 1.52r).

5.3.5. Atomic force microscopy

AFM was performed with a JPK NanoWizard 3 AFM (JPK Instruments AG). AC mode topography images were obtained in air, using silicon cantilevers (Tap150 Al-G, Budget Sensors) with a nominal spring constant of 10–130 Nm–1 and a resonance frequency of 150 kHz. Images were analyzed with the data analysis software JPK Data Processing (v. 5.0).

5.3.6. Quartz crystal microbalance with dissipation

QCM-D with Q-Sense E1 (Biolin Scientific, Sweden) set up was employed to characterize the combination of cyt *c* to the membrane on silicon dioxide sensors. Changes in the resonance frequency (ΔF) and energy dissipation (ΔD) of the oscillating sensor chip (QSX 303 SiO2) as a function of time were simultaneously recorded at multiple odd overtones (3rd, 5th, 7th, 9th, and 11th). All data shown represent recordings at the 7th overtone. In order to estimate the mass of protein attached to the different membranes, the Sauerbrey equation was applied. This equation converts the frequency shift into mass using a simple relation; $\Delta m = -C\Delta f$, where Δm is the mass, C is the proportionality constant (17.7 ng cm–2 Hz–1), and Δf is the frequency shift. After establishing a baseline in aqueous buffer solution, QCM-D measurements were conducted under continuous flow conditions. A flow rate of 50 μL/min for the process of protein addition and washing was delivered using a Reglo Digital peristaltic pump (Ismatec, Glattbrugg, Switzerland). The temperature of the flow cell was fixed at 24.0 ± 0.5 °C.

5.3.7. Fluorimetry

Fluorimetry was performed with a Spectramax M5e microplate and cuvette reader (Molecular Devices, USA) using a 10 mm light path quartz cuvette (Hellma, Germany), an excitation wavelength of 570 nm, and an emission wavelength of 595 nm. All specimens were measured immediately after QCM-D. The silica substrate was placed standing upright in the cuvette, facing the light source. AR and H2O2 were added to a final concentration of 3.3 and 0.66 mM, respectively, and the final volume was adjusted to 3 mL with 100 mM PB.

6. Bibliography

(1) Singer, S. J.; Nicolson, G. L. The Fluid Mosaic Model of the Structure of Cell Membranes. *Science* **1972**, *175* (4023), 720–731. https://doi.org/10.1126/science.175.4023.720.

(2) Uddin, M. N.; Basak, D.; Hopefl, R.; Minofar, B. Potential Application of Ionic Liquids in Pharmaceutical Dosage Forms for Small Molecule Drug and Vaccine Delivery System. *J Pharm Pharm Sci* **2020**, *23*, 158–176. https://doi.org/10.18433/jpps30965.

(3) Nam, J.; Beales, P. A.; Vanderlick, T. K. Giant Phospholipid/Block Copolymer Hybrid Vesicles: Mixing Behavior and Domain Formation. *Langmuir* **2011**, *27* (1), 1–6. https://doi.org/10.1021/la103428g.

(4) Jain, S. On the Origins of Morphological Complexity in Block Copolymer Surfactants. *Science* **2003**, *300* (5618), 460–464. https://doi.org/10.1126/science.1082193.

(5) Shen, Y.; Saboe, P. O.; Sines, I. T.; Erbakan, M.; Kumar, M. Biomimetic Membranes: A Review. *Journal of Membrane Science* **2014**, *454*, 359–381. https://doi.org/10.1016/j.memsci.2013.12.019.

(6) Antonietti, M.; Förster, S. Vesicles and Liposomes: A Self-Assembly Principle Beyond Lipids. *Adv. Mater.* **2003**, *15* (16), 1323–1333. https://doi.org/10.1002/adma.200300010.

(7) Discher, B. M. Polymersomes: Tough Vesicles Made from Diblock Copolymers. *Science* **1999**, *284* (5417), 1143–1146. https://doi.org/10.1126/science.284.5417.1143.

(8) Deng, Y.; Wang, Y.; Holtz, B.; Li, J.; Traaseth, N.; Veglia, G.; Stottrup, B. J.; Elde, R.; Pei, D.; Guo, A.; Zhu, X.-Y. Fluidic and Air-Stable Supported Lipid Bilayer and Cell-Mimicking Microarrays. *J. Am. Chem. Soc.* **2008**, *130* (19), 6267–6271. https://doi.org/10.1021/ja800049f.

(9) Schwartz, D. K. Langmuir-Blodgett Film Structure. *Surface Science Reports* **1997**, *27* (7–8), 245–334. https://doi.org/10.1016/S0167-5729(97)00003-4.

(10) Pera, I.; Stark, R.; Kappl, M.; Butt, H.-J.; Benfenati, F. Using the Atomic Force Microscope to Study the Interaction between Two Solid Supported Lipid Bilayers and the Influence of Synapsin I. *Biophysical Journal* **2004**, *87* (4), 2446–2455. https://doi.org/10.1529/biophysj.104.044214.

(11) Battaglia, G.; Ryan, A. J. Bilayers and Interdigitation in Block Copolymer Vesicles. *J. Am. Chem. Soc.* **2005**, *127* (24), 8757–8764. https://doi.org/10.1021/ja050742y.

(12) Roskamp, R. F.; Vockenroth, I. K.; Eisenmenger, N.; Braunagel, J.; Köper, I. Functional Tethered Bilayer Lipid Membranes on Aluminum Oxide. *ChemPhysChem* **2008**, *9* (13), 1920–1924. https://doi.org/10.1002/cphc.200800248.

(13) Lee, J. C.-M.; Santore, M.; Bates, F. S.; Discher, D. E. From Membranes to Melts, Rouse to Reptation: Diffusion in Polymersome versus Lipid Bilayers. *Macromolecules* **2002**, *35* (2), 323–326. https://doi.org/10.1021/ma0112063.

(14) Kumar, M.; Grzelakowski, M.; Zilles, J.; Clark, M.; Meier, W. Highly Permeable Polymeric Membranes Based on the Incorporation of the Functional Water Channel Protein Aquaporin Z. *Proceedings of the National Academy of Sciences* **2007**, *104* (52), 20719–20724. https://doi.org/10.1073/pnas.0708762104.

(15) Rakhmatullina, E.; Meier, W. Solid-Supported Block Copolymer Membranes through Interfacial Adsorption of Charged Block Copolymer Vesicles. *Langmuir* **2008**, *24* (12), 6254–6261. https://doi.org/10.1021/la8003068.

(16) Tanford, C. The Hydrophobic Effect and the Organization of Living Matter. *Science* **1978**, *200* (4345), 1012–1018. https://doi.org/10.1126/science.653353.

(17) Tu, Y.-M.; Song, W.; Ren, T.; Shen, Y.; Chowdhury, R.; Rajapaksha, P.; Culp, T. E.; Samineni, L.; Lang, C.; Thokkadam, A.; Carson, D.; Dai, Y.; Mukthar, A.; Zhang, M.; Parshin, A.; Sloand, J. N.; Medina, S. H.; Grzelakowski, M.; Bhattacharya, D.; Phillip, W. A.; Gomez, E. D.; Hickey, R. J.; Wei, Y.; Kumar, M. Rapid Fabrication of Precise High-Throughput Filters from Membrane Protein Nanosheets. *Nat. Mater.* **2020**, *19* (3), 347–354. https://doi.org/10.1038/s41563-019-0577-z.

(18) Discher, D. E. Polymer Vesicles. *Science* **2002**, *297* (5583), 967–973. https://doi.org/10.1126/science.1074972.

(19) Blanazs, A.; Armes, S. P.; Ryan, A. J. Self-Assembled Block Copolymer Aggregates: From Micelles to Vesicles and Their Biological Applications. *Macromol. Rapid Commun.* **2009**, *30* (4–5), 267–277. https://doi.org/10.1002/marc.200800713.

(20) Chen, Q.; Wilhelmina de Groot, G.; Schönherr, H.; Julius Vancso, G. Patterns of Surface Immobilized Block Copolymer Vesicle Nanoreactors. *European Polymer Journal* **2011**, *47* (2), 130–138. https://doi.org/10.1016/j.eurpolymj.2010.11.005.

(21) LoPresti, C.; Lomas, H.; Massignani, M.; Smart, T.; Battaglia, G. Polymersomes: Nature Inspired Nanometer Sized Compartments. *J. Mater. Chem.* **2009**, *19* (22), 3576. https://doi.org/10.1039/b818869f.

(22) Egli, S.; Nussbaumer, M. G.; Balasubramanian, V.; Chami, M.; Bruns, N.; Palivan, C.; Meier, W. Biocompatible Functionalization of Polymersome Surfaces: A New Approach to Surface Immobilization and Cell Targeting Using Polymersomes. *J. Am. Chem. Soc.* **2011**, *133* (12), 4476–4483. https://doi.org/10.1021/ja110275f.

(23) Graff, A.; Fraysse-Ailhas, C.; Palivan, C. G.; Grzelakowski, M.; Friedrich, T.; Vebert, C.; Gescheidt, G.; Meier, W. Amphiphilic Copolymer Membranes Promote NADH:Ubiquinone Oxidoreductase Activity: Towards an Electron-Transfer Nanodevice: Amphiphilic Copolymer Membranes Promote NADH …. *Macromol. Chem. Phys.* **2010**, *211* (2), 229–238. https://doi.org/10.1002/macp.200900517.

(24) Langowska, K.; Palivan, C. G.; Meier, W. Polymer Nanoreactors Shown to Produce and Release Antibiotics Locally. *Chem. Commun.* **2013**, *49* (2), 128–130. https://doi.org/10.1039/C2CC36345C.

(25) Rutnakornpituk, M.; Ngamdee, P.; Phinyocheep, P. Preparation and Properties of Polydimethylsiloxane-Modified Chitosan. *Carbohydrate Polymers* **2006**, *63* (2), 229–237. https://doi.org/10.1016/j.carbpol.2005.08.063.

(26) Schlaad, H.; Diehl, C.; Gress, A.; Meyer, M.; Demirel, A. L.; Nur, Y.; Bertin, A. Poly(2-Oxazoline)s as Smart Bioinspired Polymers: Poly(2-Oxazoline)s as Smart Bioinspired Polymers. *Macromol. Rapid Commun.* **2010**, *31* (6), 511–525. https://doi.org/10.1002/marc.200900683.

(27) Hoogenboom, R.; Schlaad, H. Bioinspired Poly(2-Oxazoline)s. *Polymers* **2011**, *3* (1), 467–488. https://doi.org/10.3390/polym3010467.

(28) Gaucher, G.; Dufresne, M.-H.; Sant, V. P.; Kang, N.; Maysinger, D.; Leroux, J.-C. Block Copolymer Micelles: Preparation, Characterization and Application in Drug Delivery. *Journal of Controlled Release* **2005**, *109* (1–3), 169–188. https://doi.org/10.1016/j.jconrel.2005.09.034.

(29) Malinova, V.; Belegrinou, S.; de Bruyn Ouboter, D.; Meier, W. P. Biomimetic Block Copolymer Membranes. In *Polymer Membranes/Biomembranes*; Meier, W. P., Knoll, W., Eds.; Advances in Polymer Science; Springer Berlin Heidelberg: Berlin, Heidelberg, 2009; Vol. 224, pp 87–111. https://doi.org/10.1007/978-3-642-10479-4_10.

(30) Smart, T.; Lomas, H.; Massignani, M.; Flores-Merino, M. V.; Perez, L. R.; Battaglia, G. Block Copolymer Nanostructures. *Nano Today* **2008**, *3* (3–4), 38–46. https://doi.org/10.1016/S1748-0132(08)70043-4.

(31) Pearson, R. T.; Warren, N. J.; Lewis, A. L.; Armes, S. P.; Battaglia, G. Effect of PH and Temperature on PMPC–PDPA Copolymer Self-Assembly. *Macromolecules* **2013**, *46* (4), 1400–1407. https://doi.org/10.1021/ma302228m.

(32) Shannon, M. A.; Bohn, P. W.; Elimelech, M.; Georgiadis, J. G.; Mariñas, B. J.; Mayes, A. M. Science and Technology for Water Purification in the Coming Decades. In *Nanoscience and Technology*; Co-Published with Macmillan Publishers Ltd, UK, 2009; pp 337–346. https://doi.org/10.1142/9789814287005_0035.

(33) Graff, A.; Sauer, M.; Van Gelder, P.; Meier, W. Virus-Assisted Loading of Polymer Nanocontainer. *Proceedings of the National Academy of Sciences* **2002**, *99* (8), 5064–5068. https://doi.org/10.1073/pnas.062654499.

(34) Grzelakowski, M.; Onaca, O.; Rigler, P.; Kumar, M.; Meier, W. Immobilized Protein–Polymer Nanoreactors. *Small* **2009**, *5* (22), 2545–2548. https://doi.org/10.1002/smll.200900603.

(35) Jackman, J.; Knoll, W.; Cho, N.-J. Biotechnology Applications of Tethered Lipid Bilayer Membranes. *Materials* **2012**, *5* (12), 2637–2657. https://doi.org/10.3390/ma5122637.

(36) Sackmann, E. Supported Membranes: Scientific and Practical Applications. *Science* **1996**, *271* (5245), 43–48. https://doi.org/10.1126/science.271.5245.43.

(37) Yu, K.; Eisenberg, A. Bilayer Morphologies of Self-Assembled Crew-Cut Aggregates of Amphiphilic PS- *b* -PEO Diblock Copolymers in Solution. *Macromolecules* **1998**, *31* (11), 3509–3518. https://doi.org/10.1021/ma971419l.

(38) Bermudez, H.; Brannan, A. K.; Hammer, D. A.; Bates, F. S.; Discher, D. E. Molecular Weight Dependence of Polymersome Membrane Structure, Elasticity, and Stability. *Macromolecules* **2002**, *35* (21), 8203–8208. https://doi.org/10.1021/ma020669l.

(39) Svenson, S. Self-Assembly and Self-Organization: Important Processes, But Can We Predict Them? *Journal of Dispersion Science and Technology* **2004**, *25* (2), 101–118. https://doi.org/10.1081/DIS-120030657.

(40) Taubert, A.; Napoli, A.; Meier, W. Self-Assembly of Reactive Amphiphilic Block Copolymers as Mimetics for Biological Membranes. *Current Opinion in Chemical Biology* **2004**, *8* (6), 598–603. https://doi.org/10.1016/j.cbpa.2004.09.008.

(41) Šegota, S.; Težak, D. Spontaneous Formation of Vesicles. *Advances in Colloid and Interface Science* **2006**, *121* (1–3), 51–75. https://doi.org/10.1016/j.cis.2006.01.002.

(42) Kita-Tokarczyk, K.; Grumelard, J.; Haefele, T.; Meier, W. Block Copolymer Vesicles—Using Concepts from Polymer Chemistry to Mimic Biomembranes. *Polymer* **2005**, *46* (11), 3540–3563. https://doi.org/10.1016/j.polymer.2005.02.083.

(43) Nardin, C.; Winterhalter, M.; Meier, W. Giant Free-Standing ABA Triblock Copolymer Membranes. *Langmuir* **2000**, *16* (20), 7708–7712. https://doi.org/10.1021/la000204t.

(44) Jones, M.-C.; Leroux, J.-C. Polymeric Micelles – a New Generation of Colloidal Drug Carriers. *European Journal of Pharmaceutics and Biopharmaceutics* **1999**, *48* (2), 101–111. https://doi.org/10.1016/S0939-6411(99)00039-9.

(45) XLIV. Of the Stilling of Waves by Means of Oil. Extracted from Sundry Letters between Benjamin Franklin, LL. D. F. R. S. William Brownrigg, M. D. F. R. S. and the Reverend Mr. Farish. *Phil. Trans. R. Soc.* **1774**, *64*, 445–460. https://doi.org/10.1098/rstl.1774.0044.

(46) Langmuir, I. The Mechanism of the Surface Phenomena of Flotation. *Trans. Faraday Soc.* **1920**, *15* (June), 62. https://doi.org/10.1039/tf9201500062.

(47) Dynarowicz-Łątka, P.; Dhanabalan, A.; Oliveira, O. N. Modern Physicochemical Research on Langmuir Monolayers. *Advances in Colloid and Interface Science* **2001**, *91* (2), 221–293. https://doi.org/10.1016/S0001-8686(99)00034-2.

(48) Ybert, C.; Lu, W.; Möller, G.; Knobler, C. M. Collapse of a Monolayer by Three Mechanisms. *J. Phys. Chem. B* **2002**, *106* (8), 2004–2008. https://doi.org/10.1021/jp013173z.

(49) Girard-Egrot, A. P.; Godoy, S.; Blum, L. J. Enzyme Association with Lipidic Langmuir–Blodgett Films: Interests and Applications in Nanobioscience. *Advances in Colloid and Interface Science* **2005**, *116* (1–3), 205–225. https://doi.org/10.1016/j.cis.2005.04.006.

(50) Johann, R.; Vollhardt, D.; Möhwald, H. Shifting of Fatty Acid Monolayer Phases Due to Ionization of the Headgroups. *Langmuir* **2001**, *17* (15), 4569–4580. https://doi.org/10.1021/la001781k.

(51) Kanicky, J. R.; Shah, D. O. Effect of Degree, Type, and Position of Unsaturation on the PKa of Long-Chain Fatty Acids. *Journal of Colloid and Interface Science* **2002**, *256* (1), 201–207. https://doi.org/10.1006/jcis.2001.8009.

(52) Dynarowicz-Łątka, P.; Hąc-Wydro, K. Interactions between Phosphatidylcholines and Cholesterol in Monolayers at the Air/Water Interface. *Colloids and Surfaces B: Biointerfaces* **2004**, *37* (1–2), 21–25. https://doi.org/10.1016/j.colsurfb.2004.06.007.

(53) Vié, V.; Van Mau, N.; Lesniewska, E.; Goudonnet, J. P.; Heitz, F.; Le Grimellec, C. Distribution of Ganglioside G_{M1} between Two-Component, Two-Phase Phosphatidylcholine Monolayers. *Langmuir* **1998**, *14* (16), 4574–4583. https://doi.org/10.1021/la980203p.

(54) Ma, G.; Allen, H. C. DPPC Langmuir Monolayer at the Air−Water Interface: Probing the Tail and Head Groups by Vibrational Sum Frequency Generation Spectroscopy. *Langmuir* **2006**, *22* (12), 5341–5349. https://doi.org/10.1021/la0535227.

(55) Haefele, T.; Kita-Tokarczyk, K.; Meier, W. Phase Behavior of Mixed Langmuir Monolayers from Amphiphilic Block Copolymers and an Antimicrobial Peptide. *Langmuir* **2006**, *22* (3), 1164–1172. https://doi.org/10.1021/la0524216.

(56) Baker, S. M.; Leach, K. A.; Devereaux, C. E.; Gragson, D. E. Controlled Patterning of Diblock Copolymers by Monolayer Langmuir−Blodgett Deposition. *Macromolecules* **2000**, *33* (15), 5432–5436. https://doi.org/10.1021/ma992029x.

(57) Tanaka, M.; Sackmann, E. Polymer-Supported Membranes as Models of the Cell Surface. *Nature* **2005**, *437* (7059), 656–663. https://doi.org/10.1038/nature04164.

(58) Sinner, E.-K.; Knoll, W. Functional Tethered Membranes. *Current Opinion in Chemical Biology* **2001**, *5* (6), 705–711. https://doi.org/10.1016/S1367-5931(01)00269-1.

(59) Tanaka, M.; Sackmann, E. Supported Membranes as Biofunctional Interfaces and Smart Biosensor Platforms. *phys. stat. sol. (a)* **2006**, *203* (14), 3452–3462. https://doi.org/10.1002/pssa.200622464.

(60) Spinke, J.; Yang, J.; Wolf, H.; Liley, M.; Ringsdorf, H.; Knoll, W. Polymer-Supported Bilayer on a Solid Substrate. *Biophysical Journal* **1992**, *63* (6), 1667–1671. https://doi.org/10.1016/S0006-3495(92)81742-3.

(61) Bunjes, N.; Schmidt, E. K.; Jonczyk, A.; Rippmann, F.; Beyer, D.; Ringsdorf, H.; Gräber, P.; Knoll, W.; Naumann, R. Thiopeptide-Supported Lipid Layers on Solid Substrates. *Langmuir* **1997**, *13* (23), 6188–6194. https://doi.org/10.1021/la970317l.

(62) Förtig, A.; Jordan, R.; Graf, K.; Schiavon, G.; Purrucker, O.; Tanaka, M. Solid-Supported Biomimetic Membranes with Tailored Lipopolymer Tethers. *Macromol. Symp.* **2004**, *210* (1), 329–338. https://doi.org/10.1002/masy.200450637.

(63) Schiller, S. M.; Naumann, R.; Lovejoy, K.; Kunz, H.; Knoll, W. Archaea Analogue Thiolipids for Tethered Bilayer Lipid Membranes on Ultrasmooth Gold Surfaces. *Angew. Chem. Int. Ed.* **2003**, *42* (2), 208–211. https://doi.org/10.1002/anie.200390080.

(64) Wagner, M. L.; Tamm, L. K. Tethered Polymer-Supported Planar Lipid Bilayers for Reconstitution of Integral Membrane Proteins: Silane-Polyethyleneglycol-Lipid as a Cushion and Covalent Linker. *Biophysical Journal* **2000**, *79* (3), 1400–1414. https://doi.org/10.1016/S0006-3495(00)76392-2.

(65) von Tscharner, V.; McConnell, H. M. An Alternative View of Phospholipid Phase Behavior at the Air-Water Interface. Microscope and Film Balance Studies. *Biophysical Journal* **1981**, *36* (2), 409–419. https://doi.org/10.1016/S0006-3495(81)84740-6.

(66) Brian, A. A.; McConnell, H. M. Allogeneic Stimulation of Cytotoxic T Cells by Supported Planar Membranes. *Proceedings of the National Academy of Sciences* **1984**, *81* (19), 6159–6163. https://doi.org/10.1073/pnas.81.19.6159.

(67) Tamm, L. K.; McConnell, H. M. Supported Phospholipid Bilayers. *Biophysical Journal* **1985**, *47* (1), 105–113. https://doi.org/10.1016/S0006-3495(85)83882-0.

(68) Tabaei, S. R.; Vafaei, S.; Cho, N.-J. Fabrication of Charged Membranes by the Solvent-Assisted Lipid Bilayer (SALB) Formation Method on SiO_2 and Al_2O_3. *Phys. Chem. Chem. Phys.* **2015**, *17* (17), 11546–11552. https://doi.org/10.1039/C5CP01428J.

(69) Zhao, B.; Brittain, W. J. Polymer Brushes: Surface-Immobilized Macromolecules. *Progress in Polymer Science* **2000**, *25* (5), 677–710. https://doi.org/10.1016/S0079-6700(00)00012-5.

(70) Hensarling, R. M.; Rahane, S. B.; LeBlanc, A. P.; Sparks, B. J.; White, E. M.; Locklin, J.; Patton, D. L. Thiol–Isocyanate "Click" Reactions: Rapid Development of Functional Polymeric Surfaces. *Polym. Chem.* **2011**, *2* (1), 88–90. https://doi.org/10.1039/C0PY00292E.

(71) Zdyrko, B.; Luzinov, I. Polymer Brushes by the "Grafting to" Method: Polymer Brushes by the "Grafting to" …. *Macromol. Rapid Commun.* **2011**, *32* (12), 859–869. https://doi.org/10.1002/marc.201100162.

(72) Kowal, J.; Zhang, X.; Dinu, I. A.; Palivan, C. G.; Meier, W. Planar Biomimetic Membranes Based on Amphiphilic Block Copolymers. *ACS Macro Lett.* **2014**, *3* (1), 59–63. https://doi.org/10.1021/mz400590c.

(73) Opsteen, J. A.; van Hest, J. C. M. Modular Synthesis of Block Copolymers via Cycloaddition of Terminal Azide and Alkyne Functionalized Polymers. *Chem. Commun.* **2005**, No. 1, 57. https://doi.org/10.1039/b412930j.

(74) Rakhmatullina, E.; Mantion, A.; Bürgi, T.; Malinova, V.; Meier, W. Solid-Supported Amphiphilic Triblock Copolymer Membranes Grafted from Gold Surface: Grafting of Copolymer Membranes from Gold Surface. *J. Polym. Sci. A Polym. Chem.* **2009**, *47* (1), 1–13. https://doi.org/10.1002/pola.23116.

(75) Xiao, M.; Liu, J.; Yang, J.; Wang, R.; Xie, D. Biomimetic Membrane Control of Block Copolymer Vesicles with Tunable Wall Thickness. *Soft Matter* **2013**, *9* (8), 2434. https://doi.org/10.1039/c2sm26882e.

(76) Boxer, S. Molecular Transport and Organization in Supported Lipid Membranes. *Current Opinion in Chemical Biology* **2000**, *4* (6), 704–709. https://doi.org/10.1016/S1367-5931(00)00139-3.

(77) Kalb, E.; Frey, S.; Tamm, L. K. Formation of Supported Planar Bilayers by Fusion of Vesicles to Supported Phospholipid Monolayers. *Biochimica et Biophysica Acta (BBA) - Biomembranes* **1992**, *1103* (2), 307–316. https://doi.org/10.1016/0005-2736(92)90101-Q.

(78) Richter, R.; Mukhopadhyay, A.; Brisson, A. Pathways of Lipid Vesicle Deposition on Solid Surfaces: A Combined QCM-D and AFM Study. *Biophysical Journal* **2003**, *85* (5), 3035–3047. https://doi.org/10.1016/S0006-3495(03)74722-5.

(79) Richter, R. P.; Bérat, R.; Brisson, A. R. Formation of Solid-Supported Lipid Bilayers: An Integrated View. *Langmuir* **2006**, *22* (8), 3497–3505. https://doi.org/10.1021/la052687c.

(80) Dorn, J.; Belegrinou, S.; Kreiter, M.; Sinner, E.-K.; Meier, W. Planar Block Copolymer Membranes by Vesicle Spreading: Planar Block Copolymer Membranes by Vesicle Spreading. *Macromol. Biosci.* **2011**, *11* (4), 514–525. https://doi.org/10.1002/mabi.201000396.

(81) Richter, R. P.; Brisson, A. R. Following the Formation of Supported Lipid Bilayers on Mica: A Study Combining AFM, QCM-D, and Ellipsometry. *Biophysical Journal* **2005**, *88* (5), 3422–3433. https://doi.org/10.1529/biophysj.104.053728.

(82) Göse, M.; Pescador, P.; Reibetanz, U. Design of a Homogeneous Multifunctional Supported Lipid Membrane on Layer-by-Layer Coated Microcarriers. *Biomacromolecules* **2015**, *16* (3), 757–768. https://doi.org/10.1021/bm5016688.

(83) Belegrinou, S.; Dorn, J.; Kreiter, M.; Kita-Tokarczyk, K.; Sinner, E.-K.; Meier, W. Biomimetic Supported Membranes from Amphiphilic Block Copolymers. *Soft Matter* **2010**, *6* (1), 179–186. https://doi.org/10.1039/B917318H.

(84) Agarwal, V. K. Langmuir-Blodgett Films. *Physics Today* **1988**, *41* (6), 40–46. https://doi.org/10.1063/1.881121.

(85) Brosseau, C. L.; Leitch, J.; Bin, X.; Chen, M.; Roscoe, S. G.; Lipkowski, J. Electrochemical and PM-IRRAS a Glycolipid-Containing Biomimetic Membrane Prepared Using Langmuir−Blodgett/Langmuir−Schaefer Deposition. *Langmuir* **2008**, *24* (22), 13058–13067. https://doi.org/10.1021/la802201h.

(86) Palivan, C. G.; Goers, R.; Najer, A.; Zhang, X.; Car, A.; Meier, W. Bioinspired Polymer Vesicles and Membranes for Biological and Medical Applications. *Chem. Soc. Rev.* **2016**, *45* (2), 377–411. https://doi.org/10.1039/C5CS00569H.

(87) Chemin, M.; Brun, P.-M.; Lecommandoux, S.; Sandre, O.; Le Meins, J.-F. Hybrid Polymer/Lipid Vesicles: Fine Control of the Lipid and Polymer Distribution in the Binary Membrane. *Soft Matter* **2012**, *8* (10), 2867. https://doi.org/10.1039/c2sm07188f.

(88) Schulz, M.; Glatte, D.; Meister, A.; Scholtysek, P.; Kerth, A.; Blume, A.; Bacia, K.; Binder, W. H. Hybrid Lipid/Polymer Giant Unilamellar Vesicles: Effects of Incorporated Biocompatible PIB–PEO Block Copolymers on Vesicle Properties. *Soft Matter* **2011**, *7* (18), 8100. https://doi.org/10.1039/c1sm05725a.

(89) Le Meins, J.-F.; Schatz, C.; Lecommandoux, S.; Sandre, O. Hybrid Polymer/Lipid Vesicles: State of the Art and Future Perspectives. *Materials Today* **2013**, *16* (10), 397–402. https://doi.org/10.1016/j.mattod.2013.09.002.

(90) Khan, S.; Li, M.; Muench, S. P.; Jeuken, L. J. C.; Beales, P. A. Durable Proteo-Hybrid Vesicles for the Extended Functional Lifetime of Membrane Proteins in Bionanotechnology. *Chem. Commun.* **2016**, *52* (73), 11020–11023. https://doi.org/10.1039/C6CC04207D.

(91) Chang, L.-C.; Chang, Y.-Y.; Gau, C.-S. Interfacial Properties of Pluronics and the Interactions between Pluronics and Cholesterol/DPPC Mixed Monolayers. *Journal of Colloid and Interface Science* **2008**, *322* (1), 263–273. https://doi.org/10.1016/j.jcis.2008.02.051.

(92) Leiske, D. L.; Meckes, B.; Miller, C. E.; Wu, C.; Walker, T. W.; Lin, B.; Meron, M.; Ketelson, H. A.; Toney, M. F.; Fuller, G. G. Insertion Mechanism of a Poly(Ethylene Oxide)-Poly(Butylene Oxide) Block Copolymer into a DPPC Monolayer. *Langmuir* **2011**, *27* (18), 11444–11450. https://doi.org/10.1021/la2016879.

(93) Schulz, M.; Werner, S.; Bacia, K.; Binder, W. H. Controlling Molecular Recognition with Lipid/Polymer Domains in Vesicle Membranes. *Angew. Chem. Int. Ed.* **2013**, *52* (6), 1829–1833. https://doi.org/10.1002/anie.201204959.

(94) Thoma, J.; Belegrinou, S.; Rossbach, P.; Grzelakowski, M.; Kita-Tokarczyk, K.; Meier, W. Membrane Protein Distribution in Composite Polymer–Lipid Thin Films. *Chem. Commun.* **2012**, *48* (70), 8811. https://doi.org/10.1039/c2cc32851h.

(95) Tabaei, S. R.; Choi, J.-H.; Haw Zan, G.; Zhdanov, V. P.; Cho, N.-J. Solvent-Assisted Lipid Bilayer Formation on Silicon Dioxide and Gold. *Langmuir* **2014**, *30* (34), 10363–10373. https://doi.org/10.1021/la501534f.

(96) Krywko-Cendrowska, A.; di Leone, S.; Bina, M.; Yorulmaz-Avsar, S.; Palivan, C. G.; Meier, W. Recent Advances in Hybrid Biomimetic Polymer-Based Films: From Assembly to Applications. *Polymers* **2020**, *12* (5), 1003. https://doi.org/10.3390/polym12051003.

(97) Anderson, T. H.; Min, Y.; Weirich, K. L.; Zeng, H.; Fygenson, D.; Israelachvili, J. N. Formation of Supported Bilayers on Silica Substrates. *Langmuir* **2009**, *25* (12), 6997–7005. https://doi.org/10.1021/la900181c.

(98) Yoon, B. K.; Jackman, J. A.; Park, S.; Mokrzecka, N.; Cho, N.-J. Characterizing the Membrane-Disruptive Behavior of Dodecylglycerol Using Supported Lipid Bilayers. *Langmuir* **2019**, *35* (9), 3568–3575. https://doi.org/10.1021/acs.langmuir.9b00244.

(99) Czernohlavek, C.; Schuster, B. Formation of Planar Hybrid Lipid/Polymer Membranes Anchored to an S-Layer Protein Lattice by Vesicle Binding and Rupture. *Soft Materials* **2020**, *18* (4), 443–450. https://doi.org/10.1080/1539445X.2019.1708753.

(100) Draghici, C.; Mikhalevich, V.; Gunkel-Grabole, G.; Kowal, J.; Meier, W.; Palivan, C. G. Biomimetic Planar Polymer Membranes Decorated with Enzymes as Functional Surfaces. *Langmuir* **2018**, *34* (30), 9015–9024. https://doi.org/10.1021/acs.langmuir.8b00541.

(101) Schuster, B. S-Layer Protein-Based Biosensors. *Biosensors* **2018**, *8* (2), 40. https://doi.org/10.3390/bios8020040.

(102) Hajicharalambous, C. S.; Lichter, J.; Hix, W. T.; Swierczewska, M.; Rubner, M. F.; Rajagopalan, P. Nano- and Sub-Micron Porous Polyelectrolyte Multilayer Assemblies: Biomimetic Surfaces for Human Corneal Epithelial Cells. *Biomaterials* **2009**, *30* (23–24), 4029–4036. https://doi.org/10.1016/j.biomaterials.2009.03.020.

(103) Kowal, J.; Wu, D.; Mikhalevich, V.; Palivan, C. G.; Meier, W. Hybrid Polymer–Lipid Films as Platforms for Directed Membrane Protein Insertion. *Langmuir* **2015**, *31* (17), 4868–4877. https://doi.org/10.1021/acs.langmuir.5b00388.

(104) Itel, F.; Chami, M.; Najer, A.; Lörcher, S.; Wu, D.; Dinu, I. A.; Meier, W. Molecular Organization and Dynamics in Polymersome Membranes: A Lateral Diffusion Study. *Macromolecules* **2014**, *47* (21), 7588–7596. https://doi.org/10.1021/ma5015403.

(105) Winzen, S.; Bernhardt, M.; Schaeffel, D.; Koch, A.; Kappl, M.; Koynov, K.; Landfester, K.; Kroeger, A. Submicron Hybrid Vesicles Consisting of Polymer–Lipid and Polymer–Cholesterol Blends. *Soft Matter* **2013**, *9* (25), 5883. https://doi.org/10.1039/c3sm50733e.

(106) Hu, S.-W.; Huang, C.-Y.; Tsao, H.-K.; Sheng, Y.-J. Hybrid Membranes of Lipids and Diblock Copolymers: From Homogeneity to Rafts to Phase Separation. *Phys. Rev. E* **2019**, *99* (1), 012403. https://doi.org/10.1103/PhysRevE.99.012403.

(107) Amado, E.; Kerth, A.; Blume, A.; Kressler, J. Infrared Reflection Absorption Spectroscopy Coupled with Brewster Angle Microscopy for Studying Interactions of Amphiphilic Triblock Copolymers with Phospholipid Monolayers. *Langmuir* **2008**, *24* (18), 10041–10053. https://doi.org/10.1021/la801768m.

(108) Meyer, C. E.; Abram, S.-L.; Craciun, I.; Palivan, C. G. Biomolecule–Polymer Hybrid Compartments: Combining the Best of Both Worlds. *Phys. Chem. Chem. Phys.* **2020**, *22* (20), 11197–11218. https://doi.org/10.1039/D0CP00693A.

(109) Pereira, E. M. A.; Kosaka, P. M.; Rosa, H.; Vieira, D. B.; Kawano, Y.; Petri, D. F. S.; Carmona-Ribeiro, A. M. Hybrid Materials from Intermolecular Associations between Cationic Lipid and Polymers. *J. Phys. Chem. B* **2008**, *112* (31), 9301–9310. https://doi.org/10.1021/jp801297t.

(110) Morigaki, K.; Kiyosue, K.; Taguchi, T. Micropatterned Composite Membranes of Polymerized and Fluid Lipid Bilayers. *Langmuir* **2004**, *20* (18), 7729–7735. https://doi.org/10.1021/la049340e.

(111) Rao, S.; Prestidge, C. A. Polymer-Lipid Hybrid Systems: Merging the Benefits of Polymeric and Lipid-Based Nanocarriers to Improve Oral Drug Delivery. *Expert Opinion on Drug Delivery* **2016**, *13* (5), 691–707. https://doi.org/10.1517/17425247.2016.1151872.

(112) Beales, P. A.; Khan, S.; Muench, S. P.; Jeuken, L. J. C. Durable Vesicles for Reconstitution of Membrane Proteins in Biotechnology. *Biochemical Society Transactions* **2017**, *45* (1), 15–26. https://doi.org/10.1042/BST20160019.

(113) Mashaghi, S.; van Oijen, A. M. A Versatile Approach to the Generation of Fluid Supported Lipid Bilayers and Its Applications: Engineering Protein-Functionalized Membranes. *Biotechnol. Bioeng.* **2014**, *111* (10), 2076–2081. https://doi.org/10.1002/bit.25273.

(114) Tanner, P.; Baumann, P.; Enea, R.; Onaca, O.; Palivan, C.; Meier, W. Polymeric Vesicles: From Drug Carriers to Nanoreactors and Artificial Organelles. *Acc. Chem. Res.* **2011**, *44* (10), 1039–1049. https://doi.org/10.1021/ar200036k.

(115) Renggli, K.; Baumann, P.; Langowska, K.; Onaca, O.; Bruns, N.; Meier, W. Selective and Responsive Nanoreactors. *Adv. Funct. Mater.* **2011**, *21* (7), 1241–1259. https://doi.org/10.1002/adfm.201001563.

(116) Einfalt, T.; Goers, R.; Dinu, I. A.; Najer, A.; Spulber, M.; Onaca-Fischer, O.; Palivan, C. G. Stimuli-Triggered Activity of Nanoreactors by Biomimetic Engineering Polymer Membranes. *Nano Lett.* **2015**, *15* (11), 7596–7603. https://doi.org/10.1021/acs.nanolett.5b03386.

(117) Edlinger, C.; Einfalt, T.; Spulber, M.; Car, A.; Meier, W.; Palivan, C. G. Biomimetic Strategy To Reversibly Trigger Functionality of Catalytic Nanocompartments by the Insertion of PH-Responsive Biovalves. *Nano Lett.* **2017**, *17* (9), 5790–5798. https://doi.org/10.1021/acs.nanolett.7b02886.

(118) Einfalt, T.; Witzigmann, D.; Edlinger, C.; Sieber, S.; Goers, R.; Najer, A.; Spulber, M.; Onaca-Fischer, O.; Huwyler, J.; Palivan, C. G. Biomimetic Artificial Organelles with in Vitro and in Vivo Activity Triggered by Reduction in Microenvironment. *Nat Commun* **2018**, *9* (1), 1127. https://doi.org/10.1038/s41467-018-03560-x.

(119) González-Pérez, A.; Stibius, K. B.; Vissing, T.; Nielsen, C. H.; Mouritsen, O. G. Biomimetic Triblock Copolymer Membrane Arrays: A Stable Template for Functional Membrane Proteins. *Langmuir* **2009**, *25* (18), 10447–10450. https://doi.org/10.1021/la902417m.

(120) Goers, R.; Thoma, J.; Ritzmann, N.; Di Silvestro, A.; Alter, C.; Gunkel-Grabole, G.; Fotiadis, D.; Müller, D. J.; Meier, W. Optimized Reconstitution of Membrane Proteins into Synthetic Membranes. *Commun Chem* **2018**, *1* (1), 35. https://doi.org/10.1038/s42004-018-0037-8.

(121) Stoenescu, R.; Meier, W. Vesicles with Asymmetric Membranes from Amphiphilic ABC Triblock Copolymers. *Chem. Commun.* **2002**, No. 24, 3016–3017. https://doi.org/10.1039/b209352a.

(122) Stoenescu, R.; Graff, A.; Meier, W. Asymmetric ABC-Triblock Copolymer Membranes Induce a Directed Insertion of Membrane Proteins. *Macromol. Biosci.* **2004**, *4* (10), 930–935. https://doi.org/10.1002/mabi.200400065.

(123) Tanaka, M. Polymer-Supported Membranes: Physical Models of Cell Surfaces. *MRS Bull.* **2006**, *31* (7), 513–520. https://doi.org/10.1557/mrs2006.135.

(124) Habel, J.; Ogbonna, A.; Larsen, N.; Cherré, S.; Kynde, S.; Midtgaard, S. R.; Kinoshita, K.; Krabbe, S.; Jensen, G. V.; Hansen, J. S.; Almdal, K.; Hèlix-Nielsen, C. Selecting Analytical Tools for Characterization of Polymersomes in Aqueous Solution. *RSC Adv.* **2015**, *5* (97), 79924–79946. https://doi.org/10.1039/C5RA16403F.

(125) Gormally, M. V.; McKibben, R. K.; Johal, M. S.; Selassie, C. R. D. Controlling Tyrosinase Activity on Charged Polyelectrolyte Surfaces: A QCM-D Analysis. *Langmuir* **2009**, *25* (17), 10014–10019. https://doi.org/10.1021/la900751w.

(126) Wang, J. Nanomaterial-Based Electrochemical Biosensors. *Analyst* **2005**, *130* (4), 421. https://doi.org/10.1039/b414248a.

(127) Natrajan, N.; Sheldon, B. W. Efficacy of Nisin-Coated Polymer Films To Inactivate Salmonella Typhimurium on Fresh Broiler Skin†. *Journal of Food Protection* **2000**, *63* (9), 1189–1196. https://doi.org/10.4315/0362-028X-63.9.1189.

(128) Fadnavis, N. W.; Bhaskar, V.; Kantam, M. L.; Choudary, B. M. Highly Efficient "Tight Fit" Immobilization of α-Chymotrypsin in Mesoporous MCM-41: A Novel Approach Using Precursor Immobilization and Activation. *Biotechnol. Prog.* **2003**, *19* (2), 346–351. https://doi.org/10.1021/bp025678s.

(129) Bornscheuer, U. T. Immobilizing Enzymes: How to Create More Suitable Biocatalysts. *Angew. Chem. Int. Ed.* **2003**, *42* (29), 3336–3337. https://doi.org/10.1002/anie.200301664.

(130) Garcia-Galan, C.; Berenguer-Murcia, Á.; Fernandez-Lafuente, R.; Rodrigues, R. C. Potential of Different Enzyme Immobilization Strategies to Improve Enzyme Performance. *Adv. Synth. Catal.* **2011**, *353* (16), 2885–2904. https://doi.org/10.1002/adsc.201100534.

(131) Sheldon, R. A. Enzyme Immobilization: The Quest for Optimum Performance. *Adv. Synth. Catal.* **2007**, *349* (8–9), 1289–1307. https://doi.org/10.1002/adsc.200700082.

(132) Hudson, S.; Cooney, J.; Magner, E. Proteins in Mesoporous Silicates. *Angew. Chem. Int. Ed.* **2008**, *47* (45), 8582–8594. https://doi.org/10.1002/anie.200705238.

(133) Qiu, H.; Xu, C.; Huang, X.; Ding, Y.; Qu, Y.; Gao, P. Immobilization of Laccase on Nanoporous Gold: Comparative Studies on the Immobilization Strategies and the Particle Size Effects. *J. Phys. Chem. C* **2009**, *113* (6), 2521–2525. https://doi.org/10.1021/jp8090304.

(134) Zhou, X.; Yu, T.; Zhang, Y.; Kong, J.; Tang, Y.; Marty, J.-L.; Liu, B. Nanozeolite-Assembled Interface towards Sensitive Biosensing. *Electrochemistry Communications* **2007**, *9* (7), 1525–1529. https://doi.org/10.1016/j.elecom.2007.02.018.

(135) Arıca, M. Y.; Altıntas, B.; Bayramoğlu, G. Immobilization of Laccase onto Spacer-Arm Attached Non-Porous Poly(GMA/EGDMA) Beads: Application for Textile Dye Degradation. *Bioresource Technology* **2009**, *100* (2), 665–669. https://doi.org/10.1016/j.biortech.2008.07.038.

(136) Castellana, E. T.; Cremer, P. S. Solid Supported Lipid Bilayers: From Biophysical Studies to Sensor Design. *Surface Science Reports* **2006**, *61* (10), 429–444. https://doi.org/10.1016/j.surfrep.2006.06.001.

(137) Caseli, L.; Furriel, R. P. M.; de Andrade, J. F.; Leone, F. A.; Zaniquelli, M. E. D. Surface Density as a Significant Parameter for the Enzymatic Activity of Two Forms of Alkaline Phosphatase Immobilized on Phospholipid Langmuir–Blodgett Films. *Journal of Colloid and Interface Science* **2004**, *275* (1), 123–130. https://doi.org/10.1016/j.jcis.2004.01.081.

(138) Ye, Q.; Konradi, R.; Textor, M.; Reimhult, E. Liposomes Tethered to Omega-Functional PEG Brushes and Induced Formation of PEG Brush Supported Planar Lipid Bilayers. *Langmuir* **2009**, *25* (23), 13534–13539. https://doi.org/10.1021/la902039g.

(139) Naumann, C. A.; Prucker, O.; Lehmann, T.; Rühe, J.; Knoll, W.; Frank, C. W. The Polymer-Supported Phospholipid Bilayer: Tethering as a New Approach to Substrate−Membrane Stabilization. *Biomacromolecules* **2002**, *3* (1), 27–35. https://doi.org/10.1021/bm0100211.

(140) Naumann, R.; Jonczyk, A.; Hampel, C.; Ringsdorf, H.; Knoll, W.; Bunjes, N.; Gräber, P. Coupling of Proton Translocation through ATPase Incorporated into Supported Lipid Bilayers to an Electrochemical Process. *Bioelectrochemistry and Bioenergetics* **1997**, *42* (2), 241–247. https://doi.org/10.1016/S0302-4598(96)05108-2.

(141) Gritsch, S.; Nollert, P.; Jähnig, F.; Sackmann, E. Impedance Spectroscopy of Porin and Gramicidin Pores Reconstituted into Supported Lipid Bilayers on Indium−Tin-Oxide Electrodes †. *Langmuir* **1998**, *14* (11), 3118–3125. https://doi.org/10.1021/la9710381.

(142) Knoll, W.; Köper, I.; Naumann, R.; Sinner, E.-K. Tethered Bimolecular Lipid Membranes—A Novel Model Membrane Platform. *Electrochimica Acta* **2008**, *53* (23), 6680–6689. https://doi.org/10.1016/j.electacta.2008.02.121.

(143) Granéli, A.; Rydström, J.; Kasemo, B.; Höök, F. Formation of Supported Lipid Bilayer Membranes on SiO_2 from Proteoliposomes Containing Transmembrane Proteins. *Langmuir* **2003**, *19* (3), 842–850. https://doi.org/10.1021/la026231w.

(144) Discher, B. M.; Hammer, D. A.; Bates, F. S.; Discher, D. E. Polymer Vesicles in Various Media. *Current Opinion in Colloid & Interface Science* **2000**, *5* (1–2), 125–131. https://doi.org/10.1016/S1359-0294(00)00045-5.

(145) Zhang, X.; Fu, W.; Palivan, C. G.; Meier, W. Natural Channel Protein Inserts and Functions in a Completely Artificial, Solid-Supported Bilayer Membrane. *Sci Rep* **2013**, *3* (1), 2196. https://doi.org/10.1038/srep02196.

(146) Torchilin, V. P. Recent Advances with Liposomes as Pharmaceutical Carriers. *Nat Rev Drug Discov* **2005**, *4* (2), 145–160. https://doi.org/10.1038/nrd1632.

(147) Langowska, K.; Kowal, J.; Palivan, C. G.; Meier, W. A General Strategy for Creating Self-Defending Surfaces for Controlled Drug Production for Long Periods of Time. *J. Mater. Chem. B* **2014**, *2* (29), 4684. https://doi.org/10.1039/c4tb00277f.

(148) Torchilin, V. P. Structure and Design of Polymeric Surfactant-Based Drug Delivery Systems. *Journal of Controlled Release* **2001**, *73* (2–3), 137–172. https://doi.org/10.1016/S0168-3659(01)00299-1.

(149) Kita-Tokarczyk, K.; Itel, F.; Grzelakowski, M.; Egli, S.; Rossbach, P.; Meier, W. Monolayer Interactions between Lipids and Amphiphilic Block Copolymers. *Langmuir* **2009**, *25*, 9847.

(150) Fischlechner, M.; Reibetanz, U.; Zaulig, M.; Enderlein, D.; Romanova, J.; Leporatti, S.; Moya, S.; Donath, E. Fusion of Enveloped Virus Nanoparticles with Polyelectrolyte-Supported Lipid Membranes for the Design of Bio/Nonbio Interfaces. *Nano Lett.* **2007**, *7* (11), 3540–3546. https://doi.org/10.1021/nl0723580.

(151) Harada, Y.; Noda, J.; Yatabe, R.; Ikezaki, H.; Toko, K. Research on the Changes to the Lipid/Polymer Membrane Used in the Acidic Bitterness Sensor Caused by Preconditioning. *Sensors* **2016**, *16* (2), 230. https://doi.org/10.3390/s16020230.

(152) Nakatani, F.; Ienaga, T.; Wu, X.; Tahara, Y.; Ikezaki, H.; Sano, H.; Muto, Y.; Kaneda, Y.; Toko, K. Development of a Sensor with a Lipid/Polymer Membrane Comprising Na+ Ionophores to Evaluate the Saltiness Enhancement Effect. *Sensors* **2019**, *19* (23), 5251. https://doi.org/10.3390/s19235251.

(153) Kang, M.; Lee, B.; Leal, C. Three-Dimensional Microphase Separation and Synergistic Permeability in Stacked Lipid–Polymer Hybrid Membranes. *Chem. Mater.* **2017**, *29* (21), 9120–9132. https://doi.org/10.1021/acs.chemmater.7b02845.

(154) Yatabe, R.; Noda, J.; Tahara, Y.; Naito, Y.; Ikezaki, H.; Toko, K. Analysis of a Lipid/Polymer Membrane for Bitterness Sensing with a Preconditioning Process. *Sensors* **2015**, *15* (9), 22439–22450. https://doi.org/10.3390/s150922439.

(155) Toko, K.; Hara, D.; Tahara, Y.; Yasuura, M.; Ikezaki, H. Relationship between the Amount of Bitter Substances Adsorbed onto Lipid/Polymer Membrane and the Electric Response of Taste Sensors. *Sensors* **2014**, *14* (9), 16274–16286. https://doi.org/10.3390/s140916274.

(156) Sackmann, E. *Structure and Dynamics of Membranes*; 1995; Vol. 1.

(157) Gust, D.; Moore, T. A.; Moore, A. L. Mimicking Photosynthetic Solar Energy Transduction. *Acc. Chem. Res.* **2001**, *34*, 40.

(158) Lin, Q.; London, E. Preparation of Artificial Plasma Membrane Mimicking Vesicles with Lipid Asymmetry. *PLoS One* **2014**, *9*, e87903.

(159) Steinberg-Yfrach, G.; Rigaud, J.-L.; Durantini, E. N.; Moore, A. L.; Gust, D.; Moore, T. A. Light-Driven Production of ATP Catalysed by F0F1-ATP Synthase in an Artificial Photosynthetic Membrane. *Nature* **1998**, *392*, 479.

(160) Vockenroth, I. K.; Atanasova, P. P.; Jenkins, A. T. A.; Köper, I. Incorporation of α-Hemolysin in Different Tethered Bilayer Lipid Membrane Architectures. *Langmuir* **2008**, *24*, 496.

(161) Kowal, J. Ł.; Kowal, J. K.; Wu, D.; Stahlberg, H.; Palivan, C. G.; Meier, W. P. Functional Surface Engineering by Nucleotide-Modulated Potassium Channel Insertion into Polymer Membranes Attached to Solid Supports. *Biomaterials* **2014**, *35*, 7286.

(162) Draghici, C.; Kowal, J.; Darjan, A.; Meier, W.; Palivan, C. G. “Active Surfaces” Formed by Immobilization of Enzymes on Solid-Supported Polymer Membranes. *Langmuir* **2014**, *30*, 11660.

(163) Belluati, A.; Mikhalevich, V.; Yorulmaz Avsar, S.; Daubian, D.; Craciun, I.; Chami, M.; Meier, W. P.; Palivan, C. G. How Do the Properties of Amphiphilic Polymer Membranes Influence the Functional Insertion of Peptide Pores? *Biomacromolecules* **2020**, *21*, 701.

(164) Dahlin, A.; Zäch, M.; Rindzevicius, T.; Käll, M.; Sutherland, D. S.; Höök, F. Localized Surface Plasmon Resonance Sensing of Lipid-Membrane-Mediated Biorecognition Events. *J. Am. Chem. Soc.* **2005**, *127*, 5043.

(165) El Idrissi, M.; Meyer, C. E.; Zartner, L.; Meier, W. Nanosensors Based on Polymer Vesicles and Planar Membranes: A Short Review. *J. Nanobiotechnol.* **2018**, *16*, 63.

(166) Gettel, D. L.; Sanborn, J.; Patel, M. A.; de Hoog, H.-P.; Liedberg, B.; Nallani, M.; Parikh, A. N. Mixing, Diffusion, and Percolation in Binary Supported Membranes Containing Mixtures of Lipids and Amphiphilic Block Copolymers. *J. Am. Chem. Soc.* **2014**, *136*, 10186.

(167) Schulz, M.; Olubummo, A.; Bacia, K.; Binder, W. H. Lateral Surface Engineering of Hybrid Lipid–BCP Vesicles and Selective Nanoparticle Embedding. *Soft Matter* **2014**, *10*, 831.

(168) Nam, J.; Vanderlick, T. K.; Beales, P. A. Formation and Dissolution of Phospholipid Domains with Varying Textures in Hybrid Lipo-Polymersomes. *Soft Matter* **2012**, *8*, 7982.

(169) Paxton, W. F.; McAninch, P. T.; Achyuthan, K. E.; Shin, S. H. R.; Monteith, H. L. Monitoring and Modulating Ion Traffic in Hybrid Lipid/Polymer Vesicles. *Colloids Surf., B* **2017**, *159*, 268.

(170) Amado, E.; Blume, A.; Kressler, J. Novel Non-Ionic Block Copolymers Tailored for Interactions with Phospholipids. *React. Funct. Polym.* **2009**, *69*, 450.

(171) Chimisso, V.; Maffeis, V.; Hürlimann, D.; Palivan, C. G.; Meier, W. Self-Assembled Polymeric Membranes and Nanoassemblies on Surfaces: Preparation, Characterization, and Current Applications. *Macromol. Biosci.* **2020**, *20*, 1900257.

(172) Jagoda, A.; Ketikidis, P.; Zinn, M.; Meier, W.; Kita-Tokarczyk, K. Interactions of Biodegradable Poly ([R]-3-Hydroxy-10-Undecenoate) with 1, 2-Dioleoyl-Sn-Glycero-3-Phosphocholine Lipid: A Monolayer Study. *Langmuir* **2011**, *27*, 10878.

(173) Mathé, C.; Devineau, S.; Aude, J.-C.; Lagniel, G.; Chédin, S.; Legros, V.; Mathon, M.-H.; Renault, J.-P.; Pin, S.; Boulard, Y. Structural Determinants for Protein Adsorption/Non-Adsorption to Silica Surface. *PLoS One* **2013**, *8*, e81346.

(174) Nakanishi, K.; Sakiyama, T.; Imamura, K. On the Adsorption of Proteins on Solid Surfaces, a Common but Very Complicated Phenomenon. *J. Biosci. Bioeng.* **2001**, *91*, 233.

(175) Rezwan, K.; Meier, L. P.; Gauckler, L. J. Lysozyme and Bovine Serum Albumin Adsorption on Uncoated Silica and AlOOH-Coated Silica Particles: The Influence of Positively and Negatively Charged Oxide Surface Coatings. *Biomaterials* **2005**, *26*, 4351.

(176) Ying, P.; Viana, A. S.; Abrantes, L. M.; Jin, G. Adsorption of Human Serum Albumin onto Gold: A Combined Electrochemical and Ellipsometric Study. *J. Colloid Interface Sci.* **2004**, *279*, 95.

(177) Kim, D. T.; Blanch, H. W.; Radke, C. J. Direct Imaging of Lysozyme Adsorption onto Mica by Atomic Force Microscopy. *Langmuir* **2002**, *18*, 5841.

(178) Hinnen, C. Electrochemical and Spectroreflectance Studies of the Adsorbed Horse Heart Cytochrome c and Cytochrome CD3 from D. Vulgaris, Miyazaki Strain, at Gold Electrode. *J. Electroanal. Chem. Interfacial Electrochem.* **1983**, *147*, 329.

(179) Reed, D. E.; Hawkridge, F. M. Direct Electron Transfer Reactions of Cytochrome c at Silver Electrodes. *Anal. Chem.* **1987**, *59*, 2334.

(180) Wang, L.; Wang, E. Direct Electron Transfer between Cytochrome c and a Gold Nanoparticles Modified Electrode. *Electrochem. Commun.* **2004**, *6*, 49.

(181) Patila, M.; Pavlidis, I. V.; Diamanti, E. K.; Katapodis, P.; Gournis, D.; Stamatis, H. Enhancement of Cytochrome c Catalytic Behaviour by Affecting the Heme Environment Using Functionalized Carbon-Based Nanomaterials. *Process Biochem.* **2013**, *48*, 1010.

(182) Tanne, J.; Dietzel, B.; Scheller, F. W.; Bier, F. Nanohybrid Materials Consisting of Poly [(3-Aminobenzoic Acid)-Co-(3-Aminobenzenesulfonic Acid)-Co-Aniline] and Multiwalled Carbon Nanotubes for Immobilization of Redox Active Cytochrome c. *Electroanalysis* **2014**, *26*, 732.

(183) Song, Y.; Liu, H.; Wan, L.; Wang, Y.; Hou, H.; Wang, L. Direct Electrochemistry of Cytochrome c Based on Poly (Diallyldimethylammonium Chloride)-Graphene Nanosheets/Gold Nanoparticles Hybrid Nanocomposites and Its Biosensing. *Electroanalysis* **2013**, *25*, 1400.

(184) Eguílaz, M.; Agüí, L.; Yáñez-Sedeño, P.; Pingarrón, J. M. A Biosensor Based on Cytochrome c Immobilization on a Poly-3-Methylthiophene/Multi-Walled Carbon Nanotubes Hybrid-Modified Electrode. Application to the Electrochemical Determination of Nitrite. *J. Electroanal. Chem.* **2010**, *644*, 30.

(185) Wang, Y.; Bian, X.; Liao, L.; Zhu, J.; Guo, K.; Kong, J.; Liu, B. Electrochemistry and Biosensing Activity of Cytochrome c Immobilized on a Mesoporous Interface Assembled from Carbon Nanospheres. *Microchim. Acta* **2012**, *178*, 277.

(186) Petrov, P.; Stassin, F.; Pagnoulle, C.; Jérôme, R. Noncovalent Functionalization of Multi-Walled Carbon Nanotubes by Pyrene Containing Polymers. *Chem. Commun.* **2003**, 2904.

(187) Wu, J.-F.; Xu, M.-Q.; Zhao, G.-C. Graphene-Based Modified Electrode for the Direct Electron Transfer of Cytochrome c and Biosensing. *Electrochem. Commun.* **2010**, *12*, 175.

(188) Salamon, Z.; Tollin, G. Reduction of Cytochrome c at a Lipid Bilayer Modified Electrode. *Bioelectrochem. Bioenerg.* **1991**, *320*, 447.

(189) Salamon, Z.; Tollin, G. Interfacial Electrochemistry of Cytochrome c at a Lipid Bilayer Modified Electrode: Effect of Incorporation of Negative Charges into the Bilayer on Cyclic Voltammetric Parameters. *J. Electroanal. Chem. Interfacial Electrochem.* **1991**, *321*, 321.

(190) Choi, E. J.; Dimitriadis, E. K. Cytochrome c Adsorption to Supported, Anionic Lipid Bilayers Studied via Atomic Force Microscopy. *Biophys. J.* **2004**, *87*, 3234.

(191) Salamon, Z.; Tollin, G. Interaction of Horse Heart Cytochrome c with Lipid Bilayer Membranes: Effects on Redox Potentials. *J. Bioenerg. Biomembr.* **1997**, *29*, 211.

(192) Tuominen, E. K. J.; Wallace, C. J. A.; Kinnunen, P. K. J. Phospholipid-CytochromecInteraction. *J. Biol. Chem.* **2002**, *277*, 8822.

(193) Gouveia, A.; Bajwa, E.; Klegeris, A. Extracellular Cytochrome c as an Intercellular Signaling Molecule Regulating Microglial Functions. *Biochim. Biophys. Acta, Gen. Subj.* **2017**, *1861*, 2274.

(194) Tuominen, E. K. *Phospholipid–Cytochrome c Interactions*; 2011.

(195) Salamon, Z.; Tollin, G. Surface Plasmon Resonance Studies of Complex Formation between Cytochrome c and Bovine Cytochrome c Oxidase Incorporated into a Supported Planar Lipid Bilayer. I. Binding of Cytochrome c to Cardiolipin/Phosphatidylcholine Membranes in the Absence of Oxidase. *Biophys. J.* **1996**, *71*, 848.

(196) Kalanxhi, E.; Wallace, C. J. A. Cytochrome c Impaled: Investigation of the Extended Lipid Anchorage of a Soluble Protein to Mitochondrial Membrane Models. *Biochem. J.* **2007**, *407*, 179.

(197) Santucci, R.; Sinibaldi, F.; Fiorucci, L. Human Diseases and Mitochondrial Damage: Role of Cytochrome c–Cardiolipin Interaction as a Key Regulator of Cell Fate. *Front. Med. Chem.* **2016**, *9*, 56.

(198) Boussaad, S.; Pean, J.; Tao, N. J. High-Resolution Multiwavelength Surface Plasmon Resonance Spectroscopy for Probing Conformational and Electronic Changes in Redox Proteins. *Anal. Chem.* **2000**, *72*, 222.

(199) Morandat, S.; El Kirat, K. Real-Time Atomic Force Microscopy Reveals Cytochrome c-Induced Alterations in Neutral Lipid Bilayers. *Langmuir* **2007**, *23*, 10929.

(200) Bayraktar, H.; You, C.-C.; Rotello, V. M.; Knapp, M. J. Facial Control of Nanoparticle Binding to Cytochrome c. *J. Am. Chem. Soc.* **2007**, *129*, 2732.

(201) Honig, E. P. Molecular Constitution of X-and Y-Type Langmuir-Blodgett Films. *J. Colloid Interface Sci.* **1973**, *43*, 66.

(202) Valeur, E.; Bradley, M. Amide Bond Formation: Beyond the Myth of Coupling Reagents. *Chem. Soc. Rev.* **2009**, *38*, 606.

(203) Huang, C.-J.; Cho, N.-J.; Hsu, C.-J.; Tseng, P.-Y.; Frank, C. W.; Chang, Y.-C. Type I Collagen-Functionalized Supported Lipid Bilayer as a Cell Culture Platform. *Biomacromolecules* **2010**, *11*, 1231.

(204) Kranz, R. G.; Richard-Fogal, C.; Taylor, J.-S.; Frawley, E. R. Cytochrome c Biogenesis: Mechanisms for Covalent Modifications and Trafficking of Heme and for Heme-Iron Redox Control. *Microbiol. Mol. Biol. Rev.* **2009**, *73*, 510.

(205) Zhu, H.; Mumtaz, F.; Zhang, C.; Tan, L.; Liu, S.; Zhang, Y.; Pan, C.; Wang, Y. A Rapid Approach to Prepare Poly (2-Methyl-2-Oxazoline)-Based Antifouling Coating by UV Irradiation. *Appl. Surf. Sci.* **2017**, *426*, 817.

(206) Yorulmaz Avsar, S.; Jackman, J. A.; Kim, M. C.; Yoon, B. K.; Hunziker, W.; Cho, N.-J. Immobilization Strategies for Functional Complement Convertase Assembly at Lipid Membrane Interfaces. *Langmuir* **2017**, *33*, 7332.

(207) Muenzner, J.; Pletneva, E. V. Structural Transformations of Cytochrome c upon Interaction with Cardiolipin. *Chem. Phys. Lipids* **2014**, *179*, 57.

(208) Alakoskela, J.-M.; Jutila, A.; Simonsen, A. C.; Pirneskoski, J.; Pyhäjoki, S.; Turunen, R.; Marttila, S.; Mouritsen, O. G.; Goormaghtigh, E.; Kinnunen, P. K. J. Characteristics of Fibers Formed by Cytochrome c and Induced by Anionic Phospholipids. *Biochemistry* **2006**, *45*, 13447.

(209) Pinheiro, T. J. T.; Watts, A. Resolution of Individual Lipids in Mixed Phospholipid Membranes and Specific Lipid-Cytochrome c Interactions by Magic-Angle Spinning Solid-State Phosphorus-31 NMR. *Biochemistry* **1994**, *33*, 2459.

(210) Pinheiro, T. J. T.; Watts, A. Lipid Specificity in the Interaction of Cytochrome c with Anionic Phospholipid Bilayers Revealed by Solid-State 31P NMR. *Biochemistry* **1994**, *33*, 2451.

(211) Brown, D. A.; London, E. Functions of Lipid Rafts in Biological Membranes. *Annu. Rev. Cell Dev. Biol.* **1998**, *14*, 111.

(212) Zhao, Y.; Xu, J.-X. The Operation of the Alternative Electron-Leak Pathways Mediated by Cytochrome c in Mitochondria. *Biochem. Biophys. Res. Commun.* **2004**, *317*, 980.

(213) Traylor, T. G.; Kim, C.; Richards, J. L.; Xu, F.; Perrin, C. L. Reactions of Iron (III) Porphyrins with Oxidants. Structure-Reactivity Studies. *J. Am. Chem. Soc.* **1995**, *117*, 3468.

(214) Tanner, P.; Balasubramanian, V.; Palivan, C. G. Aiding Nature's Organelles: Artificial Peroxisomes Play Their Role. *Nano Lett.* **2013**, *13*, 2875.

(215) Belluati, A.; Craciun, I.; Liu, J.; Palivan, C. G. Nanoscale Enzymatic Compartments in Tandem Support Cascade Reactions in Vitro. *Biomacromolecules* **2018**, *19*, 4023.

(216) Belikova, N. A.; Vladimirov, Y. A.; Osipov, A. N.; Kapralov, A. A.; Tyurin, V. A.; Potapovich, M. V.; Basova, L. V.; Peterson, J.; Kurnikov, I. V.; Kagan, V. E. Peroxidase Activity and Structural Transitions of Cytochrome c Bound to Cardiolipin-Containing Membranes. *Biochemistry* **2006**, *45*, 4998.

(217) Lefrançois, P.; Vajrala, V. S. R.; Arredondo, I. B.; Goudeau, B.; Doneux, T.; Bouffier, L.; Arbault, S. Direct Oxidative Pathway from Amplex Red to Resorufin Revealed by in Situ Confocal Imaging. *Phys. Chem. Chem. Phys.* **2016**, *18*, 25817.

(218) Chertkova, R. V.; Brazhe, N. A.; Bryantseva, T. V.; Nekrasov, A. N.; Dolgikh, D. A.; Yusipovich, A. I.; Sosnovtseva, O.; Maksimov, G. V.; Rubin, A. B.; Kirpichnikov, M. P. New Insight into the Mechanism of Mitochondrial Cytochrome c Function. *PLoS One* **2017**, *12*, e0178280.

(219) Rideau, E.; Dimova, R.; Schwille, P.; Wurm, F. R.; Landfester, K. Liposomes and Polymersomes: A Comparative Review towards Cell Mimicking. *Chem. Soc. Rev.* **2018**, *47* (23), 8572–8610. https://doi.org/10.1039/C8CS00162F.

(220) Belluati, A.; Craciun, I.; Meyer, C. E.; Rigo, S.; Palivan, C. G. Enzymatic Reactions in Polymeric Compartments: Nanotechnology Meets Nature. *Current Opinion in Biotechnology* **2019**, *60*, 53–62. https://doi.org/10.1016/j.copbio.2018.12.011.

(221) Balasubramanian, V.; Herranz-Blanco, B.; Almeida, P. V.; Hirvonen, J.; Santos, H. A. Multifaceted Polymersome Platforms: Spanning from Self-Assembly to Drug Delivery and Protocells. *Progress in Polymer Science* **2016**, *60*, 51–85. https://doi.org/10.1016/j.progpolymsci.2016.04.004.

(222) Morton, D.; Mortezaei, S.; Yemenicioglu, S.; Isaacman, M. J.; Nova, I. C.; Gundlach, J. H.; Theogarajan, L. Tailored Polymeric Membranes for Mycobacterium Smegmatis Porin A (MspA) Based Biosensors. *J. Mater. Chem. B* **2015**, *3* (25), 5080–5086. https://doi.org/10.1039/C5TB00383K.

(223) Diep, J.; Tek, A.; Thompson, L.; Frommer, J.; Wang, R.; Piunova, V.; Sly, J.; La, Y.-H. Layer-by-Layer Assembled Core–Shell Star Block Copolymers for Fouling Resistant Water Purification Membranes. *Polymer* **2016**, *103*, 468–477. https://doi.org/10.1016/j.polymer.2015.11.048.

(224) Li, J.-J.; Zhou, Y.-N.; Luo, Z.-H. Thermal-Responsive Block Copolymers for Surface with Reversible Switchable Wettability. *Ind. Eng. Chem. Res.* **2014**, *53* (47), 18112–18120. https://doi.org/10.1021/ie503610n.

(225) Dimitriou, M. D.; Zhou, Z.; Yoo, H.-S.; Killops, K. L.; Finlay, J. A.; Cone, G.; Sundaram, H. S.; Lynd, N. A.; Barteau, K. P.; Campos, L. M.; Fischer, D. A.; Callow, M. E.; Callow, J. A.; Ober, C. K.; Hawker, C. J.; Kramer, E. J. A General Approach to Controlling the Surface Composition of Poly(Ethylene Oxide)-Based Block Copolymers for Antifouling Coatings. *Langmuir* **2011**, *27* (22), 13762–13772. https://doi.org/10.1021/la202509m.

(226) Otsuka, H.; Nagasaki, Y.; Kataoka, K. Surface Characterization of Functionalized Polylactide through the Coating with Heterobifunctional Poly(Ethylene Glycol)/Polylactide Block Copolymers. *Biomacromolecules* **2000**, *1* (1), 39–48. https://doi.org/10.1021/bm990005s.

(227) Garni, M.; Wehr, R.; Avsar, S. Y.; John, C.; Palivan, C.; Meier, W. Polymer Membranes as Templates for Bio-Applications Ranging from Artificial Cells to Active Surfaces. *European Polymer Journal* **2019**, *112*, 346–364. https://doi.org/10.1016/j.eurpolymj.2018.12.047.

(228) Rigo, S.; Cai, C.; Gunkel-Grabole, G.; Maurizi, L.; Zhang, X.; Xu, J.; Palivan, C. G. Nanoscience-Based Strategies to Engineer Antimicrobial Surfaces. *Adv. Sci.* **2018**, *5* (5), 1700892. https://doi.org/10.1002/advs.201700892.

(229) Chapman, C. A. R.; Chen, H.; Stamou, M.; Biener, J.; Biener, M. M.; Lein, P. J.; Seker, E. Nanoporous Gold as a Neural Interface Coating: Effects of Topography, Surface Chemistry, and Feature Size. *ACS Appl. Mater. Interfaces* **2015**, *7* (13), 7093–7100. https://doi.org/10.1021/acsami.5b00410.

(230) Yorulmaz Avsar, S.; Kyropoulou, M.; Di Leone, S.; Schoenenberger, C.-A.; Meier, W. P.; Palivan, C. G. Biomolecules Turn Self-Assembling Amphiphilic Block Co-Polymer Platforms Into Biomimetic Interfaces. *Front. Chem.* **2019**, *6*, 645. https://doi.org/10.3389/fchem.2018.00645.

(231) Lin, Y.-L.; Chang, H.-Y.; Sheng, Y.-J.; Tsao, H.-K. Structural and Mechanical Properties of Polymersomes Formed by Rod–Coil Diblock Copolymers. *Soft Matter* **2013**, *9* (19), 4802. https://doi.org/10.1039/c3sm00051f.

(232) Ferhan, A. R.; Yoon, B. K.; Park, S.; Sut, T. N.; Chin, H.; Park, J. H.; Jackman, J. A.; Cho, N.-J. Solvent-Assisted Preparation of Supported Lipid Bilayers. *Nat Protoc* **2019**, *14* (7), 2091–2118. https://doi.org/10.1038/s41596-019-0174-2.

(233) Jackman, J. A.; Cho, N.-J. Supported Lipid Bilayer Formation: Beyond Vesicle Fusion. *Langmuir* **2020**, *36* (6), 1387–1400. https://doi.org/10.1021/acs.langmuir.9b03706.

(234) Le Meins, J.-F.; Sandre, O.; Lecommandoux, S. Recent Trends in the Tuning of Polymersomes' Membrane Properties. *Eur. Phys. J. E* **2011**, *34* (2), 14. https://doi.org/10.1140/epje/i2011-11014-y.

(235) Livnah, O.; Bayer, E. A.; Wilchek, M.; Sussman, J. L. Three-Dimensional Structures of Avidin and the Avidin-Biotin Complex. *Proceedings of the National Academy of Sciences* **1993**, *90* (11), 5076–5080. https://doi.org/10.1073/pnas.90.11.5076.

(236) Luong, J. H. T.; Male, K. B.; Glennon, J. D. Biotin Interference in Immunoassays Based on Biotin-Strept(Avidin) Chemistry: An Emerging Threat. *Biotechnology Advances* **2019**, *37* (5), 634–641. https://doi.org/10.1016/j.biotechadv.2019.03.007.

(237) Wu, D.; Rigo, S.; Di Leone, S.; Belluati, A.; Constable, E. C.; Housecroft, C. E.; Palivan, C. G. Brushing the Surface: Cascade Reactions between Immobilized Nanoreactors. *Nanoscale* **2020**, *12* (3), 1551–1562. https://doi.org/10.1039/C9NR08502E.

(238) Bullock, R. M.; Chen, J. G.; Gagliardi, L.; Chirik, P. J.; Farha, O. K.; Hendon, C. H.; Jones, C. W.; Keith, J. A.; Klosin, J.; Minteer, S. D.; Morris, R. H.; Radosevich, A. T.; Rauchfuss, T. B.; Strotman, N. A.; Vojvodic, A.; Ward, T. R.; Yang, J. Y.; Surendranath, Y. Using Nature's Blueprint to Expand Catalysis with Earth-Abundant Metals. *Science* **2020**, *369* (6505), eabc3183. https://doi.org/10.1126/science.abc3183.

(239) Wu, S.; Zhou, Y.; Rebelein, J. G.; Kuhn, M.; Mallin, H.; Zhao, J.; Igareta, N. V.; Ward, T. R. Breaking Symmetry: Engineering Single-Chain Dimeric Streptavidin as Host for Artificial Metalloenzymes. *J. Am. Chem. Soc.* **2019**, *141* (40), 15869–15878. https://doi.org/10.1021/jacs.9b06923.

(240) Davis, H. J.; Ward, T. R. Artificial Metalloenzymes: Challenges and Opportunities. *ACS Cent. Sci.* **2019**, *5* (7), 1120–1136. https://doi.org/10.1021/acscentsci.9b00397.

(241) Heinisch, T.; Schwizer, F.; Garabedian, B.; Csibra, E.; Jeschek, M.; Vallapurackal, J.; Pinheiro, V. B.; Marlière, P.; Panke, S.; Ward, T. R. *E. Coli* Surface Display of Streptavidin for Directed Evolution of an Allylic Deallylase. *Chem. Sci.* **2018**, *9* (24), 5383–5388. https://doi.org/10.1039/C8SC00484F.

(242) Hohner, A. O.; David, M. P. C.; Rädler, J. O. Controlled Solvent-Exchange Deposition of Phospholipid Membranes onto Solid Surfaces. *Biointerphases* **2010**, *5* (1), 1–8. https://doi.org/10.1116/1.3319326.

(243) Tabaei, S. R.; Jackman, J. A.; Kim, S.-O.; Zhdanov, V. P.; Cho, N.-J. Solvent-Assisted Lipid Self-Assembly at Hydrophilic Surfaces: Factors Influencing the Formation of Supported Membranes. *Langmuir* **2015**, *31* (10), 3125–3134. https://doi.org/10.1021/la5048497.

(244) Vijayakrishna, K.; Mecerreyes, D.; Gnanou, Y.; Taton, D. Polymeric Vesicles and Micelles Obtained by Self-Assembly of Ionic Liquid-Based Block Copolymers Triggered by Anion or Solvent Exchange. *Macromolecules* **2009**, *42* (14), 5167–5174. https://doi.org/10.1021/ma900549k.

(245) Zan, G. H.; Jackman, J. A.; Cho, N.-J. AH Peptide-Mediated Formation of Charged Planar Lipid Bilayers. *J. Phys. Chem. B* **2014**, *118* (13), 3616–3621. https://doi.org/10.1021/jp411648s.

(246) Kim, M. C.; Gillissen, J. J. J.; Tabaei, S. R.; Zhdanov, V. P.; Cho, N.-J. Spatiotemporal Dynamics of Solvent-Assisted Lipid Bilayer Formation. *Phys. Chem. Chem. Phys.* **2015**, *17* (46), 31145–31151. https://doi.org/10.1039/C5CP05950J.

(247) Kim, M. C.; Gunnarsson, A.; Tabaei, S. R.; Höök, F.; Cho, N.-J. Supported Lipid Bilayer Repair Mediated by AH Peptide. *Phys. Chem. Chem. Phys.* **2016**, *18* (4), 3040–3047. https://doi.org/10.1039/C5CP06472D.

(248) Muñoz, M. G.; Monroy, F.; Ortega, F.; Rubio, R. G.; Langevin, D. Monolayers of Symmetric Triblock Copolymers at the Air−Water Interface. 1. Equilibrium Properties. *Langmuir* **2000**, *16* (3), 1083–1093. https://doi.org/10.1021/la990142a.

(249) Yan, Y.; Xiong, W.; Li, X.; Lu, T.; Huang, J.; Li, Z.; Fu, H. Molecular Packing Parameter in Bolaamphiphile Solutions: Adjustment of Aggregate Morphology by Modifying the Solution Conditions. *J. Phys. Chem. B* **2007**, *111* (9), 2225–2230. https://doi.org/10.1021/jp065235x.

(250) Yang, Y.-L.; Sheng, Y.-J.; Tsao, H.-K. Hybridization of Lipids to Monolayer and Bilayer Membranes of Triblock Copolymers. *Journal of Colloid and Interface Science* **2019**, *544*, 53–60. https://doi.org/10.1016/j.jcis.2019.02.071.

(251) Nguyen, T. T.; Sly, K. L.; Conboy, J. C. Comparison of the Energetics of Avidin, Streptavidin, NeutrAvidin, and Anti-Biotin Antibody Binding to Biotinylated Lipid Bilayer Examined by Second-Harmonic Generation. *Anal. Chem.* **2012**, *84* (1), 201–208. https://doi.org/10.1021/ac202375n.

(252) Jaskiewicz, K.; Makowski, M.; Kappl, M.; Landfester, K.; Kroeger, A. Mechanical Properties of Poly(Dimethylsiloxane)- *Block* -Poly(2-Methyloxazoline) Polymersomes Probed by Atomic Force Microscopy. *Langmuir* **2012**, *28* (34), 12629–12636. https://doi.org/10.1021/la301608k.

(253) Canale, C.; Jacono, M.; Diaspro, A.; Dante, S. Force Spectroscopy as a Tool to Investigate the Properties of Supported Lipid Membranes. *Microsc. Res. Tech.* **2010**, *73* (10), 965–972. https://doi.org/10.1002/jemt.20834.

(254) Et-Thakafy, O.; Guyomarc'h, F.; Lopez, C. Young Modulus of Supported Lipid Membranes Containing Milk Sphingomyelin in the Gel, Fluid or Liquid-Ordered Phase, Determined Using AFM Force Spectroscopy. *Biochimica et Biophysica Acta (BBA) - Biomembranes* **2019**, *1861* (9), 1523–1532. https://doi.org/10.1016/j.bbamem.2019.07.005.

(255) El Kirat, K.; Bartkowski, M.; Haupt, K. Probing the Recognition Specificity of a Protein Molecularly Imprinted Polymer Using Force Spectroscopy. *Biosensors and Bioelectronics* **2009**, *24* (8), 2618–2624. https://doi.org/10.1016/j.bios.2009.01.018.

(256) Zhang, X.; Liu, C.; Wang, Z. Force Spectroscopy of Polymers: Studying on Intramolecular and Intermolecular Interactions in Single Molecular Level. *Polymer* **2008**, *49* (16), 3353–3361. https://doi.org/10.1016/j.polymer.2008.04.056.

(257) Zhang, X.; Tanner, P.; Graff, A.; Palivan, C. G.; Meier, W. Mimicking the Cell Membrane with Block Copolymer Membranes. *J. Polym. Sci. A Polym. Chem.* **2012**, *50* (12), 2293–2318. https://doi.org/10.1002/pola.26000.

(258) Fauquignon, M.; Ibarboure, E.; Le Meins, J.-F. Membrane Reinforcement in Giant Hybrid Polymer Lipid Vesicles Achieved by Controlling the Polymer Architecture. *Soft Matter* **2021**, *17* (1), 83–89. https://doi.org/10.1039/D0SM01581D.

(259) Nielsen, C. H. Biomimetic Membranes for Sensor and Separation Applications. *Anal Bioanal Chem* **2009**, *395* (3), 697–718. https://doi.org/10.1007/s00216-009-2960-0.

(260) Piletsky, S. A.; Panasyuk, T. L.; Piletskaya, E. V.; Nicholls, I. A.; Ulbricht, M. Receptor and Transport Properties of Imprinted Polymer Membranes – a Review. *Journal of Membrane Science* **1999**, *157* (2), 263–278. https://doi.org/10.1016/S0376-7388(99)00007-1.

(261) Clodt, J. I.; Filiz, V.; Rangou, S.; Buhr, K.; Abetz, C.; Höche, D.; Hahn, J.; Jung, A.; Abetz, V. Double Stimuli-Responsive Isoporous Membranes via Post-Modification of PH-Sensitive Self-Assembled Diblock Copolymer Membranes. *Adv. Funct. Mater.* **2013**, *23* (6), 731–738. https://doi.org/10.1002/adfm.201202015.

(262) Ozaydin-Ince, G.; Coclite, A. M.; Gleason, K. K. CVD of Polymeric Thin Films: Applications in Sensors, Biotechnology, Microelectronics/Organic Electronics, Microfluidics, MEMS, Composites and Membranes. *Rep. Prog. Phys.* **2012**, *75* (1), 016501. https://doi.org/10.1088/0034-4885/75/1/016501.

(263) Zhang, X.; Higashihara, T.; Ueda, M.; Wang, L. Polyphenylenes and the Related Copolymer Membranes for Electrochemical Device Applications. *Polym. Chem.* **2014**, *5* (21), 6121–6141. https://doi.org/10.1039/C4PY00898G.

(264) Wu, D.; Spulber, M.; Itel, F.; Chami, M.; Pfohl, T.; Palivan, C. G.; Meier, W. Effect of Molecular Parameters on the Architecture and Membrane Properties of 3D Assemblies of Amphiphilic Copolymers. *Macromolecules* **2014**, *47* (15), 5060–5069. https://doi.org/10.1021/ma500511r.

(265) Bangham, A. D. Membrane Models with Phospholipids. *Progress in Biophysics and Molecular Biology* **1968**, *18*, 29–95. https://doi.org/10.1016/0079-6107(68)90019-9.

(266) Di Leone, S.; Avsar, S. Y.; Belluati, A.; Wehr, R.; Palivan, C. G.; Meier, W. Polymer–Lipid Hybrid Membranes as a Model Platform to Drive Membrane–Cytochrome *c* Interaction and Peroxidase-like Activity. *J. Phys. Chem. B* **2020**, *124* (22), 4454–4465. https://doi.org/10.1021/acs.jpcb.0c02727.

(267) Dao, T. P. T.; Fernandes, F.; Er-Rafik, M.; Salva, R.; Schmutz, M.; Brûlet, A.; Prieto, M.; Sandre, O.; Le Meins, J.-F. Phase Separation and Nanodomain Formation in Hybrid Polymer/Lipid Vesicles. *ACS Macro Lett.* **2015**, *4* (2), 182–186. https://doi.org/10.1021/mz500748f.

(268) Dao, T. P. T.; Fernandes, F.; Ibarboure, E.; Ferji, K.; Prieto, M.; Sandre, O.; Le Meins, J.-F. Modulation of Phase Separation at the Micron Scale and Nanoscale in Giant Polymer/Lipid Hybrid Unilamellar Vesicles (GHUVs). *Soft Matter* **2017**, *13* (3), 627–637. https://doi.org/10.1039/C6SM01625A.

(269) Wacklin, H. P. Composition and Asymmetry in Supported Membranes Formed by Vesicle Fusion. *Langmuir* **2011**, *27* (12), 7698–7707. https://doi.org/10.1021/la200683e.

(270) Tero, R.; Takizawa, M.; Li, Y.-J.; Yamazaki, M.; Urisu, T. Lipid Membrane Formation by Vesicle Fusion on Silicon Dioxide Surfaces Modified with Alkyl Self-Assembled Monolayer Islands. *Langmuir* **2004**, *20* (18), 7526–7531. https://doi.org/10.1021/la0400306.

(271) Kyropoulou, M.; Yorulmaz Avsar, S.; Schoenenberger, C.-A.; Palivan, C. G.; Meier, Wolfgang. P. From Spherical Compartments to Polymer Films: Exploiting Vesicle Fusion to Generate Solid Supported Thin Polymer Membranes. *Nanoscale* **2021**, *13* (14), 6944–6952. https://doi.org/10.1039/D1NR01122G.

(272) Tabaei, S. R.; Jackman, J. A.; Kim, M.; Yorulmaz, S.; Vafaei, S.; Cho, N.-J. Biomembrane Fabrication by the Solvent-Assisted Lipid Bilayer (SALB) Method. *JoVE* **2015**, No. 106, 53073. https://doi.org/10.3791/53073.

(273) Tabaei, S. R.; Jackman, J. A.; Kim, S.-O.; Liedberg, B.; Knoll, W.; Parikh, A. N.; Cho, N.-J. Formation of Cholesterol-Rich Supported Membranes Using Solvent-Assisted Lipid Self-Assembly. *Langmuir* **2014**, *30* (44), 13345–13352. https://doi.org/10.1021/la5034433.

(274) Khakbaz, P.; Klauda, J. B. Probing the Importance of Lipid Diversity in Cell Membranes via Molecular Simulation. *Chemistry and Physics of Lipids* **2015**, *192*, 12–22. https://doi.org/10.1016/j.chemphyslip.2015.08.003.

(275) Li, Y.; Chen, X.; Gu, N. Computational Investigation of Interaction between Nanoparticles and Membranes: Hydrophobic/Hydrophilic Effect. *J. Phys. Chem. B* **2008**, *112* (51), 16647–16653. https://doi.org/10.1021/jp8051906.

(276) Wehr, R.; Gaitzsch, J.; Daubian, D.; Fodor, C.; Meier, W. Deepening the Insight into Poly(Butylene Oxide)- *Block* -Poly(Glycidol) Synthesis and Self-Assemblies: Micelles, Worms and Vesicles. *RSC Adv.* **2020**, *10* (38), 22701–22711. https://doi.org/10.1039/D0RA04274A.

(277) Ehrsam, D.; Porta, F.; Hussner, J.; Seibert, I.; Meyer zu Schwabedissen, H. E. PDMS-PMOXA-Nanoparticles Featuring a Cathepsin B-Triggered Release Mechanism. *Materials* **2019**, *12* (17), 2836. https://doi.org/10.3390/ma12172836.

(278) Itel, F.; Najer, A.; Palivan, C. G.; Meier, W. Dynamics of Membrane Proteins within Synthetic Polymer Membranes with Large Hydrophobic Mismatch. *Nano Lett.* **2015**, *15* (6), 3871–3878. https://doi.org/10.1021/acs.nanolett.5b00699.

(279) Grason, G. The Packing of Soft Materials: Molecular Asymmetry, Geometric Frustration and Optimal Lattices in Block Copolymer Melts. *Physics Reports* **2006**, *433* (1), 1–64. https://doi.org/10.1016/j.physrep.2006.08.001.

(280) Tsai, H.-C.; Yang, Y.-L.; Sheng, Y.-J.; Tsao, H.-K. Formation of Asymmetric and Symmetric Hybrid Membranes of Lipids and Triblock Copolymers. *Polymers* **2020**, *12* (3), 639. https://doi.org/10.3390/polym12030639.

(281) Dionzou, M.; Morère, A.; Roux, C.; Lonetti, B.; Marty, J.-D.; Mingotaud, C.; Joseph, P.; Goudounèche, D.; Payré, B.; Léonetti, M.; Mingotaud, A.-F. Comparison of Methods for the Fabrication and the Characterization of Polymer Self-Assemblies: What Are the Important Parameters? *Soft Matter* **2016**, *12* (7), 2166–2176. https://doi.org/10.1039/C5SM01863C.

(282) Shahane, G.; Ding, W.; Palaiokostas, M.; Orsi, M. Physical Properties of Model Biological Lipid Bilayers: Insights from All-Atom Molecular Dynamics Simulations. *J Mol Model* **2019**, *25* (3), 76. https://doi.org/10.1007/s00894-019-3964-0.

(283) Bakht, O.; Pathak, P.; London, E. Effect of the Structure of Lipids Favoring Disordered Domain Formation on the Stability of Cholesterol-Containing Ordered Domains (Lipid Rafts): Identification of Multiple Raft-Stabilization Mechanisms. *Biophysical Journal* **2007**, *93* (12), 4307–4318. https://doi.org/10.1529/biophysj.107.114967.

(284) Becucci, L.; Valensin, D.; Innocenti, M.; Guidelli, R. Dermcidin, an Anionic Antimicrobial Peptide: Influence of Lipid Charge, PH and Zn^{2+} on Its Interaction with a Biomimetic Membrane. *Soft Matter* **2014**, *10* (4), 616–626. https://doi.org/10.1039/C3SM52400K.

(285) Klenz, U.; Saleem, M.; Meyer, M. C.; Galla, H.-J. Influence of Lipid Saturation Grade and Headgroup Charge: A Refined Lung Surfactant Adsorption Model. *Biophysical Journal* **2008**, *95* (2), 699–709. https://doi.org/10.1529/biophysj.108.131102.

(286) van Meer, G.; Voelker, D. R.; Feigenson, G. W. Membrane Lipids: Where They Are and How They Behave. *Nat Rev Mol Cell Biol* **2008**, *9* (2), 112–124. https://doi.org/10.1038/nrm2330.

(287) Callan-Jones, A.; Bassereau, P. Curvature-Driven Membrane Lipid and Protein Distribution. *Current Opinion in Solid State and Materials Science* **2013**, *17* (4), 143–150. https://doi.org/10.1016/j.cossms.2013.08.004.

(288) Cooke, I. R.; Deserno, M. Coupling between Lipid Shape and Membrane Curvature. *Biophysical Journal* **2006**, *91* (2), 487–495. https://doi.org/10.1529/biophysj.105.078683.

(289) Lörcher, S.; Meier, W. Cosolvent Fractionation of PMOXA-b-PDMS-b-PMOXA: Bulk Separation of Triblocks from Multiblocks. *European Polymer Journal* **2017**, *88*, 575–585. https://doi.org/10.1016/j.eurpolymj.2016.12.006.

7. Appendix

7.1 Figures

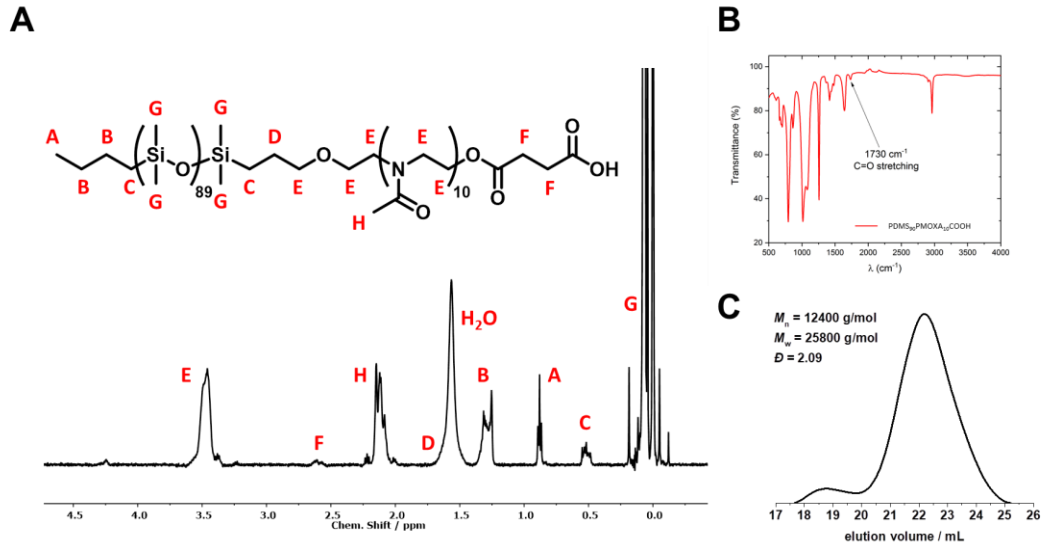

Figure 7-1. Polymer characterisation: NMR (A), FT-IR (B) and GPC (C).

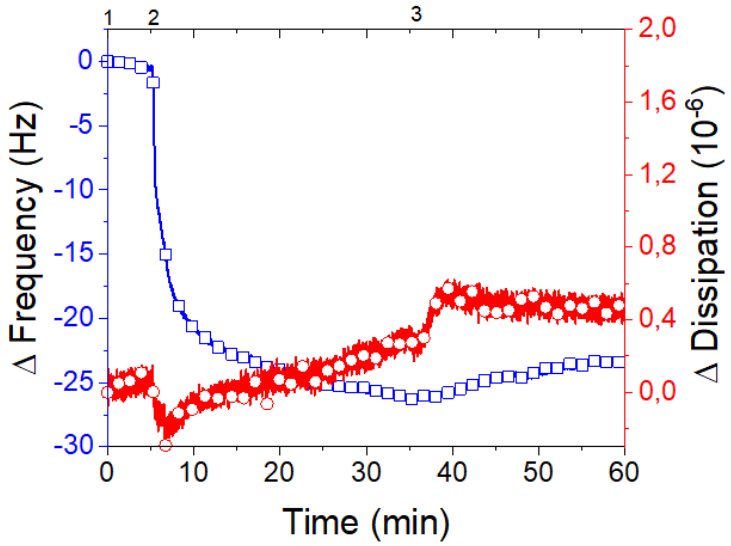

Figure 7-2. QCM-D of cyt c adsorption onto bare silica substrate. The numbers at the top of figure denote as follows; 1 injection of PB solution, 2 Injection of 0.5 mg/mL cyt c and 3 injection of PB solution.

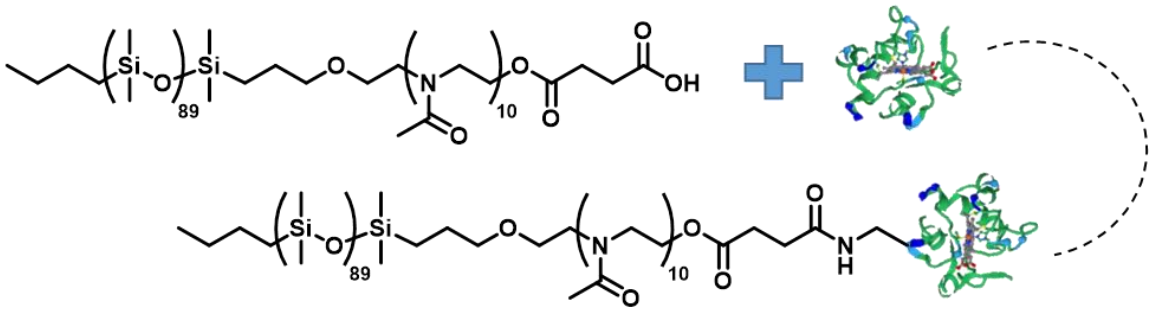

Figure 7-3. Schematic representation of polymer - cyt c conjugation through EDC/NHS chemistry.

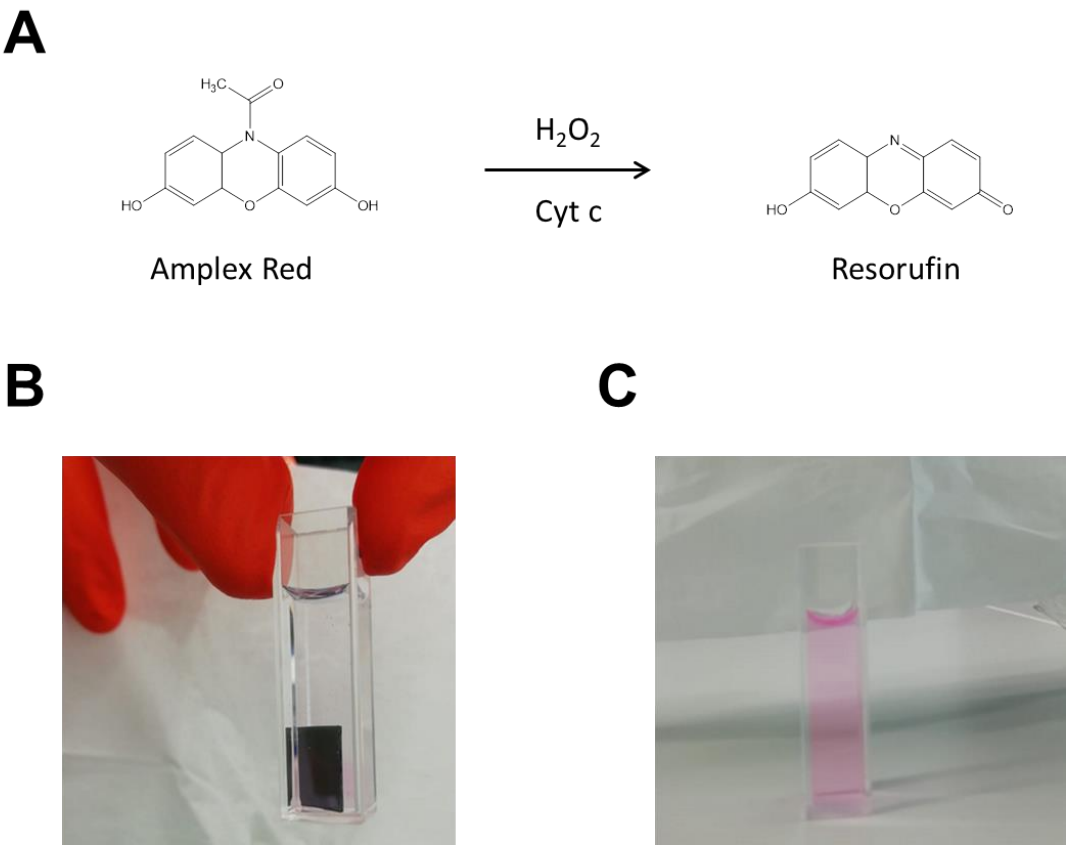

Figure 7-4. schematic representation of AR oxidation into high fluorescent species (A); change in colour of the PB solution over time in the presence of cyt c conjugated onto hybrid membrane after 30 minutes (B) and12 hours (C).

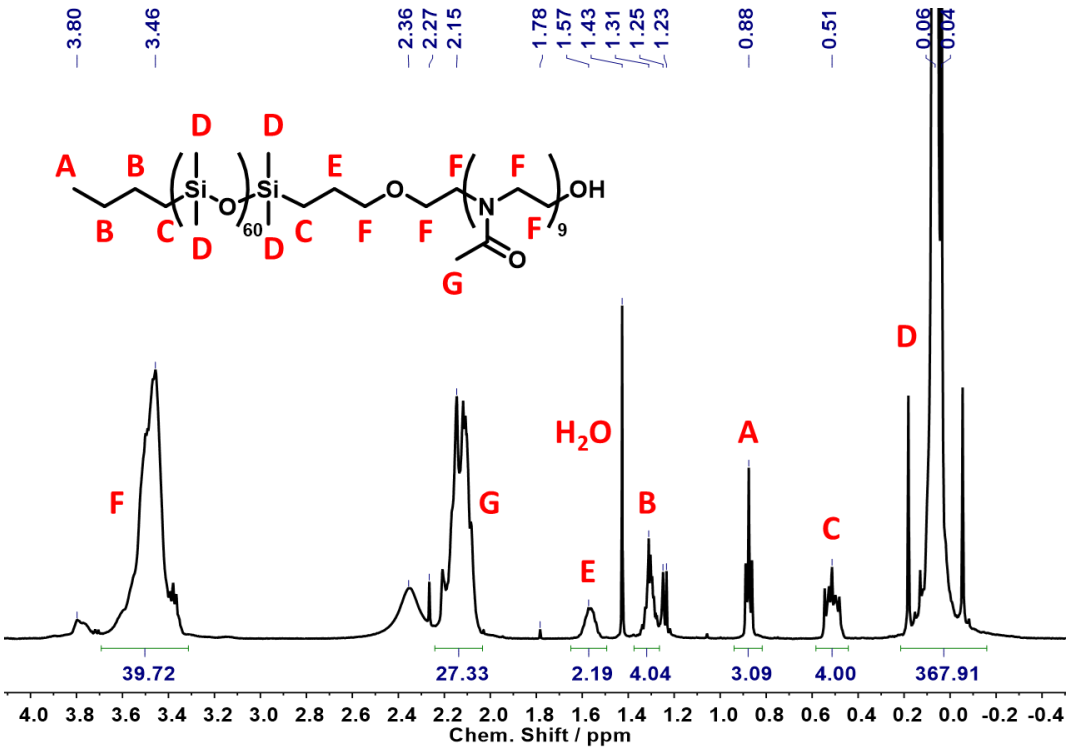

Figure 7-5. NMR spectra of $A_{61}B_9$.

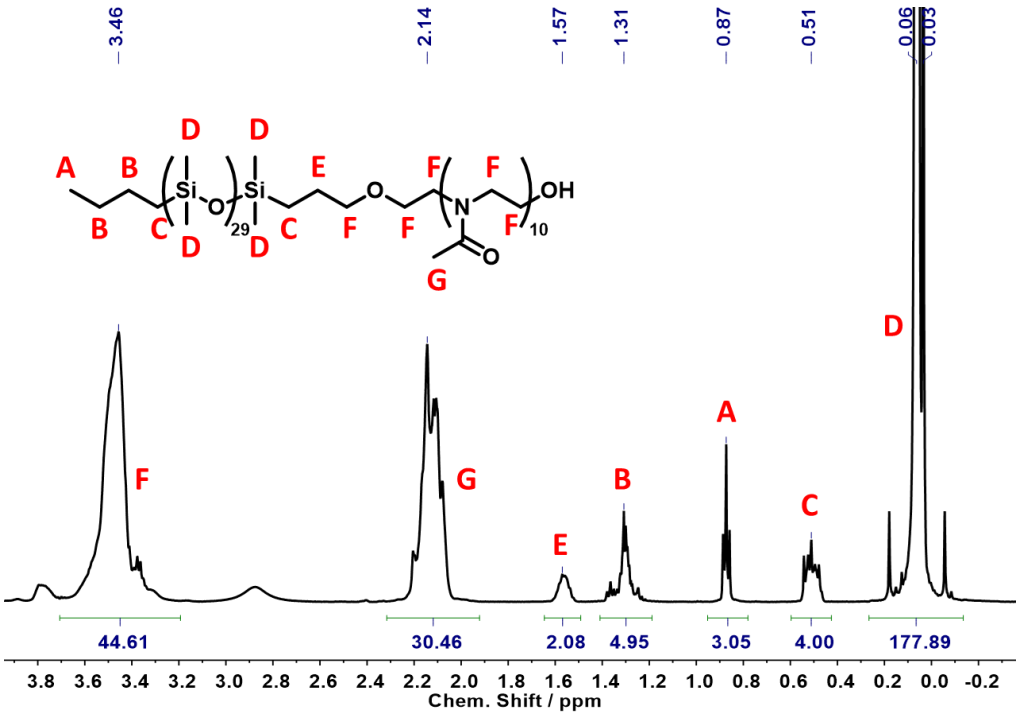

Figure 7-6. NMR spectra of $A_{30}B_{10}$.

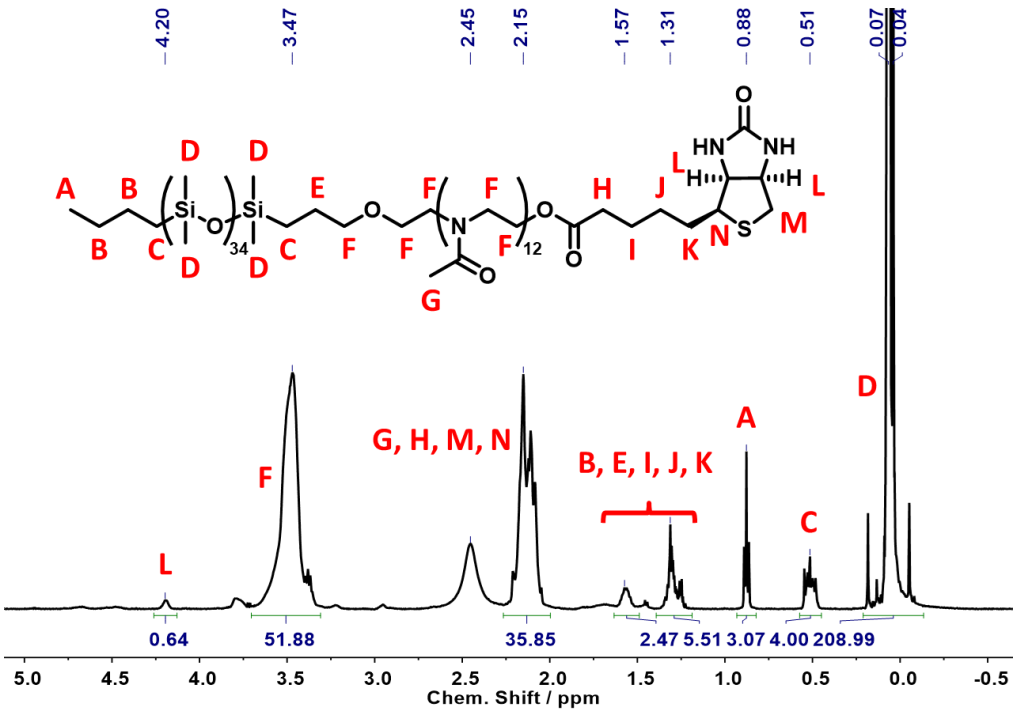

Figure 7-7. NMR spectra of biotin-$A_{35}B_{12}$.

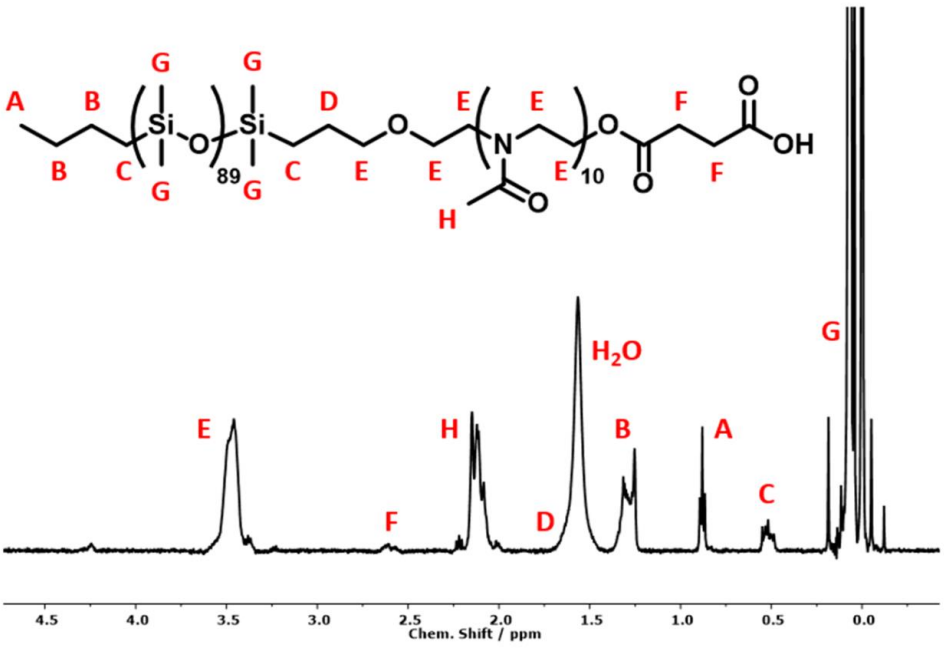

Figure 7-8. NMR spectra of $A_{89}B_{10}$.

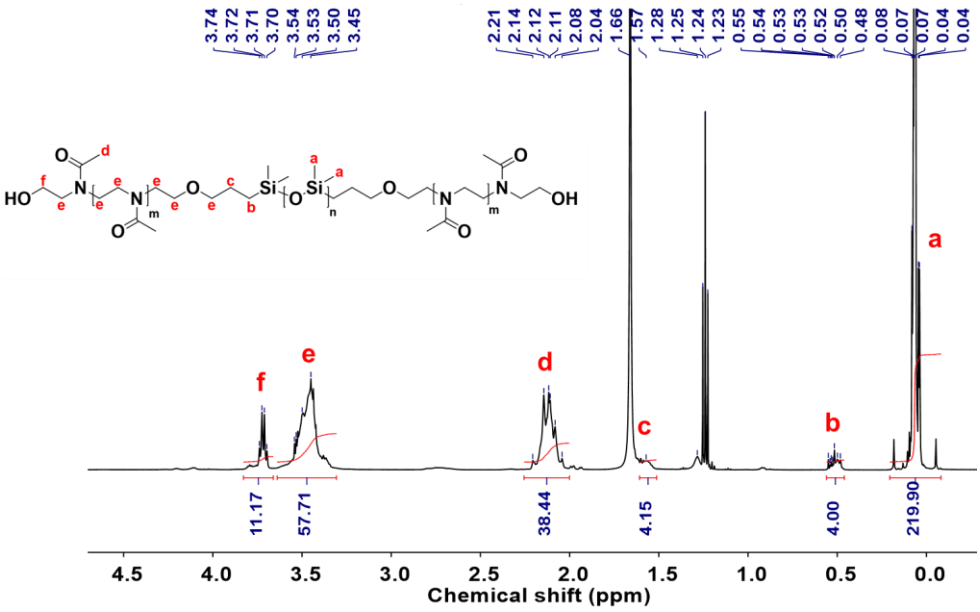

Figure 7-9. NMR spectra of $B_6A_{36}B_6$.

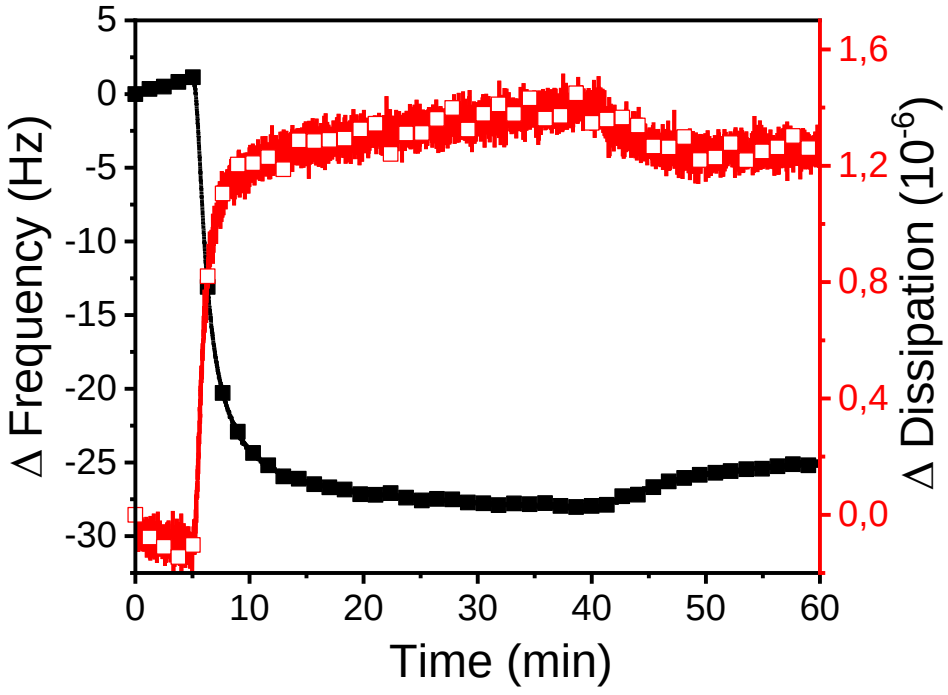

Figure 7-10. QCM-D plots of BSA attachment onto bare silica.

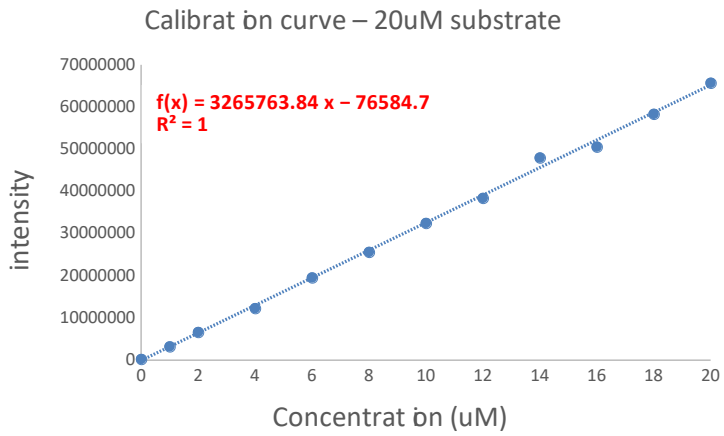

Figure 7-11. Calibration curves for determining the concentration of the product obtained by the enzymatic activity at different times by fluorimetry.

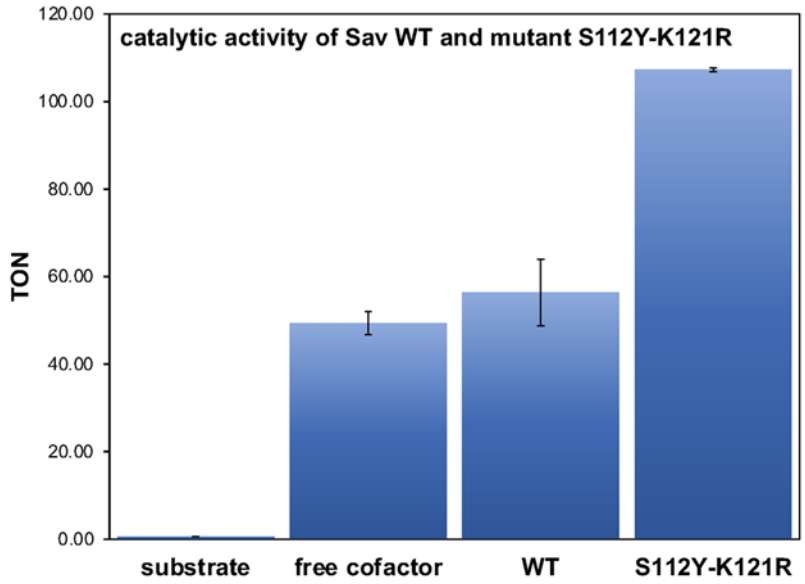

Figure 7-12. Comparison of the catalytic activity of Sav-based artificial metalloenzymes to the free cofactor in solution. Allylic deallylation of N-(allyloxycarbonyl)-aminocoumarin substrate leads to the fluorescent product aminocouamarin which was observed by TECAN measurements. Conditions: 500 µM substrate N-(allyloxycarbonyl)-aminocoumarin, 5 µM ruthenium cofactor, 10 µM Sav, 25°C, 16 h.

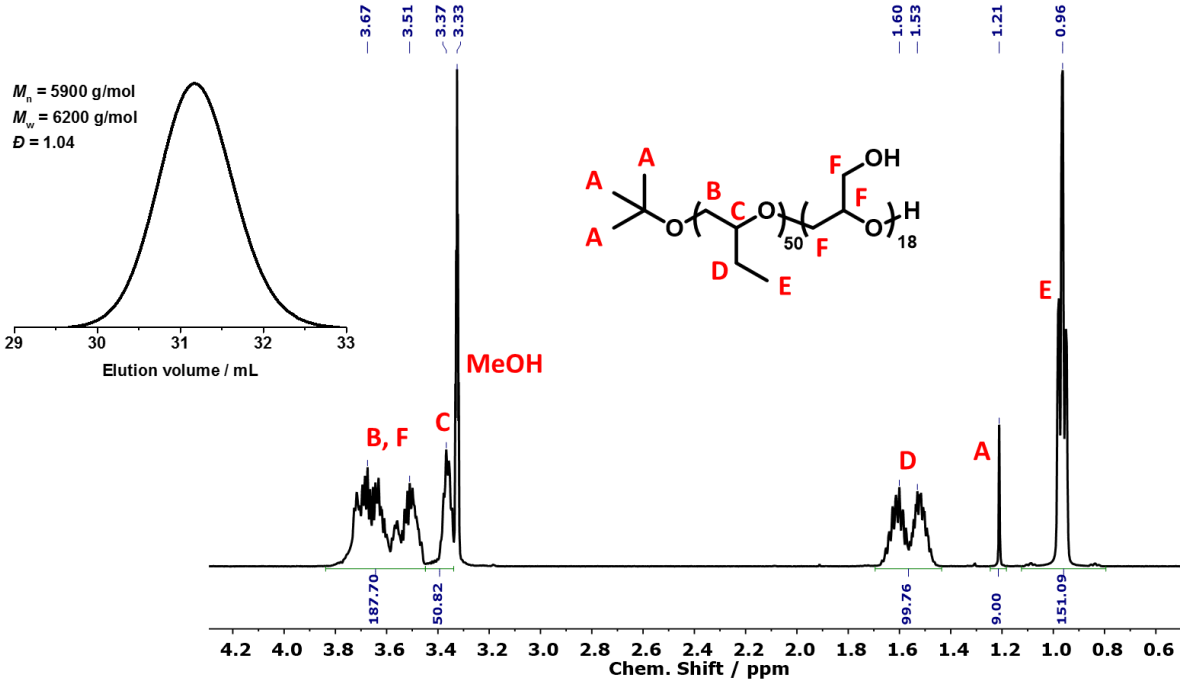

Figure 7-13. GPC and NMR spectra of PBO_{50}-PG_{18}.

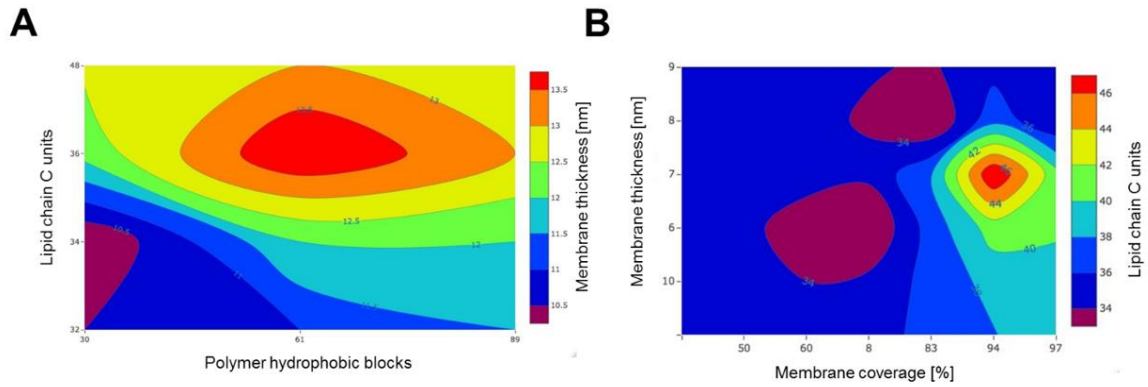

Figure 7-14. Contour plot reporting the membrane thickness in function of the PDMS-PMOXA polymers and lipids hydrophobicity (A) and membrane coverage and thickness in function of lipid hydrophobicity for membrane composed of PEO-PG polymer (B).

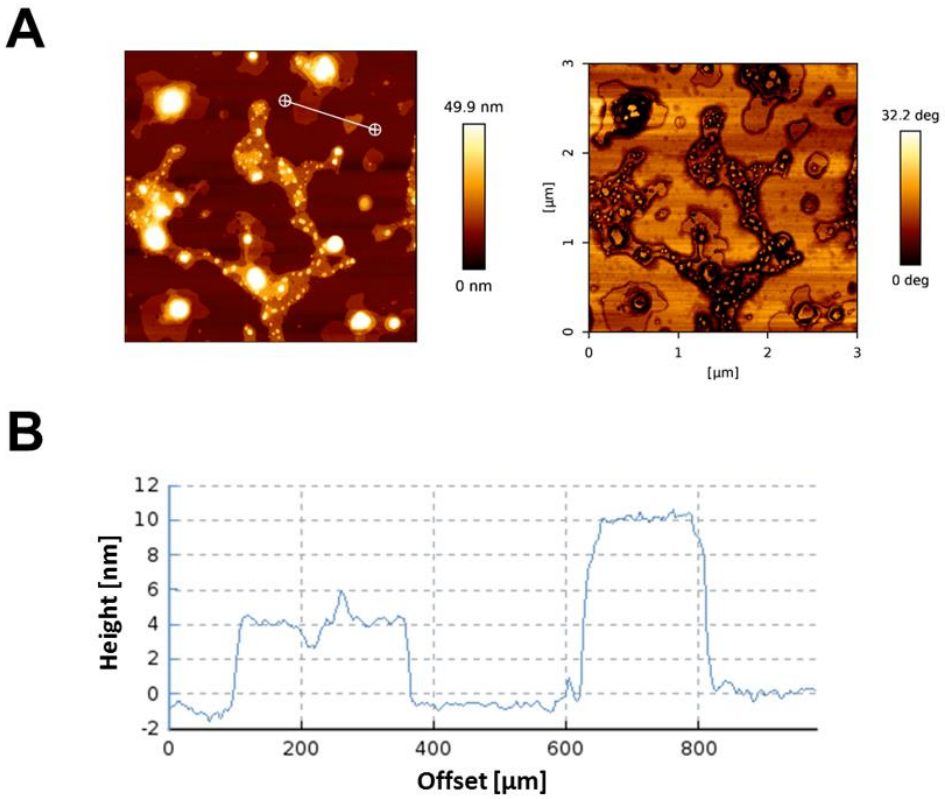

Figure 7-15. AFM characterization of membrane composed of $A_{61}B_9$ polymer and DPPC lipid (50:50 w/w): height image and phase image (A); cross section (B).

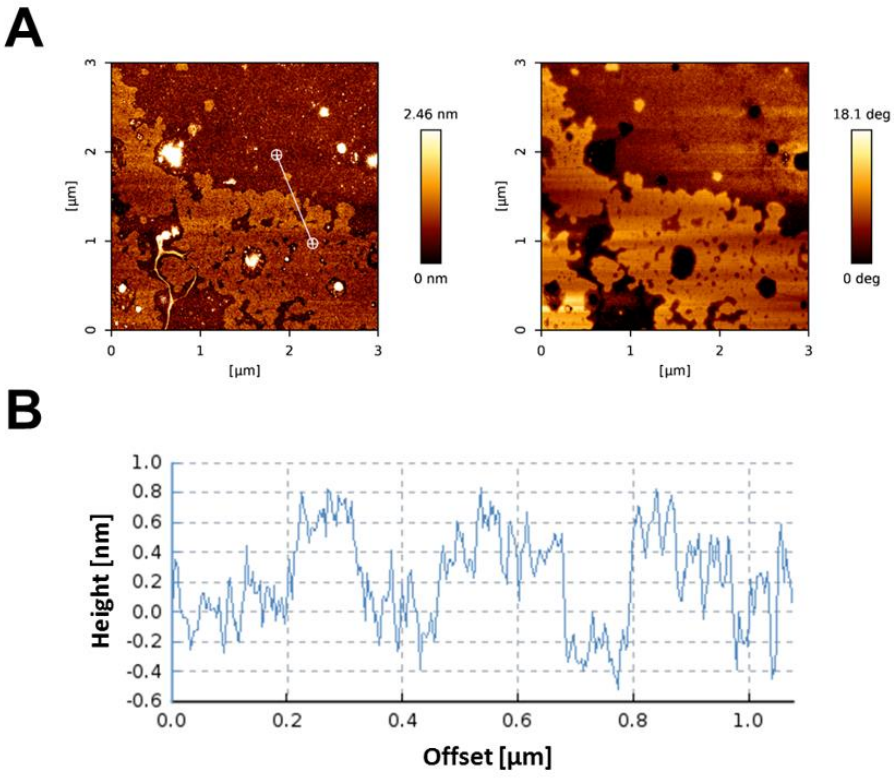

Figure 7-16. AFM characterization of membrane composed of $PBO_{50}PG_{18}$ polymer and DPPC lipid (50:50 w/w): height image and phase image (A); cross section (B).

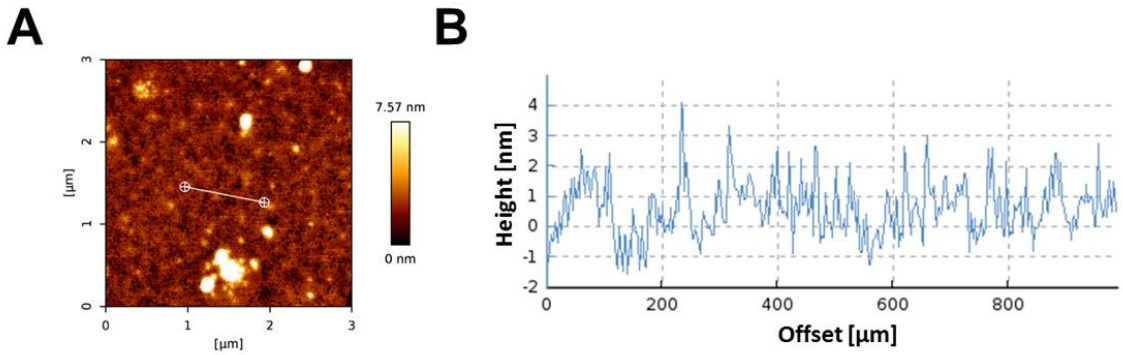

Figure 7-17. AFM characterization of membrane composed of $A_{89}B_{10}$ polymer and SM lipid (50:50 w/w): height image (A); cross section (B).

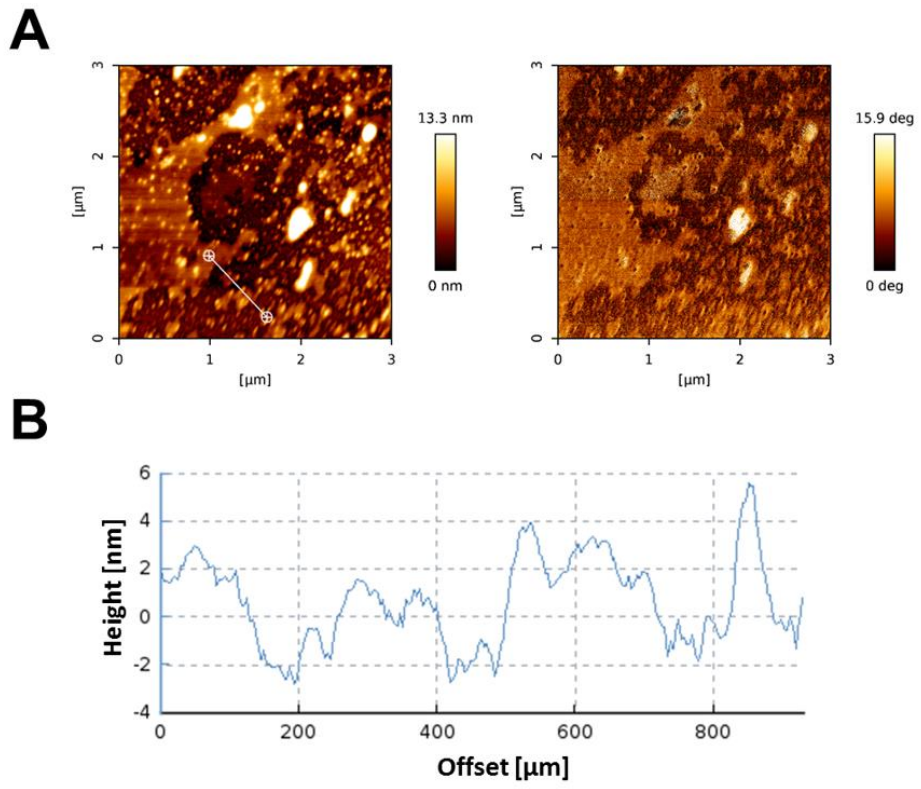

Figure 7-18. AFM characterization of membrane composed of $A_{30}B_{10}$ polymer and SM lipid (50:50 w/w): height image and phase image (A); cross section (B).

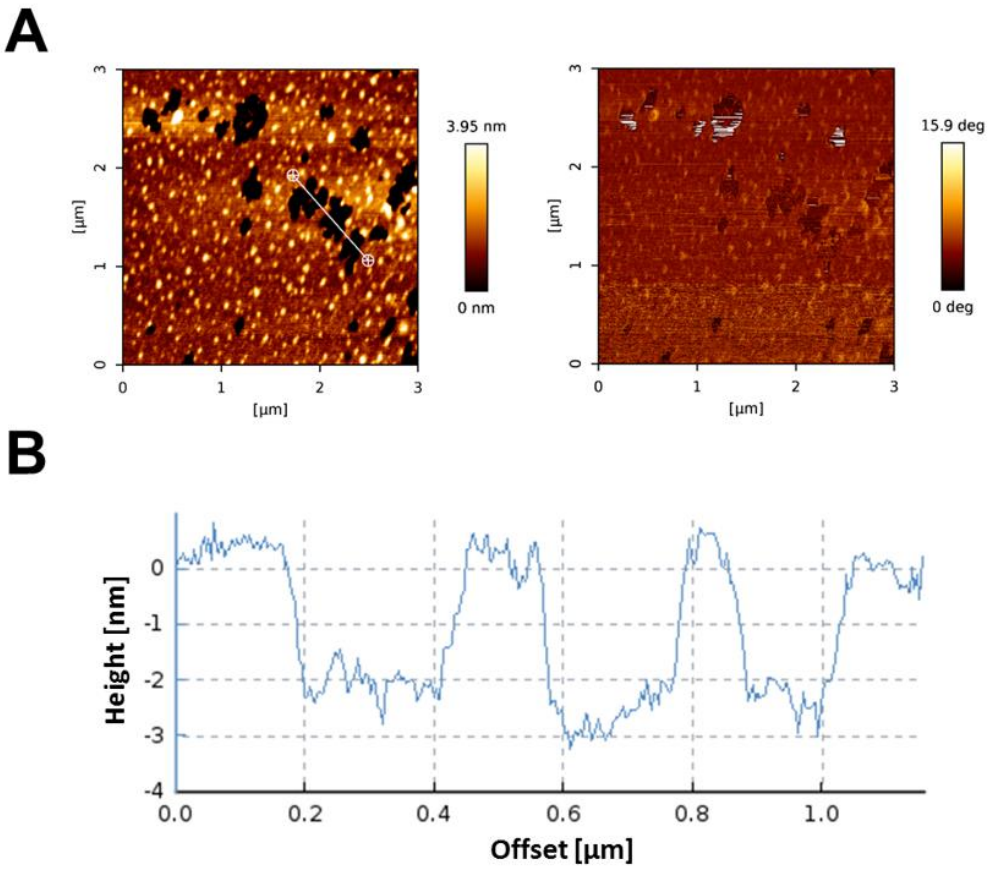

Figure 7-19. AFM characterization of membrane composed of $PBO_{50}PG_{18}$ polymer and SM lipid (50:50 w/w): height image and phase image (A); cross section (B).

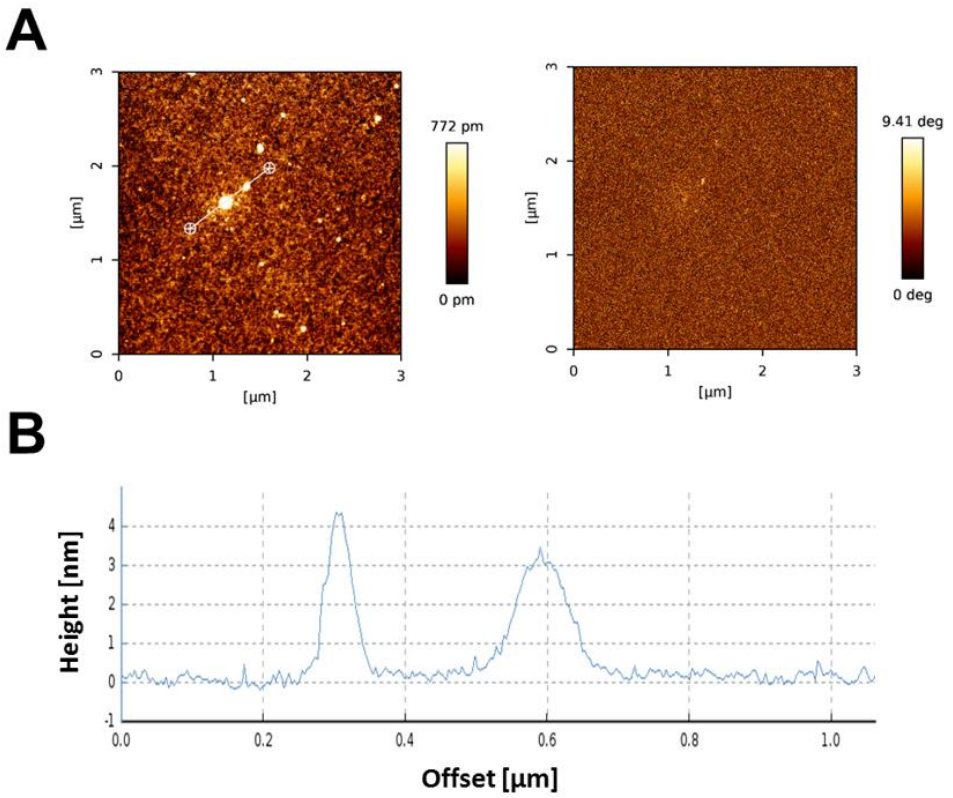

Figure 7-20. AFM characterization of membrane composed of $PBO_{50}PG_{18}$ polymer and NGPE lipid (50:50 w/w): height image and phase image (A); cross section (B).

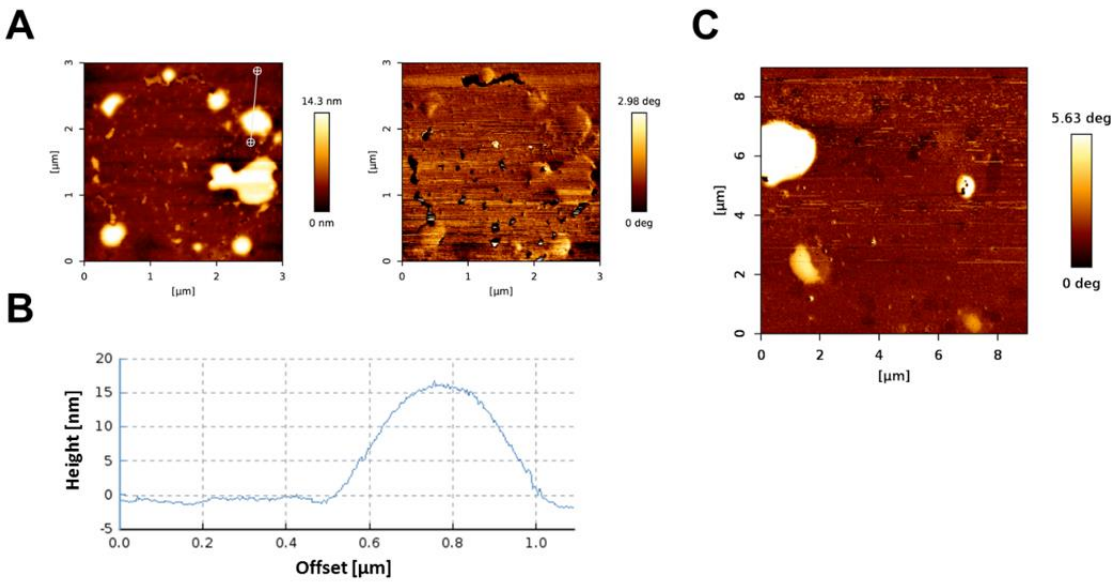

Figure 7-21. AFM characterization of membrane composed of $PBO_{50}PG_{18}$ polymer and POPE lipid (50:50 w/w): height image and phase image (A); cross section (B); phase image of $A_{61}B_9$-POPE membrane (50:50 w/w).

7.2. Tables

XMembrane type	Frequency Shift (Hz)		Mass (ng/cm2)	
	Polymer membrane	Hybrid membrane	Polymer membrane	Hybrid membrane
EDC/NHS	-8.6 ± 1.3	-5.7 ± 1.2	153 ± 24	101 ± 23
Insertion (with BSA step)	-8.1 ± 1.3	-8.4 ± 3.3	144 ± 28	148 ± 62
Insertion (without BSA step)	-8.0 ± 0.9	-7.5 ± 2.1	142 ± 16	133 ± 38

Table 7-1. QCM-D quantifications of EDC/NHS and cytochrome c combination with polymer and hybrid membranes.

Membrane type	Frequency Shift		Mass		Molecules of cyt c	
	Insertion	Conjugation	Insertion	Conjugation	Insertion	Conjugation
Polymer	-8.0 ± 0.9	-7.4 ± 0.8	142 ± 16	132 ± 18	7.1 ± 0.8	6.6 ± 0.7
Hybrid	-7.5 ± 2.1	-2.5 ± 0.7	133 ± 38	44 ± 13	6.7 ± 1.9	2.2 ± 0.6
Lipid	-2.4 ± 2.3	n.a.	42 ± 40	n.a.	2.1 ± 2.0	n.a.

Table 7-2. Quantification of cytochrome c combined with polymer and hybrid membranes.

[a]The Frequency is reported in Hz, the mass is reported in ng/cm^2, the molecules of cyt c have to be multiplied by 10^{12}. [b]Not available, the conjugation was not performed for the lipid because it has no carboxylic end group. The quantity of cyt c combined with the two strategies are compared.

Polymer	Membrane formation (4)		BSA step (6)	
	Δf (Hz)	ΔD (10-6)	Δf (Hz)	ΔD (10-6)
A30B10	-42 ± 6	0.8 ± 0.6	-46 ± 6 (-4 ± 6)	0.9 ± 0.6
A61B9	-115 ± 1	5.5 ± 0.1	-121 ± 4 (-6 ± 4)	4.9 ± 0.1
A89B10	-80 ± 10	11.5 ± 2.7	-94 ± 11 (-14 ± 11)	9.3 ± 2.9
B6A36B6	-72 ± 4	1.3 ± 0.1	-76 ± 4 (-4 ± 4)	1.1 ± 0.9

Polymer	Mass (ng)	Thickness (nm)
A30B10	696 ± 154	7 ± 1
A61B9	1777 ± 422	19 ± 2
A89B10	1424 ± 192	16 ± 1
B6A36B6	1269 ± 65	13 ± 2

Table 7-3. frequency and dissipation shift values for different one-component diblock and triblock polymer membranes. Mass and thickness of the membranes were calculated with the composite Sauerbrey model.

Biotin-A35B12 A61B9 w/w	Membrane formation (4)		BSA step (6)		Mass (ng)	Thickness (nm)
	Δf (Hz)	ΔD (10-6)	Δf (Hz)	ΔD (10-6)		
0-100	-115 ± 1	5.5 ± 0.1	-121 ± 4 (-6 ± 4)	4.9 ± 0.1	1777 ± 422	19 ± 1
20-80	-90 ± 1	2.8 ± 0.1	-95 ± 1 (-5 ± 1)	3.6 ± 0.5	1675 ± 50	17 ± 1
50-50	-72 ± 1	2.3 ± 0.5	-78 ± 1 (-6 ± 1)	1.9 ± 0.3	1415 ± 21	15 ± 2
80-20	-80 ± 2	3.2 ± 0.5	-86 ± 3 (-6 ± 4)	2.1 ± 0.3	1509 ± 63	15 ± 2
100-0	-70 ± 1	2.5 ± 0.3	-76 ± 1 (-6 ± 1)	2.1 ± 0.2	1353 ± 4	14 ± 1

Table 7-4. Frequency and dissipation shift values for the reported QCM-D graphs. Mass and thickness of the membranes were calculated with the composite Sauerbrey model.

Biotin-A35B12 A30B10 w/w	Membrane formation		BSA step	
	Δf (Hz)	ΔD (10-6)	Δf (Hz)	ΔD (10-6)
0-100	-42 ± 6	0.8 ± 0.6	-46 ± 6 (-4 ± 6)	0.9 ± 0.6
20-80	-56 ± 4	0.8 ± 0.1	-59 ± 4 (-3 ± 4)	0.3 ± 0.1
Biotin-A35B12 A30B10 w/w	Mass (ng)	Thickness (nm)		
0-100	696 ± 154	7 ± 1		
20-80	1230 ± 438	12 ± 4		

Table 7-5. Frequency and dissipation shift values for one- and two-components membranes. Mass and thickness of the membranes and mass of attached biomolecules were calculated with the composite Sauerbrey model.

Biotin-A35B12 A61B9 20:80	Membrane formation (4)		BSA step (6)	
Concentration	Δf (Hz)	ΔD (10-6)	Δf (Hz)	ΔD (10-6)
0.1 mg/mL	-57 ± 4	3.5 ± 0.7	-65 ± 1 (- 10 ± 4)	2.2 ± 0.4
0.5 mg/mL	-90 ± 1	2.8 ± 0.1	-95 ± 1 (-5 ± 1)	3.6 ± 0.5
1 mg/mL	-113 ± 0.7	3.6 ± 1.3	-117 ± 3 (-4 ± 3)	3.1 ± 1.4
Biotin-A35B12 A61B9 20:80 Concentration	Mass (ng)	Thickness (nm)		
0.1 mg/mL	977 ± 4	9.8 ± 0.1		
0.5 mg/mL	1675 ± 50	17 ± 1		
1 mg/mL	2030 ± 6	20.3 ± 0.1		

Table 7-6. Frequency and dissipation shift values for biotin-$A_{35}B_{12}$ and $A_{61}B_9$ polymers (20:80 w/w) at different concentrations. Mass and thickness of the membranes were calculated with the composite Sauerbrey model.

Membrane	Roughness (nm)	Elasticity (nN/μm)
	RMS (Rq)	
Biotin-A35B12/A61B9 20-80	1.83	16.73
Biotin-A35B12/A30B10 20-80	2.21	6.09
A61B9	1.76	8.85
A30B10	1.75	3.16
Bare silica	0.12	2.36

Table 7-7. Root Mean Squared (RMS) values of roughness and elasticity for different polymer membranes and bare silica.

Biotin-A35B12 A61B9 w/w	Avidin attachment (3)		
	Δf (Hz)	ΔD (10-6)	Mass (ng)
0-100	-2 ± 2	3.2 ± 2.8	0
20-80	-20 ± 2	3.7 ± 0.5	354 ± 35
50-50	-21 ± 1	1.9 ± 0.1	372 ± 18
80-20	-29 ± 1	2.8 ± 0.2	513 ± 18
100-0	-26 ± 2	1.8 ± 0.4	460 ± 35

Table 7-8. Frequency and dissipation shift values for the reported QCM-D graphs. Mass of the avidin attached was calculated with the composite Sauerbrey model.

Concentration	Avidin attachment (3)		
	Δf (Hz)	ΔD (10-6)	Mass (ng)
0.1 mg/mL	-10 ± 2	3.0 ± 0.4	194 ± 25
0.5 mg/mL	-20 ± 2	4.1 ± 0.6	354 ± 25
1 mg/mL	-18 ± 1	4.6 ± 1.5	327 ± 12

Table 7-9. Frequency and dissipation shift values for avidin attachment onto functional membranes at different polymer concentrations and block lenght. Mass of the avidin attached was calculated with the composite Sauerbrey model.

Biotin-A35B12 A30B12 w/w	Avidin attachment			SAV-Ru attachment		
	Δf (Hz)	ΔD (10-6)	Mass (ng)	Δf (Hz)	ΔD (10-6)	Mass (ng)
20-80	-14 ± 2	1.5 ± 0.3	247 ± 35	-18 ± 3	4.3 ± 0.9	310 ± 47
Biotin-A35B12 A30B10 w/w	SAV attachment			DNA-Biotin attachment		
	Δf (Hz)	ΔD (10-6)	Mass (ng)	Δf (Hz)	ΔD (10-6)	Mass (ng)
20-80	-16 ± 3	1.5 ± 0.2	283 ± 47	-6 ± 1	1.0 ± 0.1	110 ± 15
Biotin-A35B12 A30B10 w/w	Complementary strand attachment					
	Δf (Hz)	ΔD (10-6)	Mass (ng)			
20-80	-3 ± 1	0.1 ± 0.0	44 ± 10			

Table 7-10. Frequency and dissipation shift values for different biomolecules attachment onto membranes composed of biotin-$A_{35}B_{12}/A_{30}B_{10}$ and biotin-$A_{35}B_{12}/A_{61}B_9$ polymers (20:80 w/w) at different concentrations. Mass of the biomolecules attached was calculated with the composite Sauerbrey model.

	Substrate converted (ng)				
Time (hours)	WT membrane	YR membrane	WT bulk	YR bulk	PBS
0	0.18	0.29	0.1	0.08	0.21
4	0.89	2.48	1.58	4.1	0.02
24	1.81	3.85	2.43	5.84	0.25
48	2.38	5.08	3.85	6.51	0.02

Table 7-11. Quantification of the substrate converted by mutant and wild type ADAse in bulk or onto membrane over 48 hours. PBS was used as control.

Hybrid mixture	Membrane formation (4) Δf (Hz)	BSA step (6) Δf (Hz)	Thickness (nm)	Membrane coverage (%)
DPPC-$A_{61}B_9$ 50:50	-83 ± 23	-90 ± 27 (-7 ± 25)	15 ± 4	72 ± 22
DPPC-$A_{61}B_9$ 80:20	-54 ± 11	-54 ± 11 (-0 ± 11)	9 ± 2	97 ± 19
DPPC-$A_{61}B_9$ 20:80	-105 ± 23	-102 ± 11 (-3 ± 11)	18 ± 4	113 ± 12
DPPC-$PBO_{50}PG_{18}$ 50:50	-47 ± 12	-51 ± 12 (-4 ± 12)	8 ± 2	83 ± 19
POPC-$A_{61}B_9$ 50:50	-67 ± 0	-66 ± 1 (-1 ± 1)	12 ± 0	105 ± 1
POPC-$PBO_{50}PG_{18}$ 50:50	-43 ± 4	-44 ± 5 (-1 ± 5)	8 ± 1	97 ± 10
SM-$A_{61}B_9$ 50:50	-73 ± 4	-73 ± 0 (-0 ± 4)	13 ± 0	103 ± 0
SM-$PBO_{50}PG_{18}$ 50:50	-44 ± 3	-45 ± 4 (-1 ± 1)	7 ± 0	94 ± 7

POPE-$A_{61}B_9$ 50:50	-70 ± 10	-73 ± 10 (-3 ± 10)	12 ± 2	88 ± 12
POPE-$A_{89}B_{10}$ 50:50	-68 ± 6	-73 ± 5 (-5 ± 8)	12 ± 1	80 ± 6
POPE-$A_{30}B_{10}$ 50:50	-57 ± 0	-58 ± 0 (-1 ± 0)	10 ± 0	96 ± 0
POPE-$PBO_{50}PG_{18}$ 50:50	-57 ± 5	-67 ± 6 (-10 ± 8)	10 ± 1	60 ± 5
NGPE-$A_{61}B_9$ 50:50	-63 ± 7	-75 ± 6 (-12 ± 9)	11 ± 1	52 ± 4
NGPE-$PBO_{50}PG_{18}$ 50:50	-33 ± 1	-56 ± 1 (-23 ± 1)	6 ± 0	8 ± 0
DOPE-$A_{61}B_9$ 50:50	-82 ± 21	-84 ± 19 (-2 ± 20)	14 ± 3	90 ± 20
DOPE-$PBO_{50}PG_{18}$ 50:50	-53 ± 5	-65 ± 2 (-12 ± 5)	9 ± 0	50 ± 2

Table 7-12. Frequency shift values for membrane formation and BSA step of different hybrid membranes composed of polymer and lipids are reported. Membrane thickness and coverage were calculated.

Hybrid mixture (50:50 w/w)	Membrane coverage (%)	Phase domain separation	Islands presence
DPPC-$A_{89}B_{10}$	n.a.	yes	big
DPPC-$A_{89}B_{10}$ (in water)	n.a.	yes	no
DPPC-$A_{61}B_9$	72 ± 22	yes	big
DPPC-$PBO_{50}PG_{18}$	83 ± 19	yes	small
POPE-$A_{61}B_9$	88 ± 12	no	big
POPE-$A_{89}B_{10}$	80 ± 6	no	big
POPE-$A_{30}B_{10}$	96 ± 0	no	big
POPE-$PBO_{50}PG_{18}$	60 ± 5	not clear	big
SM-$A_{61}B_9$	103 ± 0	yes	small

SM-$A_{89}B_{10}$	n.a.	no	small
SM-$A_{30}B_{10}$	n.a.	yes	small
SM-$PBO_{50}PG_{18}$	94 ± 7	yes	small
NGPE-$A_{89}B_{10}$	n.a.	yes	no
NGPE-$A_{61}B_{9}$	52 ± 4	not clear	small
NGPE-$PBO_{50}PG_{18}$	8 ± 0	no	small

Table 7-13. Evaluation of the preserved assemble of different hybrid membranes in dry conditions.

8. Curriculum Vitae

STEFANO DI LEONE

Research Assistant

Work Experience

2021 – 2017 **Research assistant**, *University of Basel*, Switzerland
Department of Physical Chemistry
- Writing scientific publications, reports and presentations
- Assistant / Tutor of the Physical Chemistry laboratory experiments for Master students
- Mentoring and training of Master and Bachelor students
- Designing, planning and managing of the project
- Evaluating the costs and managing the budget of instruments
- Designing of a new device for membrane deposition
- Characterizing hybrid polymer supported membranes
- Investigating the interactions between artificial polymer membranes and a biomolecules

2016 **Research assistant**, *University of Bari*, Italy
Department of Science of Food and Plants
- Characterizing a new variety of pigmented durum

Education

2021 – 2017 **PhD in Nanoscience**, *University of Basel*, Switzerland
PhD title: Interaction studies between artificial polymer supported membranes and biomolecules

2014 – 2012 **Master of science in Chemistry**, *University of Bari*, Italy
Master Thesis: SERS (Surface Enhanced Raman Spectroscopy) charaterization of plasma treated silver nanocomposite substrates

2012 – 2008 **Bachelor of science in Chemistry**, *University of Bari*, Italy
Bachelor Thesis: Synthesis and characterization of sulfoxides with different functional groups

Courses Attendance and Certificates

2021 – 2019
Applied statistic in R
Dealing with data
Personal finance
Increase your word power
Intercultural communication
Negotiation skills for scientists
Productive meetings
Writing Workflow
Self-branding and self-promotion
Citation, paraphrase and plagiarism

2016 **IELTS (Academic)**

2004 **ECDL (European Computer Driving License)**

Peer - Reviewed Publication

- J. Phys. Chem. B, 2020, 124, 22, 4454−4465; doi.org/10.1021/acs.jpcb.0c02727
- Macromol. Biosci., 2020, 20, 1900291; doi.org/10.1002/mabi.201900291
- Polymers, 2020, 12(5), 1003; doi.org/10.3390/polym12051003
- Nanoscale, 2020, 12, 1551-1562; doi.org/10.1039/C9NR08502E
- Front. Chem., 2019; doi.org/10.3389/fchem.2018.00645

Basel, 24th April, 2021

Contact Information

Rudolfstrasse 44, 4054
Basel, Switzerland

+49 170 109 50 59
+39 320 350 67 05

stefano.dileone@hotmail.it
stefano.dileone@unibas.ch

https://www.linkedin.com/in/stefano-di-leone-76a035102/

Birth	30.12.1989 / Bari
Nationality	Italian
Marital Status	Unmarried
Residence Permit	L (14.06.2021)

Soft Skills

Problem-solving
Flexibility
Leadership
Communication
Teamwork
Time management
Will to learn

Softwares and OS

Microsoft Excel	■■■□□
Microsoft Powerpoint	■■■■□
Microsoft Word	■■■□□
Origin pro 8	■■■□□
Python	■■□□□
RStudio	■□□□□
Windows	■■■■□

Languages

Italian	Mother tongue
English	Fluent (C1 / C2)
German	Intermediate (B2 / C1)

Hobbies

Boardgames, Roleplaying games
Percussion instrument (drum)
Sound engineering
Volleyball, Gym, Martial arts
Draw